Investigating the Interaction between Lytic Transglycosylases and Ivyp1 & Ivyp2 in *Pseudomonas aeruginosa*

by

Joshua H Chun

A Thesis

presented to

The University of Guelph

In partial fulfilment of requirements
for the degree of

Master of Science

in

Molecular and Cellular Biology

Guelph, Ontario, Canada

ABSTRACT

Investigating the Interaction between Lytic Transglycosylases and Ivyp1 & Ivyp2 in *Pseudomonas aeruginosa*

Joshua Chun
University of Guelph, 2019

Advisor(s):
Dr. Anthony J. Clarke

The existence of the proteinaceous inhibitors of lysozyme, Ivy, has remained a paradoxical puzzle since their discovery. From the time they were shown to inhibit MltB, efforts have been made to map the interaction of Ivyp1 and Ivyp2 with all eleven lytic transglycosylases (LTs) produced by *Pseudomonas aeruginosa*. Herein, this study continues to explore the hypothesis that the Ivys function as inhibitors of LTs. In doing so, a complete pH profile has been established for all LTs along with inhibition profiles by both Ivyp1 and Ivyp2 for each LT. The pH profiles reveal that the LTs operate under a slightly acidic range of pH optima. Additionally, the first experimental evidence for interactions of Ivyp1 and Ivyp2 with the LTs MltD, MltG, Slt70 and SltB1 are reported here. Altogether, these results support the hypothesis that Ivy acts to inhibit certain LTs and present possibilities for interplay with other enzymes such as PBPs.

ACKNOWLEDGEMENTS

First and foremost, my greatest thanks go to my advisor, Dr. Anthony Clarke, who was patient not just with me but with the whole project. Failure and discouragement were not uncommon emotions to experience in this project but witnessing your relentless dedication to see it to the end provided me with the determination to do the same. Thank you for your guidance, wisdom, and support throughout this process. They were assuredly invaluable in helping me get to where I am today.

I am also grateful to the Clarke lab. Special thanks go to Stephanie Gilbert, who helped me progress in my project in a time when I felt stuck. Much of your efforts were instrumental in helping me produce some of the results in my thesis. I am also indebted to Chris Vandenende, who helped take the load off by purifying the most difficult proteins on the face of this planet. You know the ones I'm talking about.

Lastly, I am forever grateful to my wife, Rachel. Thank you for your support from beginning to end. You have always had a firm and unwavering belief in my capabilities, even in the moments when I had doubted myself. Though with bittersweet feelings this chapter in my life closes, I am confident and happy knowing that ours never will.

TABLE OF CONTENTS

Abstract ii

Acknowledgements iii

Table of Contents iv

List of Tables viii

List of Figures ix

List of Appendices xi

List of Symbols, Abbreviations or Nomenclature xii

1 Introduction 1

1.1 Antibiotic Resistance & Drug Discovery 1

1.2 *Pseudomonas aeruginosa* 2

1.3 Peptidoglycan Structure 3

1.4 Glycan Chain Hydrolases 5

1.5 Lytic Transglycosylases 5

1.5.1 Classification by Sequence and Structure 5

1.5.2 Mechanism of Action 9

1.5.3 Biological Function 10

1.5.4 Regulation by Glycan Chain Modification 11

1.5.5 Regulation by Proteinaceous Inhibitors 13

1.6 Rationale of Study, Thesis Objectives, and Hypothesis 20

2 Materials and Methods 21

2.1 Chemicals and Reagents 21

2.2 Strains and Plasmids 21

2.3 DNA Techniques 23
2.3.1 Preparation of Competent Cells 23
2.3.2 Engineering of *ivyp1* & *ivyp2* 23
2.3.3 Transformation of *E. coli* 25
2.4 Small Scale Expression of Ivyp1 & Ivyp2 (Boil Prep) 25
2.5 Large Scale Protein Production 26
2.5.1 Over-expression of Lytic Transglycosylases 26
2.5.2 Over-expression of Ivyp1 and Ivyp2 27
2.6 Cell Lysis 27
2.7 Protein Purification 27
2.7.1 Purification of *P. aeruginosa* MltA, MltD, MltF2, MltG, RlpA 27
2.7.2 Purification of *P. aeruginosa* Slt70, MltB, SltB1, SltB2, SltB3, MltF 28
2.7.3 Purification of *P. aeruginosa* Ivyp1 and Ivyp2 28
2.7.4 Gel Filtration of *P. aeruginosa* Ivyp1 and Ivyp2 29
2.8 Buffer Exchange 30
2.9 Concentration of Protein Samples 30
2.10 Protein Analysis 31
2.10.1 Sodium Dodecyl Sulfate Polyacrylamide Gel Electrophoresis (SDS-PAGE) 31
2.10.2 Protein Quantification 31
2.10.3 Protein Identification by Mass Spectrometry 31
2.11 Enzyme Activity Assays 32
2.11.1 Measurement of Lytic Activity (Turbidity Assay) 32
2.11.2 Inhibition of Lytic Activity 33
2.11.3 pH Profiles of Lytic Transglycosylases 33

2.12 Ordinary One-Way ANOVA Statistical Analysis 33
3 Results 34
3.1 Production and Purification of Ivyp1-GST and Ivyp2-GST 34
3.2 Production and Purification of Recombinant sMltA 38
3.3 Production and Purification of Recombinant sMltB 39
3.4 Production and Purification of Recombinant SltB1 40
3.5 Production and Purification of Recombinant SltB2 41
3.6 Production and Purification of Recombinant SltB3 42
3.7 Production and Purification of Recombinant sMltF 43
3.8 Production and Purification of Recombinant sMltF2 44
3.9 Production and Purification of Recombinant sRlpA 45
3.10 Confirmation of Ivyp1 and Ivyp2 Interaction with HEWL 46
3.11 Optimization of Lytic Activity Assay Conditions 47
3.11.1 sMltA 48
3.11.2 sMltB 48
3.11.3 sMltD 48
3.11.4 sMltF 48
3.11.5 sMltF2 50
3.11.6 sMltG 50
3.11.7 sRlpA 50
3.11.8 Slt70 50
3.11.9 SltB1 51
3.11.10 SltB2 51
3.11.11 SltB3 51

3.12 pH Effects on Interactions Between HEWL and Ivyp1 51
3.13 Inhibition of Lytic Activity of LTs by Ivyp1 and Ivyp2 52
3.13.1 sMltA 53
3.13.2 sMltB 53
3.13.3 sMltD 54
3.13.4 sMltF 54
3.13.5 sMltF2 54
3.13.6 sMltG 54
3.13.7 sRlpA 56
3.13.8 Slt70 56
3.13.9 SltB1 56
3.13.10 SltB2 & SltB3 56
4 Discussion 58
References 69
Appendices 76

LIST OF TABLES

Table 1.1 List of LTs and homologues in *P. aeruginosa*..... 7

Table 2.1 List of bacterial strains and genotypes used in this study..... 22

Table 2.2 List of plasmids and derivatives used in this study 22

Table 2.3 Oligonucleotide primers used in this study..... 24

Table 2.4 pH of purification buffers for LT's using NaH_2PO_4 Buffer 28

Table 3.1 pH optimum for each LT as determined in this study 50

LIST OF FIGURES

Figure 1.1. PG Structure and Reactions by PG Hydrolases 3

Figure 1.2. Classification of LTs into 6 Families 6

Figure 1.3. Mechanism of Action of LT Activity 10

Figure 1.4. Structural Analysis of Ivyc-lysozyme, MltB and Ivyp1 16

Figure 1.5. Phylogenetic Tree of the Ivy Family of Proteins 18

Figure 1.6. Turbidimetric assay of lysozyme and MltB inhibition by Ivyp1 and Ivyp2 19

Figure 3.1 SDS-PAGE Analysis of Ivyp1-GST and Ivyp2-GST Purification by Immobilized Glutathione Sepharose Chromatography 35

Figure 3.2. SDS-PAGE Analysis of GST Purification by Immobilized Glutathione Sepharose Chromatography 36

Figure 3.3 SDS-PAGE Analysis of Ivyp1 Gel Filtration 37

Figure 3.4 SDS-PAGE Analysis of Ivyp2 Gel Filtration 1 37

Figure 3.5 SDS-PAGE Analysis of Ivyp2 Gel Filtration 2 38

Figure 3.6 SDS-PAGE Analysis of sMltA Purification by Immobilized Metal Affinity Chromatography 39

Figure 3.7 SDS-PAGE Analysis of sMltB Purification by Immobilized Metal Affinity Chromatography 40

Figure 3.8 SDS-PAGE Analysis of SltB1 Purification by Immobilized Metal Affinity Chromatography 41

Figure 3.9 SDS-PAGE Analysis of SltB2 Purification by Immobilized Metal Affinity Chromatography 42

Figure 3.10 SDS-PAGE Analysis of SltB3 Purification by Immobilized Metal Affinity Chromatography 43

Figure 3.11 SDS-PAGE Analysis of sMltF Purification by Immobilized Metal Affinity Chromatography 44

Figure 3.12 SDS-PAGE Analysis of sMltF2 Purification by Immobilized Metal Affinity Chromatography 45

Figure 3.13 SDS-PAGE Analysis of sRlpA Purification by Immobilized Metal Affinity Chromatography 46

Figure 3.14 Inhibition of HEWL activity by Ivyp1 and Ivyp2 using the Turbidity Assay..... 47

Figure 3.15 pH Activity Profiles of LTs 49

Figure 3.16 Effect of pH on HEWL Inhibition by Ivyp1 52

Figure 3.17 Statistical Analysis of Apparent Inhibition Data by Ordinary One-Way ANOVA .. 53

Figure 3.18 Inhibition of LTs by Ivyp1 and Ivyp2 55

Figure 4.1 Comparison of LT Activities Assayed under Different Conditions 62

Figure 4.2 Pairwise Dali modeling of Ivyp1 to Slt70 66

LIST OF APPENDICES

Appendix A – Recipes and Formulations 76

Appendix B – Turbidity Graphs 77

Figure B 1 Inhibition of sMltA with Ivyp1 and Ivyp2 77

Figure B 2 Inhibition of sMltB with Ivyp1 and Ivyp2 77

Figure B 3 Inhibition of sMltD with Ivyp1 and Ivyp2 78

Figure B 4 Inhibition of sMltF with Ivyp1 and Ivyp2 78

Figure B 5 Inhibition of sMltF2 with Ivyp1 and Ivyp2 79

Figure B 6 Inhibition of sMltG with Ivyp1 and Ivyp2 79

Figure B 7 Inhibition of sRlpA with Ivyp1 and Ivyp2 80

Figure B 8 Inhibition of Slt70 with Ivyp1 and Ivyp2 80

Figure B 9 Inhibition of SltB1 with Ivyp1 and Ivyp2 81

Figure B 10 Inhibition of SltB2 with Ivyp1 and Ivyp2 81

Figure B 11 Inhibition of SltB3 with Ivyp1 and Ivyp2 82

LIST OF SYMBOLS, ABBREVIATIONS OR NOMENCLATURE

LT (lytic transglycosylase)

Mbp (megabase pairs)

GlcNAc (*N*-acetylglucosamine)

MurNAc (*N*-acetylmuramic acid)

m-DAP (2,6-diaminopimelic acid)

PBP (penicillin-binding protein_

Slt (Soluble lytic transglycosylase)

Mlt (Membrane-bound lytic transglycosylase)

sMlt (soluble-form of membrane-bound lytic transglycosylase)

LMM PBP (Low molecular mass penicillin-binding protein)

Ivyc (Ivy from *E. coli*)

Ivyp (Ivy from *P. aeruginosa*)

IPTG (isopropyl β-D-1-thiogalactopyranoside)

EDTA (ethylenediaminetetraacetic acid)

LB (Luria broth)

SB (SuperBroth)

Kan (kanamycin)

Amp (ampicillin)

DNA (deoxyribonucleic acid)

PCR (polymerase chain reaction)

GST (glutathione sepharose tag)

TAE (tris-acetate-EDTA)

kb (kilobase)

UV (ultraviolet)

SDS-PAGE (sodium dodecyl sulfate polyacrylamide gel electrophoresis)

MWCO (molecular weight cut-off)

ddH_2O (double distilled H_2O)

BCA (bicinchoninic acid)

BSA (bovine serum albumin)

DTT (dithiothreitol)

TCA (trichloroacetic acid)

PG (peptidoglycan)

OD (optical density)

IMAC (immobilized metal affinity chromatograph)

MIC (minimum inhibitory concentration)

CAZ (ceftazidime)

MEM (meropenem)

HEWL (hen egg white lysozyme)

1 Introduction

1.1 Antibiotic Resistance & Drug Discovery

The discovery of penicillin in 1922 by Alexander Fleming was followed by a golden age of antibiotic discovery lasting from 1940 to 1970, allowing patients to fight off infections that formerly would have led to death (1). However, mass use of antibacterial drugs has led to the rapid rise of resistant bacterial strains due to selective pressures, such that even multi-drug resistant pathogens have become commonplace (1). Strains of *Enterococcus faecium, Staphylococcus aureus, Klebsiella pneumoniae, Acinetobacter baumamnii, Pseudomonas aeruginosa,* and *Enterobacter* species (known as the ESKAPE pathogens) have been observed to "eskape" the lethal action of antibiotics (2). Additionally, we have observed a decline of new antibacterial agents being approved in the past 30 years: 16 from 1983-1987, 14 from 1988-1992, 10 from 1993-1997, 8 from 1998-2002, and 5 from 2003-2007 (3). As a result, a call to action was declared by the Infectious Disease Society of America (IDSA) for the medical research community to show greater interest in the pursuit of antimicrobial drug discovery (4).

The three most successful classes of antibiotics to date are drugs that target DNA replication (fluoroquinolones target DNA gyrase and topoisomerase), protein translation (aminoglycosides bind to 16S ribosomal RNA), and cell wall synthesis (β-lactams target penicillin binding proteins, PBPs) (5). Out of these classes, the cell wall continues to be a point of interest for drug discovery (6). This is primarily due to the fact that the numerous molecular bonds in peptidoglycan (PG) require linkages and cleavages by various types of enzymes, including amidases, endopeptidases, carboxypeptidases, glucosaminidases, transglycosylases, and transpeptidases (7). Compromising even one of these linkages could be destructive to the integrity of the cell wall. This is evident by the effectiveness of current antibiotics that target the

cell wall, of which there are two main types. The β-lactams were one of the first classes of antibiotics to be discovered and a wide variety of β-lactams have been found since their initial discovery, although resistant strains have been identified at an alarmingly similar pace. The glycopeptides, though resistant strains exist, continue to be one of the more effective "drugs of last resort" (1).

1.2 *Pseudomonas aeruginosa*

One particular organism of interest is *Pseudomonas aeruginosa*, an aerobic, motile, rod-shaped, Gram-negative bacterium (8). For the immunocompetent person, *P. aeruginosa* rarely colonizes in the form of an infection. Instead, *P. aeruginosa* is an opportunistic pathogen most commonly found in nosocomial infections and has a greater chance of colonization in people who are immunocompromised, have a disruption in their microbial flora due to antibiotic use, and/or have experienced a trauma or breach in normal cutaneous or mucosal barriers (8, 9). Thus, despite being found ubiquitously in the environment, *P. aeruginosa* is predominantly a hospital acquired infection where surgeries, antibiotic use, and immunocompromised patients are commonplace (9). Infection by *P. aeruginosa* is also a leading cause of illness and death in patients with cystic fibrosis (10).

P. aeruginosa possesses a genome of ~5-7 Mbp and included in this is the capacity to produce an extensive range of secondary metabolites and polymers, ability to use various carbon sources and electron acceptors, and the flexibility to respond and adapt to unfavourable environments (11). In addition to all of this, *P. aeruginosa* has an intrinsic resistance to a wide range of antibiotics through resistance mechanisms including biofilm production, loss or reduced copy numbers of OprD porins, overproduction of efflux pumps, and β-lactamase production (11). As a result, *P. aeruginosa* has emerged as a health threat in hospitals worldwide.

1.3 Peptidoglycan Structure

PG (also known as murein) is an essential component of the bacterial cell wall. It acts as the cellular exoskeleton providing strength and rigidity to the cell, while counter-balancing the cell's high osmotic pressure (12). It also provides a scaffold for the anchoring of other cell-wall components such as proteins (13) and teichoic acids (14). PG is made up of glycan strands cross-linked by short peptides (7). Each glycan strand is composed of alternating *N*-acetylglucosamine (GlcNAc) and *N*-acetylmuramic acid (MurNAc) moieties linked by β (1→4) bonds (Fig. 1.1) (7). The D-lactyl group of each MurNAc residue is substituted with a stem peptide composed of L-Ala-γ-D-Glu-m-DAP-D-Ala-D-Ala (where m-DAP is 2,6-diaminopimelic acid) in Gram-negative

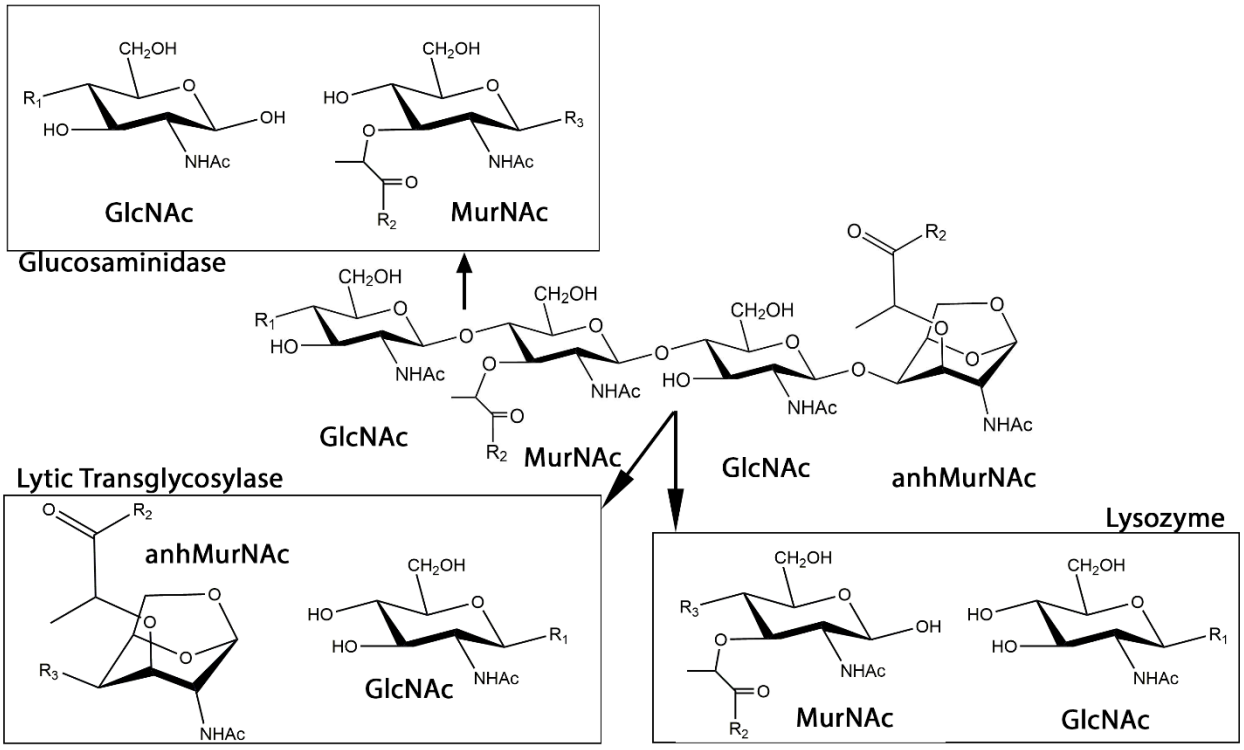

Figure 1.1. PG Structure and Reactions by PG Hydrolases - The structure of PG is shown with alternating GlcNAc and MurNAc moieties and a terminal 1,6-anhydroMurNAc moiety. Reaction products of glucosaminidase, lytic transglycosylases, and lysozymes are shown in their respective boxes. R_1 denotes MurNAc, R_2 denotes peptide stem, and R_3 denotes GlcNAc.

bacteria and L-Ala-γ-D-Glu-L-Lys-D-Ala-D-Ala in Gram-positive bacteria (15). Generally, the terminal D-Ala residue is released upon incorporation into the PG by action of either crosslinking transpeptidases or carboxypeptidases (15).

The greatest variance between peptide stems occurs at residue 3, as evidenced by the m-DAP and L-Lys substitutions between Gram-negative and Gram-positive bacteria, respectively. In certain species, other amino acids encountered at this position include yet other diamino acids (L-Orn, LL-DAP, m-lanthionine, L-2,4-diaminobutyric acid, D-Lys) or monoamino acids (L-homoserine, L-Ala, L-Glu) (16). An example of a peptide stem variation is the substitution of D-Lac for the terminal (residue 5) D-Ala in bacterial species, conferring resistance to glycopeptides (17). Glycopeptides, such as vancomycin and teicoplanin, bind to the terminal D-Ala-D-Ala of the pentapeptide precursor rendering it unable to form cross-links (17). A D-Ala-D-Lac substitution forms only four out of the five essential hydrogen bonds with vancomycin (17). Although a seemingly minor difference, this change results in a 1000-fold reduction in binding affinity thereby allowing for proper synthesis of the cell wall (17).

Several variations exist in cross-links between PG chains. However, the most common form of cross-linking is between the side chain amino group of the diamino acid residue 3 of one peptide stem (acyl acceptor) and the D-Ala carboxyl group of residue 4 of another peptide stem (acyl donor) (16). This cross-linking is catalyzed by the transpeptidase activity of PBPs (18). Cross-linking between residues 3 and 4 of separate peptide stems without an intermediate bridge is referred to as "direct cross-linking" and is most common in Gram-negative bacteria (16). In Gram-positive bacteria, a peptide bridge connects the peptide stems via a head-to-tail linkage (16). A tetrapeptide stem bridge (i.e. L-Ala-γ-D-Glu(Gly)-L-Lys-D-Ala in *Micrococcus luteus*)

and bridges consisting of runs of single amino acid residues (i.e. $(Gly)_5$ in *Staphylococcus aureus*) are two variants among many others (16).

1.4 Glycan Chain Hydrolases

Cellular growth and division require the action of lytic enzymes to break down PG for additional polymers to be inserted in place. Currently, three different groups of glycosidases are known to exist, which can cleave the β-1,4-glycosidic bonds of the glycan chain: β-*N*-acetylglucosaminidases, lytic transglycosylases (LTs), and lysozymes. B-*N*-Acetylglucosaminidases hydrolytically cleave the bonds between GlcNAc and MurNAc, while LTs and lysozymes cleave the bonds between MurNAc and GlcNAc (Fig. 1.1) (7). Lysozymes catalyze a hydrolytic cleavage and are generally expressed in animal and plant species, though structures of lysozyme from phage and bacterial species have also been reported (7, 19, 20). In contrast, LTs perform a non-hydrolytic cleavage and are generally found in bacterial species and phages (21). This non-hydrolytic cleavage results in the formation of a non-reducing 1,6-anhydroMurNAc (7). The research presented in this thesis focuses on the properties of LTs.

1.5 Lytic Transglycosylases

1.5.1 Classification by Sequence and Structure

LTs are found in both soluble forms (Slt; soluble lytic transglycosylase) in the periplasm and in membrane-bound forms (Mlt; membrane-bound lytic transglycosylase) bound to the inner or outer membrane. Despite low sequence similarity, they share structural similarity in the catalytic domain with goose-type lysozyme (22). LTs were originally classified into four families based on sequence similarity of known LTs from *Escherichia coli*, *P. aeruginosa*, and λ phage (Fig. 1.2) (23).

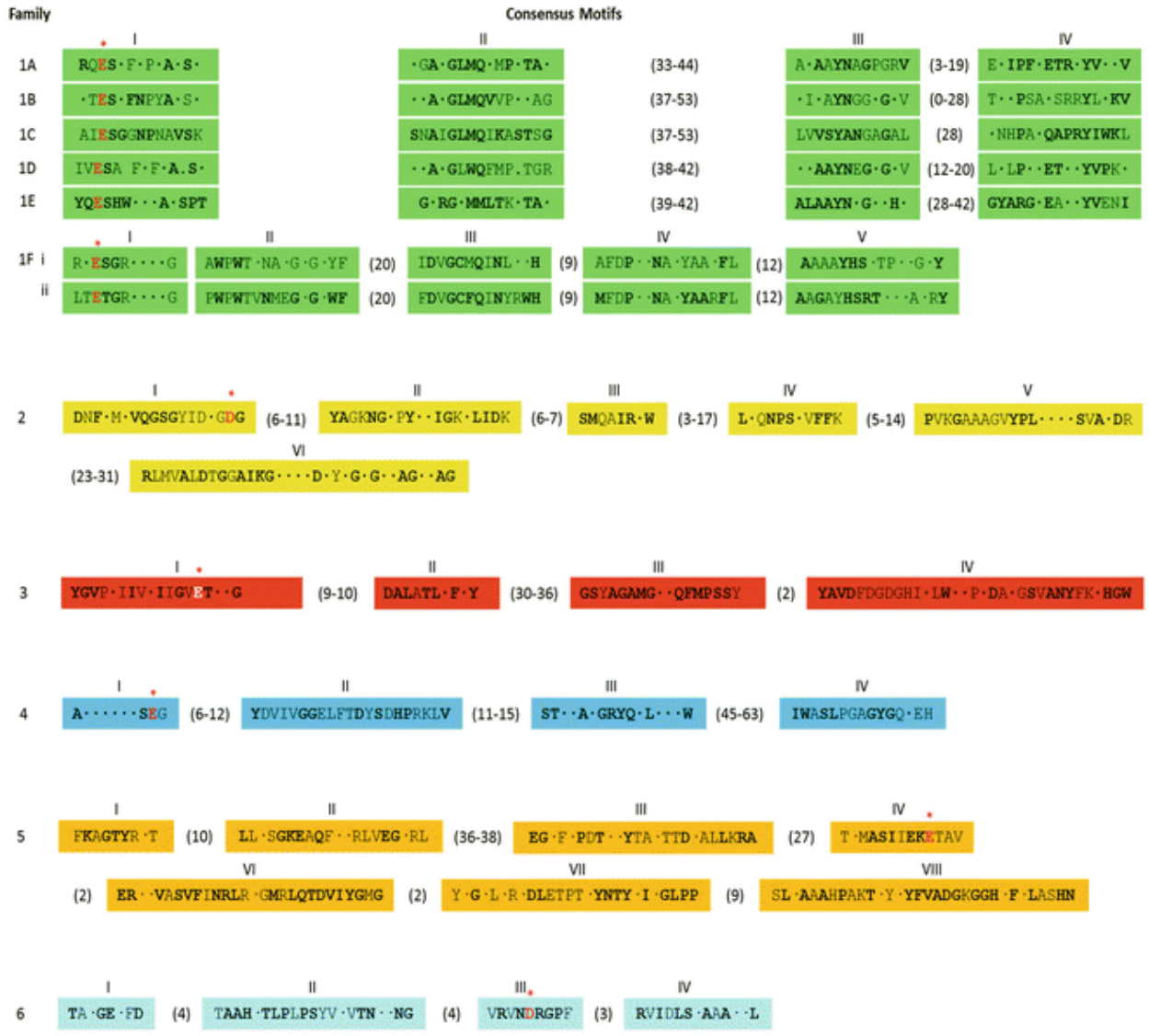

Figure 1.2. Classification of LTs into 6 Families – As described in the text, the six families of LTs are shown with their respective consensus motifs. Residues labelled in red denote the catalytic acid/base and parentheses denotes the numbers of residues between motifs. This figure was taken from (24).

Family 1 is a superfamily containing 6 sub-families: 1A (Slt70), 1B (MltC), 1C (MltE), 1D (MltD), 1E (MltF), and 1F (SltF) (Table 1.1) (23). To date, crystal structures have been determined for families 1A, 1B, 1C, and 1E (25–29). Each subfamily of this superfamily contains three motifs that are generally conserved. Motif 1 is a pair of E and S residues strictly conserved in all members of this superfamily (23). Structural characterization of Slt (subfamily

1A) via X-ray crystallography revealed that the invariant glutamate is the single catalytic residue responsible for the intramolecular cleavage reaction (25, 26). Motif 2, also found in goose-type lysozyme, is composed of G-L-M-Q residues and is present in family 1A, 1C and 1E LTs, while variants of this motif include G-L-M-M (1B) and G-L/I-W-Q (1D) (23). Motif 3 consists of a A-Y-N motif, also found in goose-type lysozyme, and is present in all members of family 1 except for 1E, which consists of a Y-A-N pattern (23). Finally, a fourth C-terminal consensus motif was identified, showing low sequence similarity between subfamilies, but high consensus within each subfamily. Thus, these motifs characteristic to each subfamily were proposed for use as a signature for further identification of unknown LTs (23).

Table 1.1 List of LTs and homologues in *P. aeruginosa*

Family	Sub-Family	LTs	Catalytic Residue	*P. aeruginosa*
1	A	Slt70 (or Slt)	Glu	Slt70
	B	MltC	Glu	-
	C	MltE	Glu	-
	D	MltD	Glu	MltD
	E	MltF	Glu	MltF, MltF2
	F	SltF	Glu	-
2	-	MltA	Asp	MltA
3	-	MltB	Glu	MltB, SltB1, SltB2, SltB3
4	-	λ-bacteriophage	Glu	-
5	-	MltG	Glu	MltG
6	-	RlpA	Asp	RlpA

Family 2 LTs share sequence similarity with MltA and contain six consensus motifs. This is the only family that does not resemble the goose-type lysozyme fold in the catalytic domain. Instead, the enzymes resemble an endoglucanase V fold, which is associated with enzymes that cleave the β-1,4-glycosidic linkage in cellulose (22, 31). Additionally, family 2 LTs do not use glutamate as the catalytic acid/base and instead use an aspartate residue to accomplish the same function (23).

The third family of LTs shares sequence similarity to MltB and contains five consensus motifs. Motif 1 is an E-T motif that shares strong similarity with the E-S motif found in the family 1 lytic transglycosylases (23). Structural characterization of Slt35 (a soluble homolog from *E. coli*) revealed that the invariant glutamate from this motif plays an identical catalytic functional role as the glutamate from motif I of family 1 (32). A second invariant glutamate residue is positioned in motif 4 to comprise an E-F hand, which has been implicated to play a role in heat stability and cell-surface associations (32).

Finally, family 4 is made up of λ bacteriophage enzymes. This family contains four consensus motifs, and similar to families 1 and 3, also contains the invariant catalytic glutamate in motif 1 (23). Like families 1 and 3, the crystal structure reveals that the catalytic domain resembles the goose-type lysozyme (33).

Since this initial classification, two other families have been added: family 5 (MltG is archetype) and family 6 (RlpA is archetype) (24, 34, 35). Family 5 contains eight consensus motifs. Like the family 3 enzymes, one of these motifs contains the invariant catalytic glutamate containing E-T motif, but positioned further down in motif 4 (35). Family 6 contains six consensus motifs. Similar to the family 2 enzymes, a putative catalytic aspartate residue is found in motif III, instead of the conventional glutamate residue (34). To date, one enzyme from every family of LTs has been identified in *E. coli*, except from families 1F (SltF from *R. spheroides*) and 4 (λ bacteriophage), for a total of 9 LTs (34–36). *P. aeruginosa* lacks enzymes from families 1B and 1C (in addition to 1F and 4), but has two homologues in family 1E (MltF, MltF2) and four in family 3 (MltB, SltB1, SltB2, SltB3) for a total of 11 LTs (Table 1.1) (34, 35, 37).

1.5.2 Mechanism of Action

The mechanism of action of LTs differs from lysozymes in that their non-hydrolytic cleavage results in the formation of a terminal 1,6-anhydroMurNAc instead of a reducing MurNAc. The mechanism of action was determined by inhibition studies with bound NAG-thiazoline and is thought to occur in the following manner (Fig. 1.3) (38). MurNAc and GlcNAc residues first bind to the active site at subsites -1 and +1, respectively (36). An acidic residue (Glu/Asp) is positioned between the subsites -1 and +1 and is believed to function as the catalytic acid/base. The catalytic Glu/Asp first acts as a general acid and protonates the glycosidic oxygen to facilitate cleavage of the glycosidic bond and releasing the GlcNAc moiety (38). This results in the formation of a putative oxocarbenium transition state, which is stabilized as an oxazolinium ion intermediate involving the *N*-acetyl group of the MurNAc residue at subsite -1 (38). The resulting deprotonated Asp/Glu residue now acts as a catalytic base to abstract a proton from the C-6 hydroxyl of this MurNAc, leading to the intramolecular nucleophilic attack at C-1 and releasing the *N*-acetyl group from oxazolinium ion formation (38). The product, 1,6-anhydroMurNAc is then released from the active site.

Structural studies on MltE from *E. coli* and its catalytic variants confirmed the initial step of this mode of action, mainly that the catalytic Glu/Asp acts as a general acid to protonate the oxygen of the glycosidic bond (39, 40). One point of contention is that the bond breakage in response to glutamate proton transfer is synchronized with the bond formation by the C6-oxygen, rather than the formation of an oxazolinium species (39). This is mainly due to the presence of a clamping loop (S73-S75), which acts to enhance the electrostatic contacts between the catalytic glutamate and substrate (39). However, the S75 of MltE is not conserved in all LTs and in the case of *E. coli* Slt70 a valine is present at the same position, likely creating a different loop

structure. Dik et al. concede that the possibility of mechanism with an oxazolinium species is indeed possible for such an LT (39).

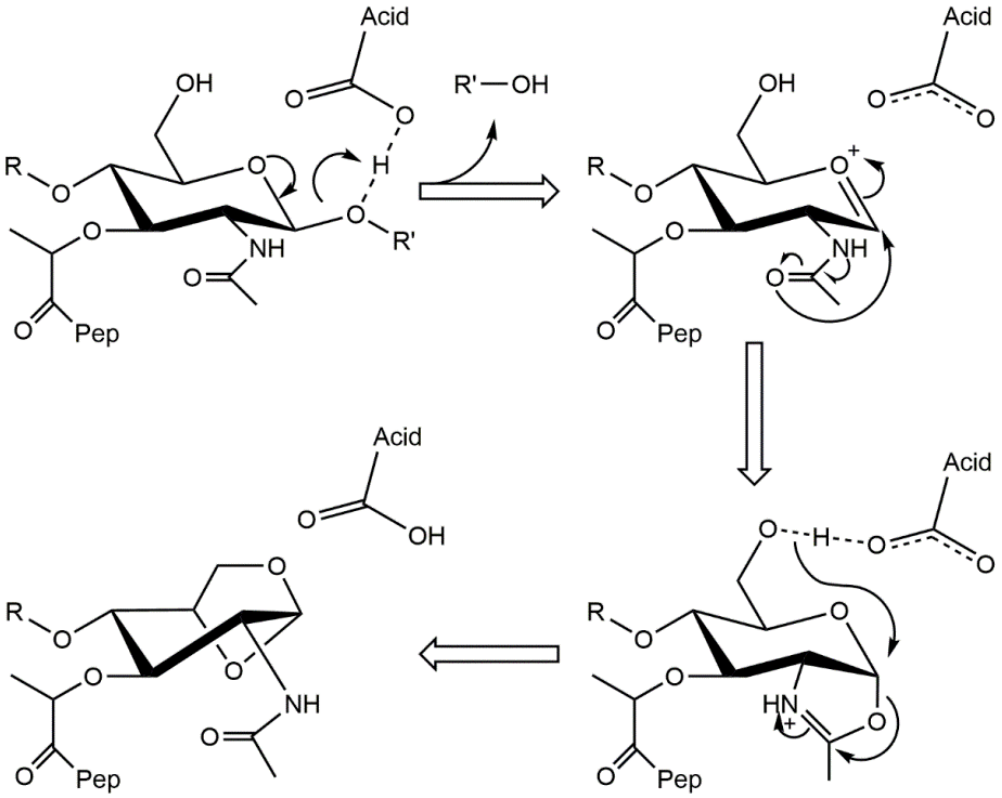

Figure 1.3. Mechanism of Action of LT Activity – The mechanism of action of general LTs, as described in the text, is shown here. R and R` denote GlcNAc residues, while Pep denotes the peptide stem.

1.5.3 Biological Function

LTs are important cell-wall remodeling enzymes that allow many different processes to occur. Cell wall remodeling involves constant turnover of PG as the sacculus expands and divides (41). Though little is known regarding the specific function of each family of LTs, current evidence suggests that the family 1 enzymes are important for assembly of conjugation and secretion systems (42), family 2 enzymes for septation and separation of dividing cells (43), family 3 enzymes for flagella and pili formation and sporulation (42), and family 4 for bacteriophage-induced lysis (36).

Furthermore, LT activity has been shown to be crucial for β-lactam resistance via regulation of β-lactamase expression. This is thought to occur by the interaction of certain muropeptides with AmpR as co-inducers or co-effectors to regulate AmpC β-lactamase expression (41). The co-inducer molecule that induces AmpC expression is 1,6-anhydroMurNAc-tripeptide, while the co-effector that represses AmpC expression is UDP-MurNAc-pentapeptide (44, 45). The steps leading up to the initiation of AmpC expression are thought to occur in the following manner. Low molecular mass PBPs (LMM PBPs) remove the terminal D-Ala residue from the peptide stem by exolytic carboxypeptidase activity (41). Binding of β-lactams to LMM PBPs results in the inability of the PBPs to perform their carboxypeptidase activity (41). LTs then catalyze the production of GlcNAc-1,6-anhydroMurNAc, which is transported into the cytoplasm from the periplasm by AmpG and then cleaved by NagZ to produce GlcNAc and 1,6-anhydroMurNAc (41, 46). AmpD is an amidase that cleaves the peptide stem of muropeptides and its expression is repressed during induction of β-lactamase expression (47). As a result, the final muropeptide structure 1,6-anhydroMurNAc-pentapeptide accumulates in the cytoplasm and induces β-lactamase expression by derepressing the AmpR regulator (41). Indeed, further research on the effect of LTs on β-lactam susceptibility revealed that mutants lacking multiple LTs were more susceptible to β-lactams (37, 48, 49). Thus, understanding regulation of LT activity is crucial for the purposes of developing drugs that can be used synergistically with β-lactamases.

1.5.4 Regulation by Glycan Chain Modification

One mode of regulating LT activity is through modifications of the glycan chains (50). This also serves a dual purpose of protecting the bacteria from cleavage of its PG by exogenous

lysozyme. There are three main types of glycan chain modifications: *N*-deacetylation, *O*-acetylation, and *N*-glycolylation.

N-Deacetylation of the C2 amine is found primarily in Gram-positive cells and occurs in both GlcNAc and MurNAc (51, 52). It has been shown to reduce the lytic activity of lysozyme, whereas chemically acetylating the PG restores lysozyme activity (53, 54). However, not much is known about the effect of *N*-deacetylation on the activity of autolysins (glucosaminidases and LTs) (55). The enzymes PdaA and PgdA deacetylate MurNAc and GlcNAc residues, respectively, and although both enzymes are topologically different, they contain similar folds in the deacetylase domain and catalytic core (55–58).

N-Glycolylation of the C2 amine (instead of *N*-acetylation) of GlcNAc occurs primarily in *Mycobacterium tuberculosis* and related genera within the *Actinomycetales* (52, 59). Although the role of this glycolyl residue is not fully known, the polar hydroxyl group is believed to stabilize the cell envelope, while potentially providing protection against lysozyme.

O-Acetylation of the C6 hydroxyl group of MurNAc, and in some cases GlcNAc, occurs in pathogenic Gram-positive and some Gram-negative cells (60, 61). Like *N*-deacetylation, *O*-acetylation has been shown to be the determinant of lysozyme resistance, particularly in *Staphylococcus* species (62). Additionally, *O*-acetylation precludes the activity of LTs, since LTs require a free C6 hydroxyl in order to form the 1,6-anhydro ring (55). Thus, it has been suggested that another function of *O*-acetylation is the spatial and temporal regulation of LTs in Gram negative species that require the action of LTs to remodel their cell wall (63–65).

Two models of *O*-acetylation currently exist, each being unique to Gram positive and Gram negative, respectively. The first involves the OatA protein, which has an N-terminal acyltranslocase domain that transports acetyl group across the membrane, as well as a C-terminal

catalytic domain which carries out the acetylation (51). In the second model, the two domains exist in two separate enzymes: PatA is responsible for the acetyl transport, while PatB catalyzes the acetyl transfer onto MurNAc (51). *O*-Acetylation is one of the research topics of interest in the Clarke lab.

1.5.5 Regulation by Proteinaceous Inhibitors

Research has been conducted on a second mode of muramidase control, involving proteinaceous inhibitors. The first proteinaceous inhibitor of lysozyme was discovered by serendipity from *E. coli* and was aptly named inhibitor of vertebrate lysozyme (Ivy) by the Claverie group (66). This French research group had been characterizing ORFan proteins and had discovered that one of these proteins, Ivy, co-purified with lysozyme, which was included in the cell lysis mixture to facilitate disruption of cell wall during sonication (66).

The researchers then went on to demonstrate by using the turbidimetric assay that Ivy could inhibit the lytic activity of lysozyme (66). Ivy was pre-incubated in a culture of *Micrococcus luteus* and lysozyme was subsequently added in a 1:1 ratio with Ivy (66). The resulting optical density progress curve produced a slightly downward concave, reflecting a slow-binding kinetic model (66). Additionally, increasing concentrations of Ivy resulted in a near complete inhibition of lytic activity, suggesting that Ivy is a tight-binding inhibitor (66). The authors concluded from the presence of a signal peptide that Ivy is likely to be localized to the periplasm, which is consistent with its proposed function as a defender of the cell wall (66). In addition, they noted the peculiarity of the occurrence of Ivy in the Gram-negative *E. coli*, which can sufficiently defend their PG from lysozyme due to the presence of an outer membrane (66). Finally, a preliminary search for orthologs revealed a hit in the *Pseudomonas aeruginosa* genome with 30% identical residues in the most similar regions (66).

The Michiels group in Belgium followed up on this study to determine whether the inhibition of lysozyme by Ivy could be observed in Gram-negative cells under stress conditions that resulted in perturbation of the outer membrane (67). First, the researchers obtained cell extracts by sonication and periplasmic proteins by osmotic shock from Ivy overexpression strains, knockout mutants, and wild-type strains of *E. coli*. Using these fractions, the researchers then performed a turbidimetric assay with *M. luteus* to determine whether these Ivy-containing (or absent) fractions inhibited lysozyme activity. The results showed that the fractions extracted from Ivy overexpression strains inhibited the activity of lysozyme, while the knockout mutants failed to inhibit lytic activity (67). The researchers then incubated each strain with lysozyme in membrane-permeabilizing conditions (lactoferrin or high pressure) and plated the mixture to measure lysozyme sensitization. In the absence of membrane permeabilizing conditions, the outer membrane was an effective barrier against lysozyme (67). However, the presence of membrane-permeabilizing conditions induced lysozyme sensitivity in an Ivy-dependent manner (67). Overexpression strains exhibited virtually no sensitivity to lysozyme, whereas knockout mutants were strongly sensitive and wild-type strains only partially sensitive (67). These results showed that Ivy expression contributes to lysozyme resistance in Gram-negative cells under membrane-permeabilizing conditions.

The structure of Ivy was determined by X-ray crystallography (68). Ivy from *E. coli* and *P. aeruginosa* were given the names Ivyc and Ivyp, respectively, and the crystal structures of both proteins were solved (68). Additionally, the Ivyc-lysozyme complex structure was determined, revealing the protein-protein interactions and mechanism of lysozyme inhibition (68). The crystal structure for Ivyc reveals a novel fold with a homodimer as the physiologically active unit (68). Each monomer is composed of a central β-sheet made up of five antiparallel strands and is

flanked on the concave side by an amphipathic α-helix and on the convex side by two short α-helices (68) (Fig. 1.4). The two β-sheets of each monomer come together to form a horseshoe-like fold with the amphipathic α-helices in the center (68). The structure of Ivyp is topologically similar to Ivyc. However, the greatest difference between the two structures is that the functional unit of Ivyp is a monomer and not a homodimer (68). The Ivyc-lysozyme complex structure reveals Ivyc again as a homodimer with each monomer bound to one molecule of lysozyme, revealing a 1:1 binding between Ivyc and lysozyme. This homodimer configuration allows for greater surface area interaction between Ivyc and lysozyme, resulting in a higher inhibitory activity of Ivyc compared to Ivyp (68). The structure also reveals the mechanism of inhibition, where a loop (CKPHDC) protruding from the Ivyc molecule occludes the lysozyme active site. In particular, the histidine residue at the center of this loop excludes a conserved water molecule from the active site and forms two hydrogen bonds with an aspartate (D52) and glutamate (E35) (Fig. 1.4), two of three residues responsible for the enzymatic activity of lysozyme (68). Comparison between the Ivyc and Ivyc-lysozyme structure reveals that there is no conformation change in the loop structure. The rigidity of this loop can be explained by the flanking cysteine residues that form a disulfide bond, as well as the lysine and aspartate residues which form a salt bridge. Functional studies involving site-directed mutagenesis confirmed the importance of the histidine residue. A histidine to aspartate substitution resulted in a 300-fold increase in K_i due to the repulsion of negatively charged aspartate and glutamate residues (68). Additionally, phylogenetic analysis revealed that this CKPHDC loop is absolutely conserved in homologues of Ivyc.

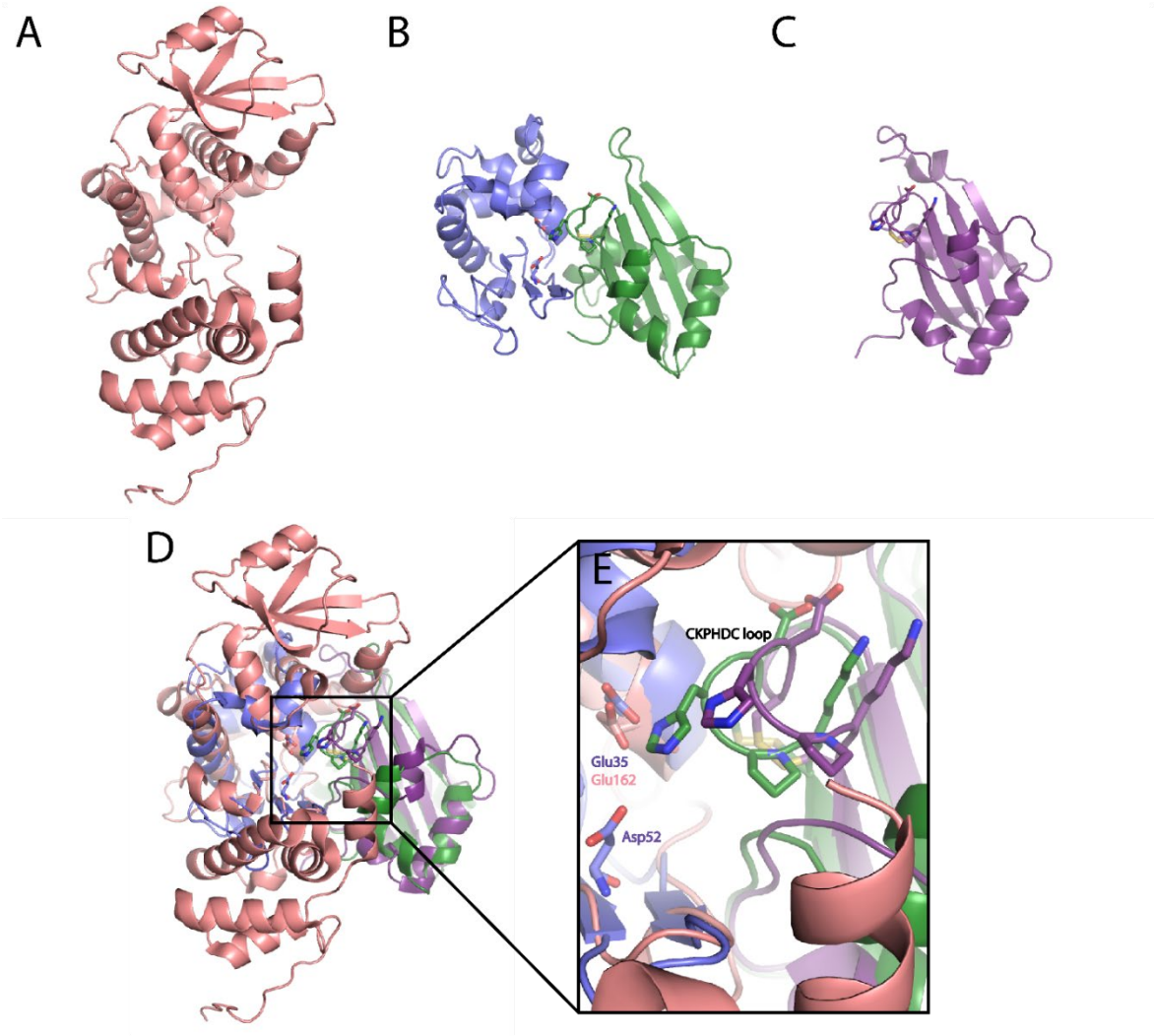

Figure 1.4. Structural Analysis of Ivyc-lysozyme, MltB and Ivyp1 – The structure of *E. coli* MltB (peach) (A), Ivyc(green)-lysozyme(blue) monomer complex (B), and Ivyp1 (purple) monomer (C) are shown above. All structures were superimposed (D) using Dali and Pymol (see text for Z-scores and rmsd). The single catalytic glutamate of MltB and both acidic residues of lysozyme (Glu35, Asp52) are shown interacting with the CKPHDC inhibitory loop of Ivyp1 and Ivyc.

Phylogenetic analysis led to some puzzling observations. The first observation was that Ivy homologues were only found in Proteobacteria (68). It had been suggested in the initial discovery of Ivy that although they had discovered an *E. coli* variant of the Ivy protein, Ivy would prove to be particularly advantageous in the Gram-positive bacteria, which have an exposed PG (66). Thus, the identification of Ivy in only Gram-negative species, which protect

their PG by their outer membrane, is paradoxical. The second observation was that, though several *E. coli* orthologues shared conservation of the CKPHDC loop structure, some homologues exhibited a noncanonical loop sequence (see Figure 1.4) (68). These Ivy homologues were referred to as paralogues and were found only within the *Pseudomonas* species with a CExxDxC loop sequence. Additionally, only *P. aeruginosa* was found to contain both the orthologue and paralogue versions of Ivy in its genome. However, functional analysis of the Ivyp homologues revealed that the Ivyp ortholog (Ivyp1) inhibited lysozyme, but the Ivyp paralogue (Ivyp2) did not (68). The researchers suggested that Ivyp1 acts as a second line of defense against lysozyme, a common component of the vertebrate immune system (68). On the other hand, Ivyp2 may inhibit other microbicidal agents of the immune system, such as PLUNC antibacterial proteins abundant in vertebrate genomes (68, 69). However, these speculations are insufficient in addressing the phylogenetic paradox and functional variations found in the Ivyp1 and Ivyp2 proteins.

The Clarke group at the University of Guelph addressed these inconsistencies by proposing that the primary function of the Ivy proteins is to inhibit LT activity, and that the inhibition of lysozyme is merely a "fortuitous coincidence" (70). In line with the Claverie group's observations, the Clarke group confirmed Ivy proteins distributed only within the Proteobacteria species (70) (Figure 1.5). The homologues of Ivy were divided into the Ivy1 proteins containing the consensus CKPHDC loop sequence and the Ivy2 proteins containing the consensus CEXXDXC motif (70). The researchers also noted a previous study on *O*-acetylation of PG, which revealed that, despite widespread occurrence of *O*-acetylation in both Gram-positive and Gram-negative cells, this modification was absent in *E. coli* and *P. aeruginosa* species (71). A BLAST search of the *E. coli* and *P. aeruginosa* genomes for genes encoding O-acetylating

enzymes (*oatA and poa* clusters) returned no hits (70). Analysis of isolated PG from both *E. coli* and *P. aeruginosa* indeed revealed that less than 1% of muramic acid in the PG was *O*-acetylated, whereas species that modify their PG have typically 30-60% of their PG *O*-acetylated (70). Finally, the researchers performed a turbidimetric assay by pre-incubating Ivyp with *M. luteus* cells and subsequently adding MltB. They showed that both Ivyp1 and Ivyp2 could inhibit MltB with equal potency (Figure 1.6).

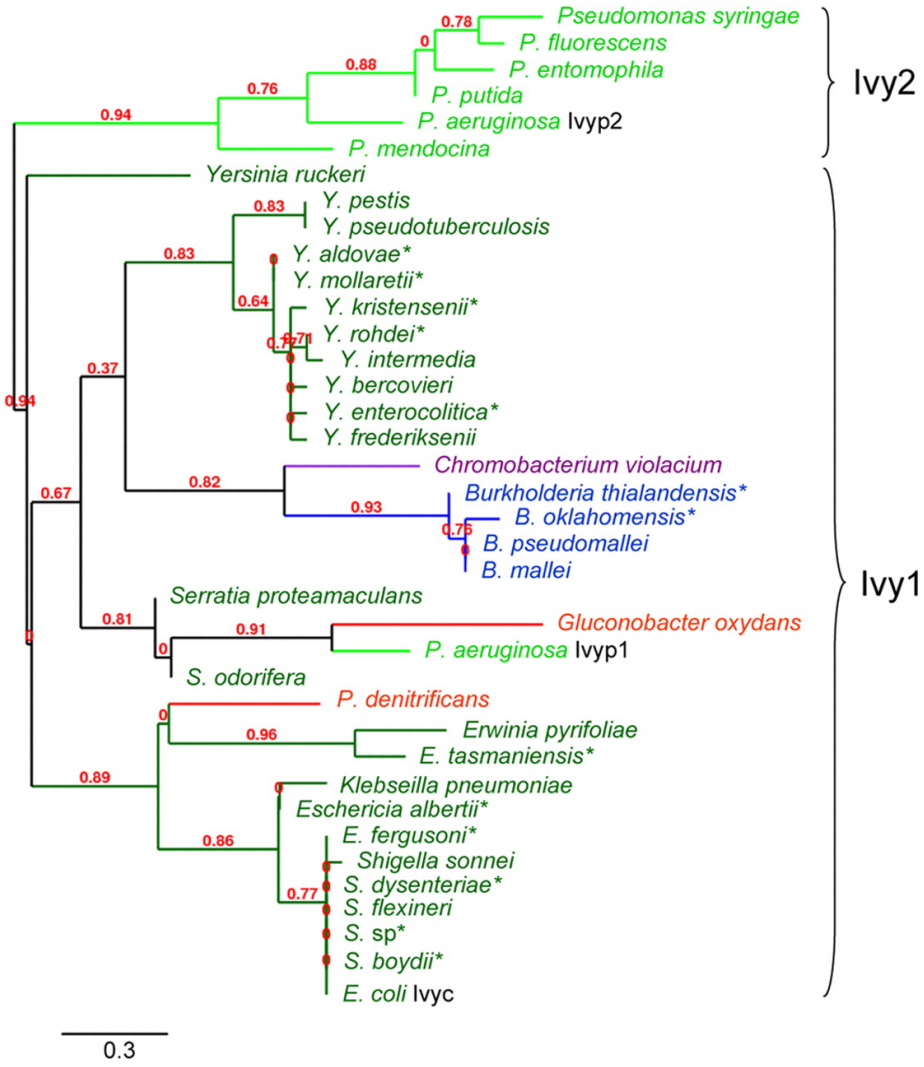

Figure 1.5. Phylogenetic Tree of the Ivy Family of Proteins – Each species has been coloured according to its proteobacterial classification: alpha (red), beta (Burkholderiaceae, blue; Neisseriaceae, purple), and gamma (Enterobacteriacaea, dark green; Pseudomonadaceae, light green). Members of the Ivy1 family are characterized by the CKPHDC consensus motif and members of the Ivy2 proteins are characterized by the CEXXDXC motif. This figure was taken from (70).

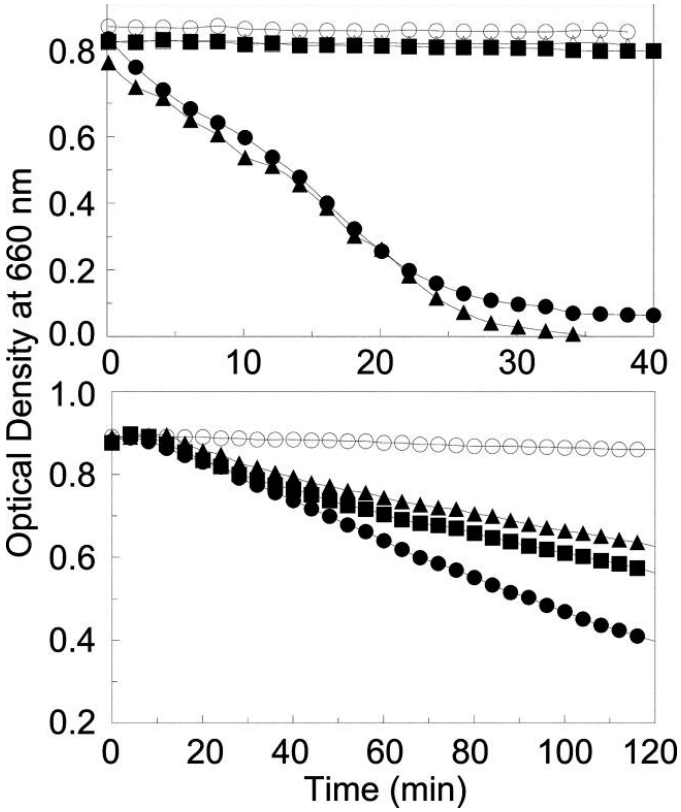

Figure 1.6. Turbidimetric assay of lysozyme and MltB inhibition by Ivyp1 and Ivyp2 – Measurement of M. luteus optical density over time. Open circles denote control samples (absence of enzymes). Top panel: lysozyme in the absence (black circles) and presence of 5.9μM Ivyp1 (black squares) and 3.9μM Ivyp2 (black triangles). Bottom panel: MltB in the absence (black circles) and presence of 8.7μM Ivyp1 (black squares) and 5.7μM (black triangles). This figure was taken from (70).

These results address the underlying paradox of the Ivy proteins in Gram-negative cells. *O*-Acetylation of PG offers a level of control for LT activity; however, these modifications are absent in *E. coli* and *P. aeruginosa*. Additionally, genes encoding the Ivy proteins have only been discovered in bacteria that do not *O*-acetylate their PG. Coupled with the observation that the Ivy proteins exhibited inhibition of MltB lytic activity, these findings suggest that the primary function of the Ivy proteins is to regulate LTs. Additionally, defense against lysozymes may be a coincidental secondary function that has arisen due to shared substrate specificity.

Since the discovery of Ivy, a second family of proteinaceous lysozyme inhibitors has been discovered by the Michiels group: periplasmic lysozyme inhibitor of c-type lysozyme (PliC) and

membrane-bound lysozyme inhibitor of c-type lysozyme (MliC) (72). The group performed experiments similar to their inhibition tests with Ivy and revealed that MliC from *E. coli* and *P. aeruginosa* can also inhibit lysozyme activity and that overexpression in *E. coli* cells made the cells more resistant to lysozyme (72). Indeed, experiments performed by Joseph Ciufo, a former MSc. student in the Clarke lab, showed that MliC could inhibit the activity of some LTs in *P. aeruginosa*, namely MltA, MltB, and MltF.

1.6 Rationale of Study, Thesis Objectives, and Hypothesis

Originally regarded as a lysozyme inhibitor, Ivy has now been dubbed a putative LT inhibitor based on the inhibition of *P. aeruginosa* MltB by both Ivyp1 and Ivyp2. However, these results are not conclusive, as evidence for LT inhibition was limited to only one of the eleven LTs in *P. aeruginosa*. On the other hand, this redundancy of LTs (5 families, and 3 subfamilies within family 1) may explain the presence of two homologues of Ivy found only in *P. aeruginosa*, in contrast to the single homologue found in other Proteobacteria. Experiments have not yet been conducted to determine whether the Ivy proteins target all LTs or if there are other undiscovered regulatory mechanisms that contribute to the overall control of LT activity. Keeping in mind that regulation of LTs via *O*-acetylation is absent in *P. aeruginosa* (and *E. coli*), further research must be done to solidify our understanding of the Ivy-LT relationship. This would be accomplished by confirming the inhibition of all LTs by Ivyp1 and Ivyp2. Furthermore, the claim that Ivy is an inhibitor of LTs would be solidified with confirmation of the molecular interactions at a structural level (X-ray crystallography).

The research presented herein seeks to test the hypothesis that the primary function of the Ivyp proteins (Ivyp1 and Ivyp2) of *P. aeruginosa* is to regulate the activity of LTs by a mode of inhibition at the substrate level.

2 Materials and Methods

2.1 Chemicals and Reagents

DNase I, RNase A, isopropyl β-D-1-thiogalactopyranoside (IPTG), and ethylenediaminetetraacetic acid (EDTA)-free protease inhibitor tablets were purchased from Roche Diagnostics (Laval, QC). For cloning, T4 DNA ligase, restriction enzymes (XhoI, EcoRI), and all other DNA-modifying enzymes were purchased from Promega (Fitchburg, WI). Ni^{2+} NTA resin and TALON cobalt resin used for LT purification were purchased from Qiagen (Valencia, CA) and Takara Bio USA Inc. (Mountain View, CA), respectively. Glutathione Sepharose 4B and Benzamidine Sepharose 6B, both used for Ivyp purification, were purchased from GE Healthcare (Chicago, IL). Acrylamide and glycerol were purchased from Fischer Scientific (Nepean, ON). All reagents for growth media, including Luria Broth (LB, 10 g/L tryptone peptone, 5 g/L yeast extract, 10 g/L sodium chloride) and SuperBroth (SB, 32 g/L tryptone peptone, 20 g/L yeast extract, 5 g/L sodium chloride), were purchased from Difco Laboratories (Detroit, MI). All other reagents and chemicals, including antibiotics, were purchased from Sigma-Aldrich (Oakville, ON).

2.2 Strains and Plasmids

The bacterial strains and plasmids used in this study are listed in Tables 2.1 and 2.2, respectively. All *E. coli* strains were maintained on LB broth or agar at 37 °C for short-term use and stored at -80 °C in 25 % glycerol for long-term use.

Table 2.1 List of bacterial strains and genotypes used in this study

Strain	Genotype	Source/Reference
***E. coli* DH5α**	F$^-$ *Φ80lacZΔM15* Δ(*lac*ZYA-*arg*F) U169 *rec*A1 *end*A1 *hsd*R17(r_K^-, m_K^+) *pho*A *sup*E44 *thi*-1 *gyr*A96 *rel*A1 λ$^-$	Invitrogen
***E. coli* BL21 (DE3)**	F-*omp*T *hsd*S_B (r_B-, m_B-) *gal dcm* (DE3)	Novagen
***E. coli* BL21 (DE3) pLysS**	F-*omp*T *hsd*S_B (r_B-, m_B-) *gal dcm* (DE3) pLysS (Cam^R)	Qiagen/Novagen
***E. coli* BL21 Star (DE3)**	F-*omp*T *hsd*S_B (r_B-, m_B-) *galdcmrne*131 (DE3)	Novagen
E. coli Shuffle T7	F′ *lac*, *pro*, *lacI*^{q} / *Δ(ara-leu)7697 araD139 fhuA2 lacZ::T7 gene1 Δ(phoA)PvuII phoR ahpC* galE (or U) galK λatt*::pNEB3-r1-*cDsbC* ($Spec^R$, *lacI*^{q}) *ΔtrxB rpsL150*(Str^R) *Δgor Δ(malF)3*	New England Biolabs Inc.
***M. luteus* ATCC 4698**	Type Strain, freeze-dried	Sigma-Aldrich

Table 2.2 List of plasmids and derivatives used in this study

Plasmid	Characteristics	Source
pNBAC54-1	pET-30a derivative with recombinant *P. aeruginosa mltB* encoding $sMltB_{\Delta 2\text{-}17}$, C-terminal His-6-tag; Kan^R	N. Blackburn
pNBAC258-2	pET-28a(+) derivative with recombinant *P. aeruginosa sltB1* encoding SltB1, C-terminal His-6-tag; Kan^R	N. Blackburn
pACCV-4	pET-28a(+) derivative with recombinant *P. aeruginosa mltA* encoding $sMltA_{\Delta 2\text{-}25}$, C-terminal His-6-tag; Kan^R	C. Vandenende
pACCV-21	pET-28a(+) derivative with recombinant *P. aeruginosa mltF* encoding sMltF, N-terminal His-6-tag; Kan^R	C. Vandenende
pACCV-23	pET-28a(+) derivative with recombinant *P. aeruginosa slt70* encoding Slt70, N-terminal His-11-tag; Kan^R	C. Vandenende
pACCV-28	pET-28a(+) derivative with recombinant *P. aeruginosa sltB3* encoding SltB3, N-terminal His-6-tag; Kan^R	C. Vandenende
pACCV-29	pET-28a(+) derivative with recombinant *P. aeruginosa sltB2* encoding SltB2, N-terminal His-6-tag; Kan^R	C. Vandenende
pACCV-31	pET-28a(+) derivative with recombinant *P. aeruginosa mltF2* encoding $sMltF2_{\Delta 2\text{-}21}$, N-terminal His-6-tag; Kan^R	C. Vandenende
pACCV-32	pET-28a(+) derivative with recombinant *P. aeruginosa mltD* encoding $sMltD_{\Delta 2\text{-}34}$, N-terminal His-6-tag; Kan^R	C. Vandenende
pACCV-33	pET-28a(+) derivative with recombinant *P. aeruginosa rlpA* encoding $sRlpA_{\Delta 2\text{-}29}$, N-terminal His-6-tag; Kan^R	C. Vandenende
pACCV-37	pBAD SUMO derivative with recombinant *P. aeruginosa mltG* encoding $sMltG_{\Delta 2\text{-}24}$, N-terminal SUMO-tag; Amp^R	C. Vandenende
pACCC-1-FN	pET-28a(+) derivative with recombinant *P. aeruginosa ivyp1* encoding Ivyp1, N-terminal His-6-tag; Kan^R	C. Clarke

pACCC-3-FN	pET-28a(+) derivative with recombinant *P. aeruginosa ivyp2* encoding Ivyp2, N-terminal His-6-tag; Kan^R	C. Clarke
pGEX-4T-1	Arabinose inducible, Tac expression, N-terminal GST-tag, thrombin cleavage site, Amp^R	GE Healthcare Life Sciences
pACJC-1	pGEX-4T-1 derivative with recombinant *P. aeruginosa ivyp1* encoding $Ivyp1_{\Delta 1\text{-}24}$, N-terminal GST-tag; Amp^R	This study
pACJC-2	pGEX-4T-1 derivative with recombinant *P. aeruginosa ivyp2* encoding $Ivyp2_{\Delta 1\text{-}23}$, N-terminal GST-tag; Amp^R	This study

2.3 DNA Techniques

2.3.1 Preparation of Competent Cells

An overnight culture of *E. coli* DH5α, *E. coli* BL21 Star (DE3) or *E. coli* BL21 (DE3) pLysS was each sub-cultured 1/20 into fresh 10mL LB media and incubated for 1.5-2 h. Cultures were chilled on ice, centrifuged (4696 × *g*, 10 min, 4 °C), and resuspended in 10mL Solution α (see Appendix A). Cells were again collected by centrifugation (4696 × *g*, 20 min, 4 °C) and resuspended in 1 mL Solution β (see Appendix A). Cells were then chilled on ice for 2-3 h before being aliquoted into 50μL volumes, flash-frozen in dry-ice/ethanol, and stored at -80 °C for long-term storage.

2.3.2 Engineering of *ivyp1* & *ivyp2*

pACCC-1-FN and pACCC-3-FN were used as plasmid DNA templates for PCR amplification of the *ivyp1* and *ivyp2* gene fragments from *P. aeruginosa*. All oligonucleotide primers used in this study are listed in Table 2.3 and were acquired from Integrated DNA Technologies (Coralville, IA). Both *ivyp1* and *ivyp2* were amplified by PCR using primers that contained *EcoRI* and *XhoI* restriction enzyme sites to facilitate the incorporation of a GST-tag from pGEX-4T-1 at the N-terminus of the protein product along with a linker containing a thrombin cleavage site. PCR amplifications were performed according to the master mix and protocol outlined in the KAPA Hifi HotStart PCR Kit and achieved in 50 μL volumes using a

Bio-Rad MyCycler Thermal Cycler system. PCR was set up with a gradient of 12 different annealing temperatures (55 ± 10 °C) and all products were separated in a 1% (w/v) agarose gel in TAE buffer (see Appendix A) via electrophoresis along with 1kb DNA ladder (NEB). DNA was visualized by staining with Sybr Safe DNA gel stain (Invitrogen Life Technologies, Burlington, ON) and exposure to UV light. DNA corresponding to *ivyp1* and *ivyp2* gene fragments was excised and purified using the Thermo Scientific GeneJET Gel Extraction Kit. DNA concentrations were measured using a Beckman DU Series 350 UV/Vis spectrophotometer (Beckman Coulter Inc., Mississauga, ON) and sequenced by the Genomic Facility of the Advanced Analysis Center, University of Guelph.

Amplified and purified fragments were digested with *EcoRI* and *XhoI*, ligated with pGEX-4T-1 plasmid properly digested by the same restriction enzymes, and transformed into *E. coli DH5α* (see 2.3.3). Individual constructs/colonies were isolated from transformants, screened for correct size-insert by colony PCR, and sequenced to confirm sequence identity. The final products were pACJC-1 and pACJC-2, pGEX-4T-1 plasmids containing Ivyp1$_{\Delta 1\text{-}24}$ and Ivyp2$_{\Delta 1\text{-}23}$ respectively with an N-terminal GST-tag and thrombin cleavage site linker. It should be noted that attempts at cloning, though successful for pACJC-1, were unsuccessful for pACJC-2 and thus pACJC-2 had to be prepared by GenScript.

Table 2.3 Oligonucleotide primers used in this study

Primer Name	Oligonucleotide Sequence (5'-3')	Target/Final Vector	Description
Ivyp1$_{Fwd}$	TTACAAGAATTCGAGGAGCAGC	pGEX-4T-1/pACJC-1	Forward primer for Ivyp1$_{\Delta 1\text{-}24}$
Ivyp1$_{Rev}$	ATTAGTCTCGAGTCACTTCCAG	pGEX-4T-1/pACJC-1	Reverse primer for Ivyp1$_{\Delta 1\text{-}24}$
Ivyp2$_{Fwd}$	TTACAAGAATTCGCCGACAGGG	pGEX-4T-1/pACJC-2	Forward primer for Ivyp2$_{\Delta 1\text{-}23}$
Ivyp2$_{Rev}$	ATTAGTCTCGAGTCAGTACCAG	pGEX-4T-1/pACJC-2	Reverse primer for Ivyp2$_{\Delta 1\text{-}23}$

2.3.3 Transformation of *E. coli*

Chemically competent *E. coli* cells were thawed on ice and incubated with 2µL plasmid DNA on ice for 30 min. Sample was heat-shocked at 42°C for 30 sec followed by a 5min incubation on ice. LB was then added to a 1mL total volume and cells were allowed to grow at 37 °C for 60 min with shaking at 250 rpm. The dilution was spread plated (0.1 mL) on LB agar supplemented with appropriate antibiotics and incubated overnight at 37 °C. An overnight culture was prepared the next day by inoculating an isolated colony in 5 mL LB with appropriate antibiotics and incubated at 37 °C at 250 rpm shaking for overnight growth. Glycerol stocks were prepared by combining a 1:1 ratio of overnight culture and sterile 50 % (v/v) glycerol, followed by immediate storage in -80 °C.

2.4 Small Scale Expression of Ivyp1 & Ivyp2 (Boil Prep)

Overnight cultures were prepared from glycerol stocks of *E. coli* BL21 Star (DE3) cells containing pACJC-1 and pACJC-2 plasmids with 5 mL LB containing ampicillin and grown overnight at 37 °C with 250 rpm shaking. Cultures were then diluted 1:100 into 10 mL LB, grown at 37 °C until early-exponential phase (OD_{600} ~0.6) and gene expression was induced with either 1 mM or 0.1 mM IPTG. Proteins were then over-expressed at 37 °C for 2 h or 4 h, or at 15 °C for 4 h or overnight. An uninduced culture was also incubated at 37 °C and grown overnight. Cells were collected by centrifugation (1 mL, 21000 × *g*, 5 min), resuspended in 20 µL ddH_2O, heated at 100°C for 5 min, and loaded onto an SDS-PAGE with 5× sample buffer for analysis (140 V, 80 min).

2.5 Large Scale Protein Production

Proteins were overexpressed and purified according to Sections 2.5.1 and 2.7 except for Slt70 and MltD which were prepared by Stephanie Gilbert, and MltG which was prepared by Chris Vandenende, lab technicians in the Clarke lab.

2.5.1 Over-expression of Lytic Transglycosylases

Overnight starter cultures of 50 mL LB with appropriate antibiotics were prepared from glycerol stocks of the following: *E. coli* BL21 Star (DE3) containing pACCV-23 (*slt70*), pACCV-4 (*mltA*), pNBAC54-1 (*mltB*), pNBAC258-2 (*sltB1*), pACCV-29 (*sltB2*), pACCV-28 (*sltB3*), pACCV-32 (*mltD*), pACCV-31 (*mltF2*), pACCV-37 (*mltG*), and pACCV-33 (*rlpA*) and *E. coli* T7 Shuffle containing pACCV-21 (*mltF*). One litre of LB containing appropriate antibiotic was inoculated with 15 mL overnight culture and grown at 37 °C until early exponential phase (OD_{600} ~0.6), with the exception of cells containing pACCV-3 (*mltA*) and pNBAC54-1 (*mltB*) which were grown in SB. Expression was induced with 0.1 mM IPTG and allowed to over-express for 4 h at 37 °C. Cells were collected by centrifugation (JA-10, 11300 × *g*, 15 min, 4 °C) and the pellet was resuspended in 20 mL of lysis buffer. There were two main modes of purification utilizing different buffer components. The first utilized Na_2HPO_4 buffer and was used for the purification of Slt70, MltB, SltB1, SltB2, SltB3, and MltF. The lysis buffer for these LTs was composed of 50 mM Na_2HPO_4 pH 8.0, containing 300 mM NaCl, 10 % glycerol, 0.1 % Triton X-100. The second buffer system used Tris-HCl and was used for the purification of MltA, MltD, MltF2, MltG, and RlpA. The lysis buffer for these LTs was composed of 50 mM Tris-HCl pH 8.0, containing 300 mM NaCl, 10 % glycerol, 0.05 % Brij-35, 5 mM EDTA, and 10 mM imidazole.

2.5.2 Over-expression of Ivyp1 and Ivyp2

An overnight culture of 50 mL LB supplemented with 100 µg/mL ampicillin was prepared from a glycerol stock of *E. coli* BL21 Star (DE3) containing either the pACJC-1 or pACJC-2 plasmid of interest and grown at 37 °C overnight. One litre of SuperBroth containing 100 µg/mL ampicillin was inoculated with 15 mL overnight culture and grown at 37 °C until early exponential phase (OD_{600} ~0.6). Proteins expression was induced with 0.1 mM IPTG and allowed to over-express for 4 h at 37 °C. Cells were collected by centrifugation (JA-10, 11300 × *g*, 15min, 4 °C) and the pellet was resuspended in 20 mL of 1× PBS pH 7.4, 10 % glycerol.

2.6 Cell Lysis

Upon thawing, EDTA-free protease inhibitor cocktail tablets were added to the cell suspension and allowed to incubate for 5 min. Cells were lysed by sonication (3 pulses, 2.5 min, 10 s ON 10 s OFF, 50 % amplitude, 5 min rest between pulses). Using a Sonic Vibra Cell high intensity ultrasonic processor fitted with a microprobe. The cell lysate was clarified by centrifugation (JA-25.5, 27200 × *g*, 20 min, 4 °C) using an Avanti J-30I high performance centrifuge and the supernatant was collected for protein purification.

2.7 Protein Purification

2.7.1 Purification of *P. aeruginosa* MltA, MltD, MltF2, MltG, RlpA

Cell-free lysate was incubated with 1 mL cOmplete His-Tag Purification Resin in a 30 mL gravity column under nutation for 1 h at 4 °C. The flow-through fraction was collected and the resin was washed with 30 mL (1 column volume) lysis buffer (50 mM Tris-HCl pH 8.0, 300 mM NaCl, 10 % glycerol, 0.05 % Brij-35, 5 mM EDTA, 10 mM imidazole). This was followed by a second (lysis buffer, 50 mM imidazole) and third (lysis buffer, 100 mM imidazole) wash with 30 mL each. Purified proteins were eluted in approximately 15 mL of elution buffer (lysis

buffer, 250 mM imidazole) followed by washes with higher imidazole concentrations (500 mM, 750 mM, 1 M) to ensure complete elution.

2.7.2 Purification of *P. aeruginosa* Slt70, MltB, SltB1, SltB2, SltB3, MltF

Cell-free lysate was incubated with 1 mL of HisPur Cobalt Resin in a 30 mL gravity column under nutation for 1 h at 4 °C. Flow-through fraction was collected and the resin was washed with 60 mL (2 × 30 mL column volume) lysis buffer (50 mM NaH_2PO_4 pH 8.0, 300 mM NaCl, 10 % glycerol, 0.1 % Triton X-100) and then subsequently washed with 60 mL of wash buffer. In certain cases, a third wash of 60 mL was performed. Purified proteins were eluted in approximately 15 mL of elution buffer.

Table 2.4 pH of purification buffers for LT's using NaH_2PO_4 Buffer

LT	pH			
	Lysis	**First Wash**	**Second Wash**	**Elution**
Slt70	8.0	7.0	6.0	5.0
MltB	8.0	7.5	6.5	5.5
SltB1	8.0	7.5	6.5	5.5
SltB2	8.0	7.0	-	5.0 / 4.5
SltB3	8.0	7.0	-	5.0 / 4.5
MltF	8.0	7.0	-	5.0 / 4.5

2.7.3 Purification of *P. aeruginosa* Ivyp1 and Ivyp2

Cell-free lysate was incubated with 5 mL Glutathione Sepharose 4B GST-tagged protein purification resin from GE Healthcare Life Sciences (Mississauga, ON) in a 30 mL gravity column under nutation for 1 h at 4 °C. Flow-through fraction was collected and the resin was washed with 150 mL (5 column volumes) 1× PBS pH 7.4, 10 % glycerol. Bound Ivyp-GST was

eluted with 15 mL (3 × 5 mL) 50 mM Tris-HCl pH 8.5, 10 mM glutathione. Tagged Ivyp-GST was cleaved by adding thrombin (1-3 U/mg protein) and incubating at room temperature for 16+ hours. Note that due to the large amount of protein obtained, the amount of thrombin used for cleavage was reduced (from the recommended 10 U/mg) in order to preserve thrombin.

For thrombin removal, 3 mL GE Healthcare Benzamidine Sepharose 4 Fast Flow resin (FisherScientific) was equilibrated with binding buffer (50 mM Tris-HCl pH 8.0, 0.5 M NaCl). The thrombin digest mixture was passed through the resin 5 times before washing the column with 6 mL (2 × 3 mL bed volume) binding buffer to elute protein residing in resin dead volume.

For GST-tag removal, the sample was incubated with 5 mL Glutathione Sepharose purification resin (equilibrated with 1× PBS pH 7.4, 10 % glycerol) under nutation for 1 h at 4 °C. Flow-through fraction was collected and the column was washed with 10 mL (2 × 5 mL bed volume) 1× PBS pH 7.4, 10 % glycerol. Depending on the extent of GST-tag removal (as determined by SDS-PAGE), this process was repeated once more. Note that achieving 100% removal of GST-tag was impossible and thus gel filtration (size exclusion) chromatography must be employed.

2.7.4 Gel Filtration of *P. aeruginosa* Ivyp1 and Ivyp2

To prepare for gel filtration, Ivyp sample was concentrated according to methods outlined in Section 2.9 to a volume <500 µL. HiLoad 16/600 Superdex 200pg was equilibrated with 240 mL 1× PBS pH 7.4, 10 % glycerol using the NGC Quest 10 Chromatography System from Bio-Rad. The ~500 µL sample was loaded onto the column and 1× PBS pH 7.4, 10% glycerol buffer was applied isocratically for 150 mL at a flow rate of 1 mL/min. Under these conditions, Ivyp started eluting at ~90 mL, creating a well-defined peak that was pure when analyzed on an SDS-PAGE

gel. All peaks were collected in 1 mL aliquots. Samples were again concentrated according to the methods outlined in Section 2.9.

2.8 Buffer Exchange

Elution fractions from LT purification were dialyzed using Fisherbrand Regenerated Cellulose Dialysis Tubing (10 kDa MWCO) against 2 L of 10 mM sodium acetate buffer, pH 5.0, containing 10 mM $MgCl_2$, 10 % (v/v) glycerol in 4°C for 2 h, followed by another dialysis against 2 L of the same buffer in 4 °C for 16 h. Prior to determination of pH activity profiles, the LTs were dialyzed into 10 mM sodium acetate, pH 5.0, containing 10 mM $MgCl_2$, 10 % glycerol only for the first purification. After the optimal pH was determined, the LTs were dialyzed against 10mM sodium acetate, 10 mM $MgCl_2$, 10 % glycerol at the optimal pH for that LT in subsequent purifications.

2.9 Concentration of Protein Samples

Ultrafiltration with 10 kDa MWCO Amicon Ultra-15 Centrifugal Filter units (EMD Millipore Corp., Billerica, MA) was used for protein concentration in the case of LTs; 3 kDa MWCO filter units were used for Ivyp1 and Ivyp2 concentration. Protein concentration was performed by centrifugation of filtration units containing protein samples at pulses of (4696 × *g*, 10 min, 4 °C) until final volume of 1 mL was reached for LTs and <0.5 mL for Ivyps. Effectively, the Ivyps were concentrated to >400 μM for an optimal setup of the enzyme activity assays.

2.10 Protein Analysis

2.10.1 Sodium Dodecyl Sulfate Polyacrylamide Gel Electrophoresis (SDS-PAGE)

For analysis of protein samples in each purification step, 12 % separating and 4 % stacking gels were used (see Appendix A). Protein samples were mixed with 5× sample buffer (see Appendix A) before being loaded into the gel (5 µL) alongside BLUeye Prestained Protein ladder from FroggaBio Scientific Solutions (Toronto, ON). Gels were run at 140 V for 80 min, after which they were washed with ddH_20, microwaved in Coomassie stain (see Appendix A) and incubated with shaking for 30 min, washed with ddH_2O, microwaved in destain (see Appendix A) and incubated with shaking 60 min, and finally washed again with ddH_20. The gels were scanned for imaging immediately using Gel Doc XR+ Gel Documentation System from Bio-Rad (Mississauga, ON, Canada).

2.10.2 Protein Quantification

Protein concentration was determined using the Pierce BCA Protein Assay Kit (Thermo Scientific). Protein samples were added to a 50:1 mixture of BCA:$CuSO_4$ at a 1:8 ratio. The same was done for dilutions of bovine serum album (BSA) ranging from 0-1.0 mg/mL to create a protein standard curve. The samples were then incubated at 37 °C for 30 min before the absorbance was read immediately at 595 nm wavelength using the BioTek Synergy H1 microplate reader.

2.10.3 Protein Identification by Mass Spectrometry

For mass spectrometry analysis, 2 mg Ivyp1 and Ivyp2 was dissolved in 6 M guanidine HCl, 50 mM Tris-HCl pH 8.0, 4 mM DTT to a total volume of 100 µL. The sample was heated at 95 °C for 20 min before allowing it to cool and adding 600 µL 50 mM NH_4HCO_3 pH 7.8. Promega Sequencing Grade Modified trypsin (Fisher Scientific) was added to a final

protease:protein ratio of 1:50 and incubated at 37 °C for 1 h. Trypsin activity was inactivated by adding TCA to a final concentration of 10 %. The sample was then analyzed using the Agilent LC-UHD Q-Tof at the Mass Spectrometry Facility in the Advanced Analysis Centre, University of Guelph.

2.11 Enzyme Activity Assays

2.11.1 Measurement of Lytic Activity (Turbidity Assay)

The turbidity assay developed by Hash (1967) was used to monitor changes in OD_{600} of solubilized PG from *Micrococcus luteus* cells in the presence of HEWL, LTs and/or Ivyps. Lyophilized *M. luteus* cells were resuspended in the activity buffer (10 mM NaOAc, 10 mM $MgCl_2$) to a working concentration of 0.8 mg/mL. The optimal pH for each LT was determined by completing pH-activity studies. In order to make the PG accessible to the LTs, whole cells were lysed via sonication (2.5 min, 10 s ON 10 s OFF, 50 % amplitude). A master mix of each triplicate was prepared in 1.5 mL microfuge tubes containing 2× concentration of the LTs of interest in the activity buffer of appropriate pH before being divided into three 100 µL aliquots in a 96-well plate. Sonicated *M. luteus* cells were added to each well at a 1:1 volume ratio using a multichannel pipette and the mixture was pipetted up and down 8-10 times to ensure complete homogeneity. Special care was taken to perform this step as quickly as possible so as not to miss the initial rate, V_0, of the reaction, but as carefully as possible to avoid the formation of bubbles which can interfere with the OD_{600} reading. The decrease in turbidity at OD_{600} was measured immediately afterwards with a Biotek Synergy H1 plate reader. Two hundred µL volumes were used for each reaction in a 96-well plate and the measurements were performed at ambient temperature.

2.11.2 Inhibition of Lytic Activity

To test how the potential interaction between the Ivyps and LTs could affect the lytic activity of the LTs, the turbidity assay was performed as described in 2.12.1. Master mixes of each triplicate were prepared off ice in 1.5 mL microfuge tubes containing both the LT of interest and either Ivyp1 or Ivyp2 in the activity buffer of appropriate pH and then preincubated for 10 min before being aliquoted into 96-well plates and adding *M. luteus* cells. The interaction between LTs and Ivyps was tested at 1:5, 1:10, and 1:20 ratios.

2.11.3 pH Profiles of Lytic Transglycosylases

To determine pH optima of LT activities, a similar approach was taken in measuring the change in turbidity of *M. luteus* cells over time at OD_{600}. Lyophilized *M. luteus* cells were resuspended in ddH_2O to a final concentration of 0.4 mg/mL and lysed via sonication (2.5 min, 10 s ON 10 s OFF, 50 % amplitude). The pH test buffer (100 mM Tris, 50 mM MES, 50 mM acetic acid) was prepared with pH's ranging from 4.0-8.0 (0.5 intervals, 9 total). LTs were diluted in the pH test buffer at each pH and *M. luteus cells* were added to initiate the enzymatic reaction. The decrease in OD_{600} was measured immediately afterwards. Each experiment was conducted in triplicates.

2.12 Ordinary One-Way ANOVA Statistical Analysis

Ordinary one-way ANOVA was performed using GraphPad Prism v8.0. Using this method, the p-value was determined by comparing the means of each LT:Ivyp ratio (n=3) to one another.

3 Results

The goal of the research conducted for this thesis was to test the hypothesis that Ivyp1 and Ivyp2 function as inhibitors of LTs in *P. aeruginosa* by performing a series of turbidity-based inhibition assays. Though prior work had been completed for some of the LTs, it was deemed necessary to start from the beginning by first determining the pH dependency of each LTs before profiling their inhibition by Ivyp1 and Ivyp2.

3.1 Production and Purification of Ivyp1-GST and Ivyp2-GST

The cloning of *ivyp1* into a pGEX-4T1 vector and transformation of the vector into a BL21 Star (DE3) expression strain was performed without any trouble according to the methods laid out in Section 2.3. However, there was some difficulty in the cloning process for production of recombinant Ivyp2. Therefore, in the interest of time available for the project, *ivyp2* engineered into the pGEX-4T1 was ordered in from GenScript and subsequently transformed into a BL21 Star (DE3) expression strain.

Overproduction of Ivyp1 and Ivyp2 was followed by subsequent purification by affinity chromatography using glutathione-Sepharose resin. SDS-PAGE analysis showed that proteins were purified to apparent homogeneity (Fig. 3.1). A rough concentration determination by absorbance spectrophotometry at 280nm revealed ~60mg each of Ivyp1-GST and Ivyp2-GST purified at this point. Overnight digestion with 200U thrombin led to incomplete digestion of Ivyp1-GST (Fig. 3.1). Further investigation revealed that though thrombin is catalytic in the pH range 5-10, it has an optimal pH of 8.3. Initially upon purification, elution fractions were dialyzed from the 50 mM Tris-HCl pH 8.5, 10 mM glutathione elution buffer into a 1× PBS, pH 7.4, 10 % glycerol dialysis buffer. Removal of this step led to more efficient cleavage of the GST tag (Fig. 3.1).

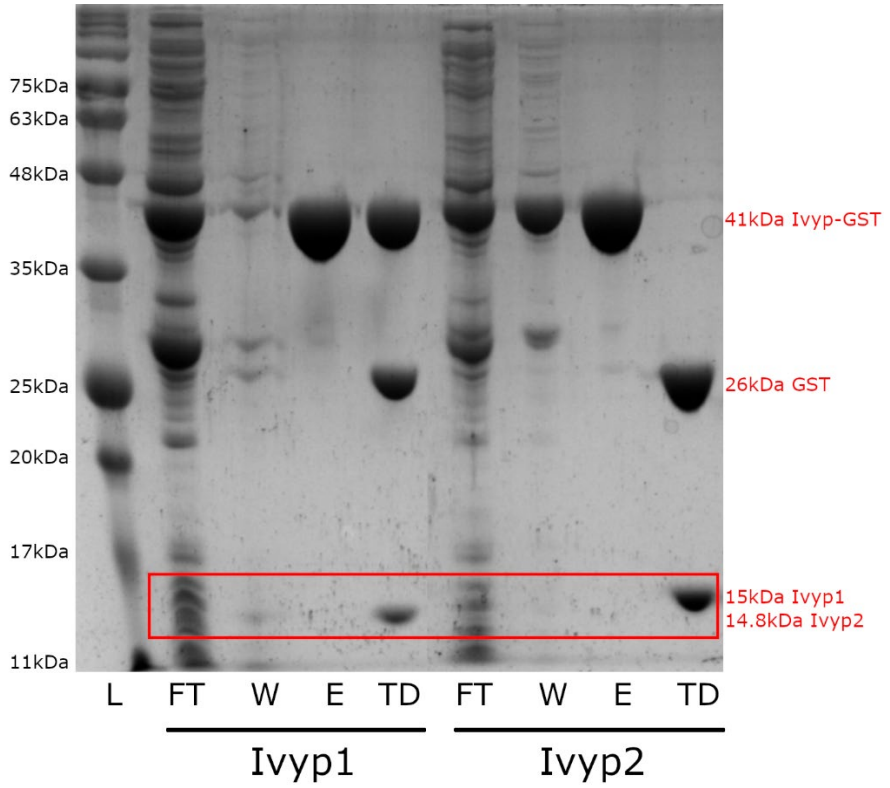

Figure 3.1 SDS-PAGE Analysis of Ivyp1-GST and Ivyp2-GST Purification by Immobilized Glutathione Sepharose Chromatography – Purification samples were run alongside (L) BLUelf Prestained Protein Ladder. Fractions collected for Ivyp1 (left) and Ivyp2 (right) are as follows: FT (flowthrough), W (wash), E (elution), and TD (thrombin digest).

Attempts were made to remove the free GST-tag, again by affinity chromatography by immobilized glutathione-Sepharose. The initial attempt to bind GST-tagged Ivyp1 and free-GST proved effective as the corresponding band sizes decreased in the first elution compared to the thrombin digest sample, whereas the band size for Ivyp1 remained largely unchanged (Fig. 3.2). A wash to elute all bound GST revealed that a first pass through the column was successful in binding half of the GST in the sample (Fig. 3.2). However, a second (Fig. 3.2) and subsequent passes (data not shown) of samples through the column revealed minimal success in effectively isolating a pure sample of Ivyp1. An additional purification step was required, and size exclusion chromatography was employed to separate Ivyp1 (14.8kDa) and Ivyp2 (15kDa) from free-GST (26kDa) and Ivyp1-GST/Ivyp2-GST (~41kDa). Depending on the use of affinity

chromatography to remove GST, either one or two cycles of size exclusion chromatography was necessary. In the case of Ivyp1, one cycle of size exclusion chromatography was enough to separate the sample (Fig. 3.3). Pure Ivyp1 fractions (fractions 10-17, Fig. 3.3) were pooled and concentrated.

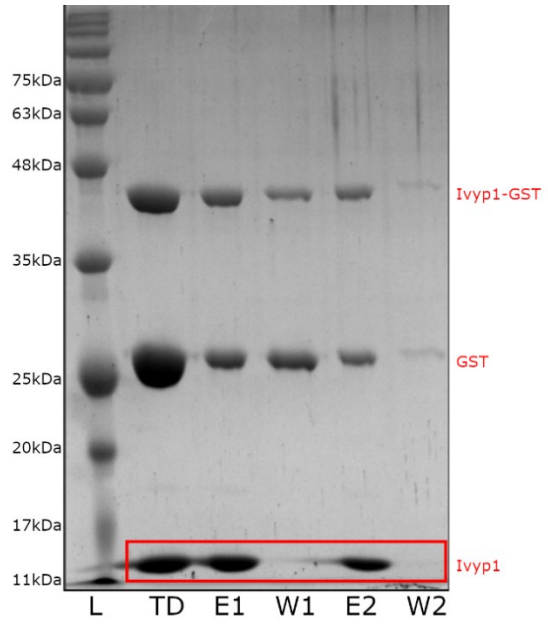

Figure 3.2. SDS-PAGE Analysis of GST Purification by Immobilized Glutathione Sepharose Chromatography – Purification samples for Ivyp1 were run alongside (L) BLUelf Prestained Protein Ladder. Fractions were collected for TD (thrombin digest), E1 (elution after first pass), W1 (column wash after first pass), E2 (elution after second pass), and W2 (column wash after second pass).

In contrast, affinity chromatography by glutathione-Sepharose was not conducted in the case of Ivyp2, resulting in an inefficient separation of products after performing size exclusion chromatography for the first time (Fig. 3.4). All samples containing Ivyp2 were collected and a second round of size exclusion chromatography was performed. This resulted in a much better separation of products (Fig. 3.5), whereupon fractions 21-35 were collected and concentrated for testing. It should be noted that in a separate purification batch, a subsequent purification by affinity chromatography using glutathione-Sepharose resin following thrombin digest resulted in

only one cycle of gel filtration being necessary (data not shown). The purifications of both Ivyp1 and Ivyp2 routinely resulted in a final yield of 10-15 mg of protein per litre cell culture.

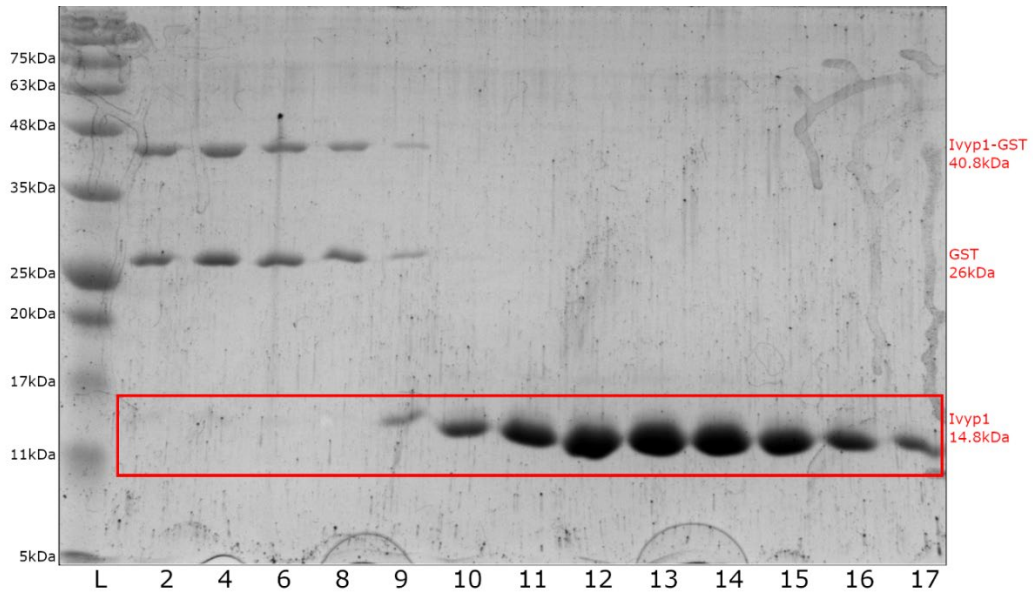

Figure 3.2 SDS-PAGE Analysis of Ivyp1 Gel Filtration – Purification samples were run alongside (L) BLUelf Prestained Protein Ladder. Fractions corresponding to the start, climax, and end of each peak from the chromatograph were selected (2, 4, 6, 8-17) and are represented here.

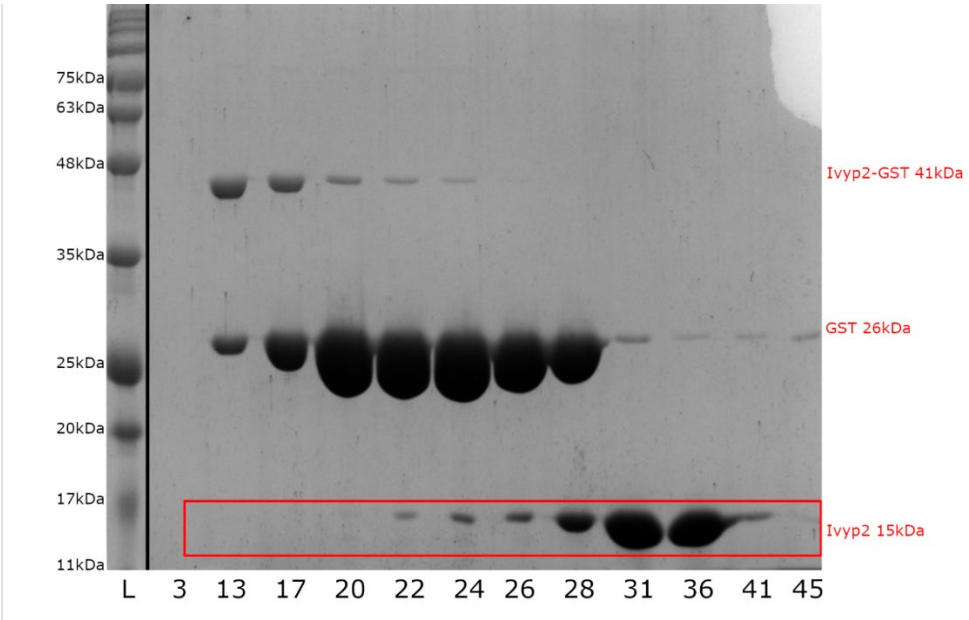

Figure 3.3 SDS-PAGE Analysis of Ivyp2 Gel Filtration 1 – Purification samples were run alongside (L) BLUelf Prestained Protein Ladder. Fractions corresponding to the start, climax, and end of each peak from the chromatograph were selected (3, 13, 17, 20, 22, 24, 26, 28, 31, 36, 41, 15) and are represented here.

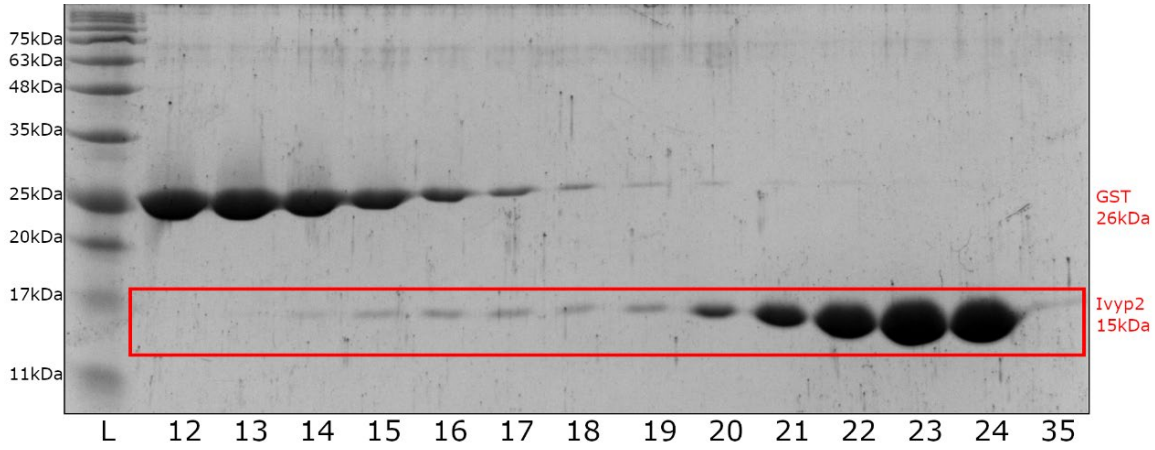

Figure 3.4 SDS-PAGE Analysis of Ivyp2 Gel Filtration 2 – Purification samples were run alongside (L) BLUelf Prestained Protein Ladder. Fractions corresponding to the start, climax, and end of each peak from the chromatograph were selected (12-24, 35) and are represented here.

3.2 Production and Purification of Recombinant sMltA

The *P. aeruginosa* PAO1 *mltA* gene was previously engineered into a pET28a(+) plasmid to produce recombinant MltA without its putative lipidation site (Δ1-37) and with an N-terminal 6His-tag (C. Vandenende, unpublished). This construct was labelled sMltA for "soluble MltA". Overexpression of engineered *mltA* in an *E. coli* BL21 Star (DE3) expression strain was followed by purification by affinity chromatography using TALON cobalt resin. No further purification steps were necessary as sMltA was purified to apparent homogeneity with yields of 0.5-0.7mg per litre cell culture and apparent mass of 43.2kDa (Fig. 3.6). After purification, sMltA was dialyzed against 2 × 2 L of 10 mM NaOAc, pH 4.5, containing 10 mM $MgCl_2$ and 10 % glycerol. Being relatively unstable, even when stored at 4 °C, sMltA was used immediately upon purification; activity has not been tested following storage at -80 °C.

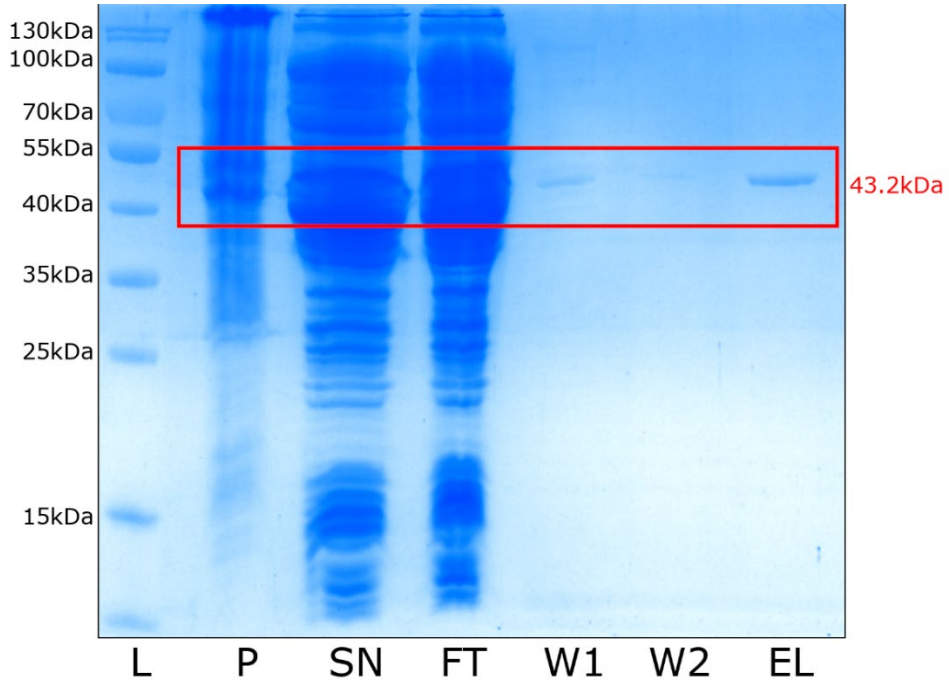

Figure 3.5 SDS-PAGE Analysis of sMltA Purification by Immobilized Metal Affinity Chromatography – Purification samples were run alongside (L) PageRuler Prestained Protein Ladder. Fractions were collected as follows: P (pellet), SN (supernatant), FT (flowthrough), W1 (wash 1), W2 (wash 2) and EL (elution).

3.3 Production and Purification of Recombinant sMltB

The *P. aeruginosa* PAO1 *mltB* gene was previously engineered into a pET30a(+) plasmid to produce recombinant MltA without its putative lipidation site (Δ2-17) and with a C-terminal hexa-His-tag (73). This construct was labelled sMltB for "soluble MltB". Overexpression of engineered *mltB* in an *E. coli* BL21 Star (DE3) expression strain was followed by affinity chromatography using TALON cobalt resin. No further purification steps were necessary as sMltB was purified to apparent homogeneity with yields of 1.0-1.3 mg per litre cell culture and apparent mass of 40.3 kDa (Fig. 3.7). After purification, sMltB was dialyzed against 2 × 2 L of 25 mM NaH_2PO_4, pH 5.8, containing 100 mM $NaCl_2$ and 0.1 % Triton X-100. sMltB was found to be active immediately after purification, as well as after storing in -80 °C.

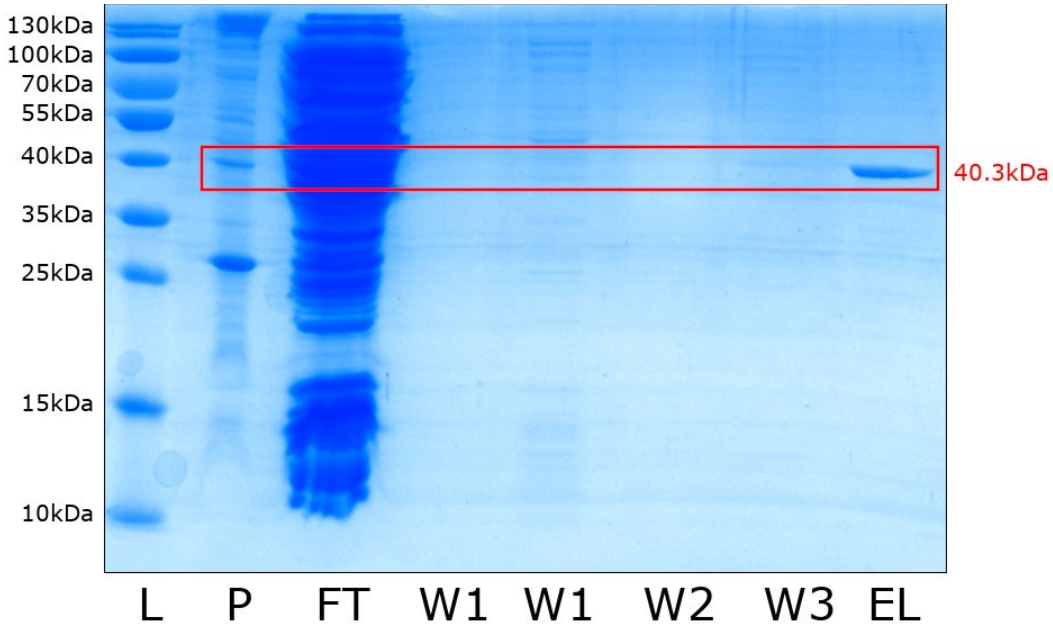

Figure 3.6 SDS-PAGE Analysis of sMltB Purification by Immobilized Metal Affinity Chromatography – Purification samples were run alongside (L) PageRuler Prestained Protein Ladder. Fractions were collected as follows: P (pellet), FT (flowthrough), W1 (wash 1), W2 (wash 2), W3 (wash 3), and EL (elution).

3.4 Production and Purification of Recombinant SltB1

The *P. aeruginosa* PAO1 *sltB1* gene was previously engineered into a pET30a(+) plasmid to produce recombinant SltB1 with a C-terminal hexa-His-tag (74). Overexpression of *sltB1* in an *E. coli* BL21 Star (DE3) expression strain was followed by affinity chromatography using TALON cobalt resin. No further purification steps were necessary as SltB1 was purified to be the predominant species (fraction E1f) with yields of 4-6 mg per litre cell culture and apparent mass of 37.9 kDa (Fig. 3.8). After purification, SltB1 was dialyzed against 2 × 2 L of 10 mM NaOAc, pH 4.5, containing 10 mM $MgCl_2$ and 10 % glycerol. SltB1 was found to be catalytically active immediately after purification, as well as after storing in -80 °C.

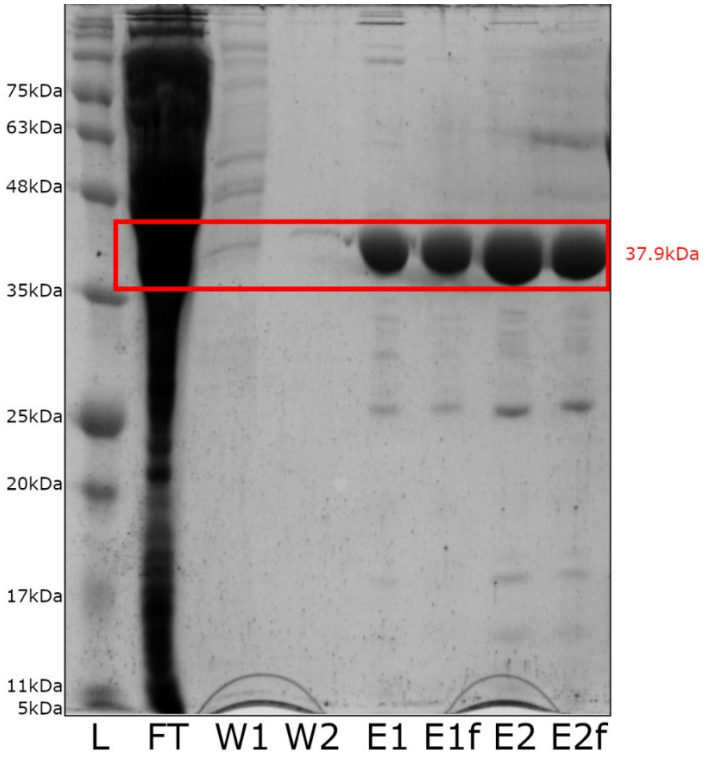

Figure 3.7 SDS-PAGE Analysis of SltB1 Purification by Immobilized Metal Affinity Chromatography – Purification samples were run alongside (L) BLUelf Prestained Protein Ladder. Fractions were collected as follows: FT (flowthrough), W1 (wash 1), W2 (wash 2), E1 (elution 1), E1f (elution 1, filtered), E2 (elution 2), E2f (elution 2, filtered).

3.5 Production and Purification of Recombinant SltB2

The *P. aeruginosa* PAO1 *sltB2* gene was previously engineered into a pET28a(+) plasmid to produce recombinant SltB2 with an N-terminal hexa-His-tag (C. Vandenende, unpublished). Overexpression of *sltB2* in an *E. coli* BL21 Star (DE3) expression strain was followed by affinity chromatography using TALON cobalt resin. No further purification steps were necessary as SltB2 was purified to apparent homogeneity (fraction E2) with yields of 3-5 mg per litre cell culture and apparent mass of 41 kDa (Fig. 3.9). After purification, SltB2 was dialyzed against 2 × 2 L of 10 mM NaOAc, pH 4.5, containing 10 mM $MgCl_2$ and 10 % glycerol. SltB2 was found to be active immediately after purification, as well as after storing in -80 °C.

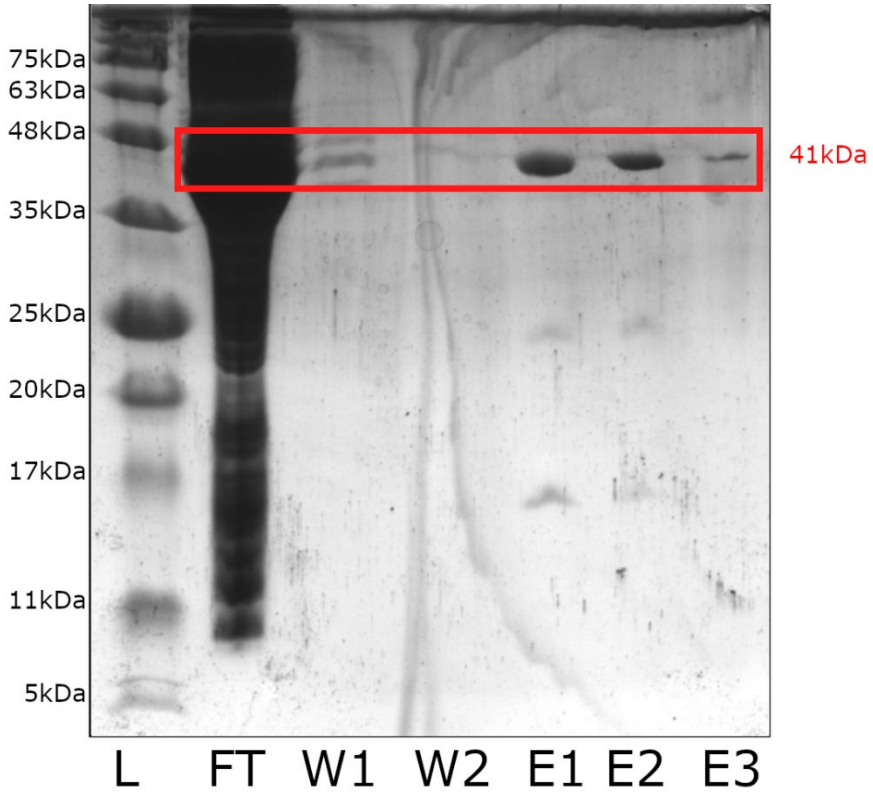

Figure 3.8 SDS-PAGE Analysis of SltB2 Purification by Immobilized Metal Affinity Chromatography – Purification samples were run alongside (L) BLUelf Prestained Protein Ladder. Fractions were collected as follows: FT (flowthrough), W1 (wash 1), W2 (wash 2), E1 (elution 1), E2 (elution 2) and E3 (elution 3; identical to elution 2).

3.6 Production and Purification of Recombinant SltB3

The *P. aeruginosa* PAO1 *sltB3* gene was previously engineered into a pET28a(+) plasmid to produce recombinant SltB3 with an N-terminal hexa-His-tag (C. Vandenende, unpublished). Overexpression of *sltB3* in an *E. coli* BL21 Star (DE3) expression strain was followed by affinity chromatography using TALON cobalt resin. The presence of contamination in the elution was evident, though to minimal degrees when compared to presence of SltB3 (Fig. 3.10). Thus, no further purification steps were employed. Purification led to final yields of 15-20mg per litre cell culture and apparent mass of 44.7 kDa (Fig. 3.10). After purification, SltB3 was dialyzed against 2 × 2 L of 10 mM NaOAc, pH 4.5, containing 10 mM $MgCl_2$ and 10 % glycerol. SltB3 was found to be active immediately after purification, as well as after storing in -80 °C.

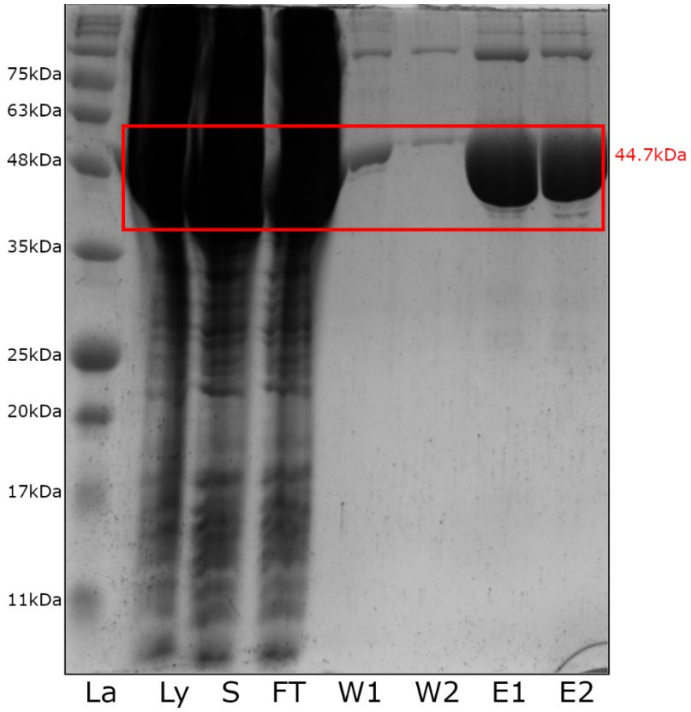

Figure 3.9 SDS-PAGE Analysis of SltB3 Purification by Immobilized Metal Affinity Chromatography – Purification samples were run alongside (La) BLUelf Prestained Protein Ladder. Fractions were collected as follows: Ly (lysate), SN (supernatant), FT (flowthrough), W1 (wash 1), W2 (wash 2), E1 (elution 1) and E2 (elution 2).

3.7 Production and Purification of Recombinant sMltF

The *P. aeruginosa* PAO1 *mltF* gene was previously engineered into a pET28a(+) plasmid to produce recombinant sMltF with an N-terminal hexa-His-tag (C. Vandenende, unpublished). Overexpression of engineered *mltF* in an *E. coli* BL21 Star (DE3) expression strain was followed by affinity chromatography using TALON cobalt resin. No further purification steps were necessary as sMltF was purified to be the predominant species (fraction E1, E2) with yields of 7-8 mg per litre cell culture and apparent mass of 52.9 kDa (Fig. 3.11). After purification, sMltF was dialyzed against 2 × 2 L of 10 mM NaOAc, pH 4.5, containing10 mM $MgCl_2$ and 10% glycerol. Being unstable, even after storage at 4°C, sMltF was used immediately following its purification; activity has not been tested upon storing at -80 °C.

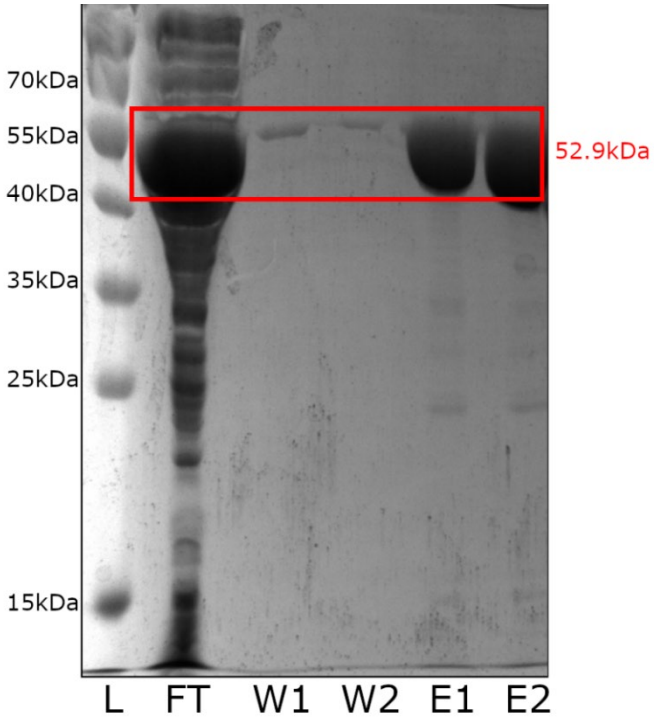

Figure 3.10 SDS-PAGE Analysis of sMltF Purification by Immobilized Metal Affinity Chromatography – Purification samples were run alongside (L) PageRuler Prestained Protein Ladder. Fractions were collected as follows: FT (flowthrough), W1 (wash 1), W2 (wash 2), E1 (elution 1), and E2 (elution 2).

3.8 Production and Purification of Recombinant sMltF2

The *P. aeruginosa* PAO1 *mltF2* gene was previously engineered into a pET28a(+) plasmid to produce recombinant MltF2 without its putative lipidation site (Δ2-21) and with an N-terminal hexa-His-tag (C. Vandenende, unpublished). This construct was labelled sMltF2 for "soluble MltF2". Overexpression of *smltF2* in an *E. coli* BL21 Star (DE3) expression strain was followed by affinity chromatography using Ni^{2+} resin. No further purification steps were necessary as sMltB was purified to apparent homogeneity with yields of 4-6 mg per litre cell culture and apparent mass of 52.3 kDa (Fig. 3.12). After purification, sMltF2 was dialyzed against 2 × 2 L of 10 mM NaOAc, pH 5.0, containing 10 mM $MgCl_2$ and 10 % glycerol. sMltF2 was found to be active immediately after purification. Activity after storage in -80 °C has not been tested.

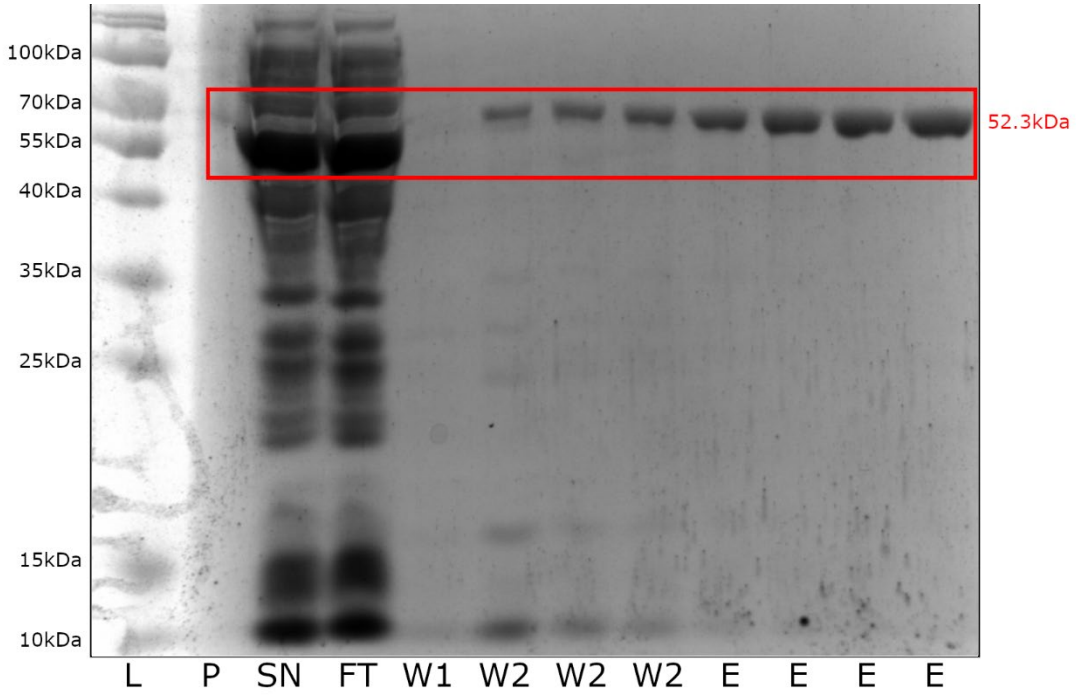

Figure 3.11 SDS-PAGE Analysis of sMltF2 Purification by Immobilized Metal Affinity Chromatography – Purification samples were run alongside (L) PageRuler Prestained Protein Ladder. Fractions were collected as follows: P (pellet), SN (supernatant), FT (flowthrough), W1 (wash 1), W2 (wash 2) and E (elution).

3.9 Production and Purification of Recombinant sRlpA

The *P. aeruginosa* PAO1 *rlpA* gene was previously engineered into a pET28a(+) plasmid to produce recombinant RlpA without its putative lipidation site (Δ2-29) and with an N-terminal hexaHis-tag (C. Vandenende, unpublished). This construct was labelled sRlpA for "soluble RlpA". Overexpression of engineered *rlpA* in an *E. coli* BL21 Star (DE3) expression strain was followed by affinity chromatography using Ni^{2+} resin. The presence of contamination in the elution was evident, though to minimal degrees when compared to presence of sRlpA (Fig. 3.13). Thus, no further purification steps were employed. Purification led to final yields of 15-20 mg per litre cell culture and apparent mass of 34.5 kDa (Fig. 3.13). After purification, sRlpA was dialyzed against 2 × 2 L of 10 mM NaOAc, pH 6.0, containing 10 mM $MgCl_2$ and 10 %

glycerol. sRlpA was found to be active immediately after purification. Activity after storage in -80°C has not been tested.

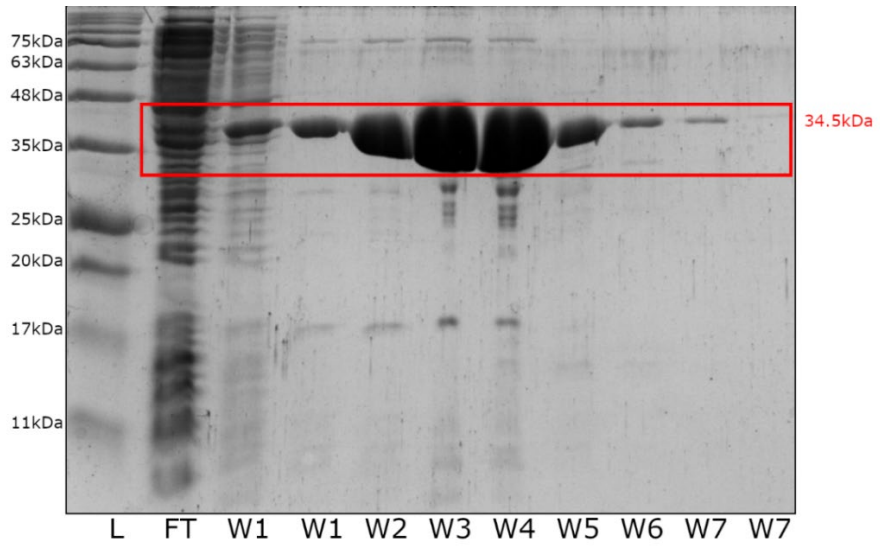

Figure 3.12 SDS-PAGE Analysis of sRlpA Purification by Immobilized Metal Affinity Chromatography – Purification samples were run alongside (L) BLUelf Prestained Protein Ladder. Fractions were collected as follows: FT (flowthrough), W1 (wash 1, 50mM imidazole), W2 (wash 2, 100mM imidazole), W3 (wash 3, 250mM imidazole), W4 (wash 4, 500mM imidazole), W5 (wash 5, 750mM imidazole), W6 (wash 6, 1M imidazole), and W7 (wash 7, final flushes with 1M imidazole).

3.10 Confirmation of Ivyp1 and Ivyp2 Interaction with HEWL

Upon gene cloning and purifying new constructs of Ivyp1 and Ivyp2, turbidity assays were performed to confirm previous results, namely that Ivyp1 can inhibit HEWL activity while Ivyp2 cannot. The results of the turbidity assay showed that a 1:1 ratio of Ivyp1:HEWL resulted in the complete loss of activity of HEWL, while a 1:1 ratio of Ivyp2:HEWL resulted in no change in HEWL activity (Fig. 3.14).

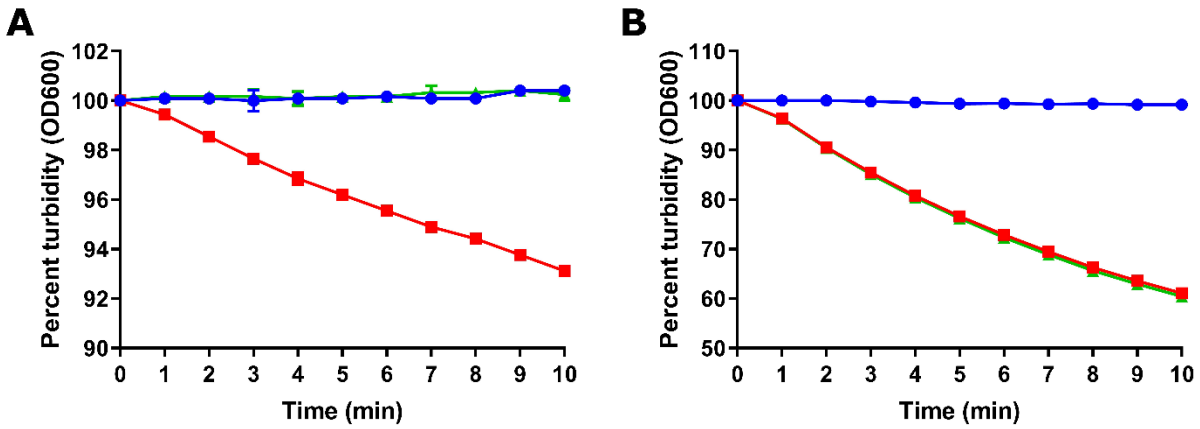

Figure 3.13 Inhibition of HEWL activity by Ivyp1 and Ivyp2 using the Turbidity Assay – Representative curves measuring HEWL activity in the presence of Ivyp1 (A) and Ivyp2 (B) at a 1:1 ratio of LT:Ivyp. *M. luteus* whole cells were used as substrate against 400nM HEWL in 100mM NaH_sPO_4 pH 7.5, containing 100mM NaCl. HEWL in the presence (green) and absence (red) of inhibitors are compared to cells-only negative control (blue).

3.11 Optimization of Lytic Activity Assay Conditions

Though previous work had been done to optimize the assay conditions for the LTs, it was deemed necessary to "re-optimize" for each LT because the activity profile based on pre-established conditions were virtually indistinguishable from negative controls. I set about performing pH-activity profiles for each LT, testing activity at pH values ranging from 4.0-8.0 with intervals of 0.5. The three-component buffer 50 mM acetic acid, 50 mM MES, 100 mM Tris was used for its broad range of pH (4.0-8.0) in addition to its ability to maintain a virtually constant ionic strength (75). This resulted in the determination of pH optima that were contrary to those identified in the past. Previously established pH activity profiles placed the optimal pH at 5.5-6.0, whereas the results of these experiments showed that the general pH optimum trended towards a more acidic pH (<5.0). Re-establishing the pH activity curves also resulted in observed increases in lytic activity, thus making it easier to identify if inhibition by Ivyp1 or Ivyp2 was occurring. The following presents the data obtained with each LT using 0.4 mg/mL *M. luteus* cells suspended in the acetate-MES-Tris tripartite buffer.

3.11.1 sMltA

The turbidity assay was performed with 400 nM sMltA in the presence of 10 μg/mL BSA as previous work with sMltA showed increase in sMltA activity with the addition of BSA (76). The pH activity profile revealed sMltA had optimal lytic activity at acidic pH conditions (pH 4.0) with decreasing rates of activity as pH was increased (Fig. 3.15A). Lytic activity was virtually nonexistent at pH 6.0 (Fig. 3.15A).

3.11.2 sMltB

With 400 nM sMltB, the initial pH activity profile revealed this LT had optimal lytic activity at two pH values, pH 4.5 and pH 7.0–7.5 (Fig. 3.15B). Suspecting inhibition of sMltA activity by MES, and perhaps Tris, a simple acetate buffer system of 10 mM NaOAc containing 10 mM MgCl2 was used. Under these conditions, the pH optimum was determined to occur at pH 5.5 (Fig. 3.15B), which concurs with previously reported results (73).

3.11.3 sMltD

The pH activity profile revealed 100 nM sMltD had optimal lytic activity at slightly acidic pH conditions (pH 5.0), though a moderate level of activity was maintained with increasing pH (Fig. 3.15C). A sharp drop-off in activity was observed with even more acidic conditions.

3.11.4 sMltF

sMltF (400 nM) had optimal lytic activity under acidic pH conditions (pH 4.0), though the activity seemed to increase with increasing pH after a steep decline at pH 4.5–5.0 (Fig. 3.15D). This may be a result of the bimodal nature of sMltF as previously described by Mobashery's group (27). However, it should be noted that the error associated with these data is considerable.

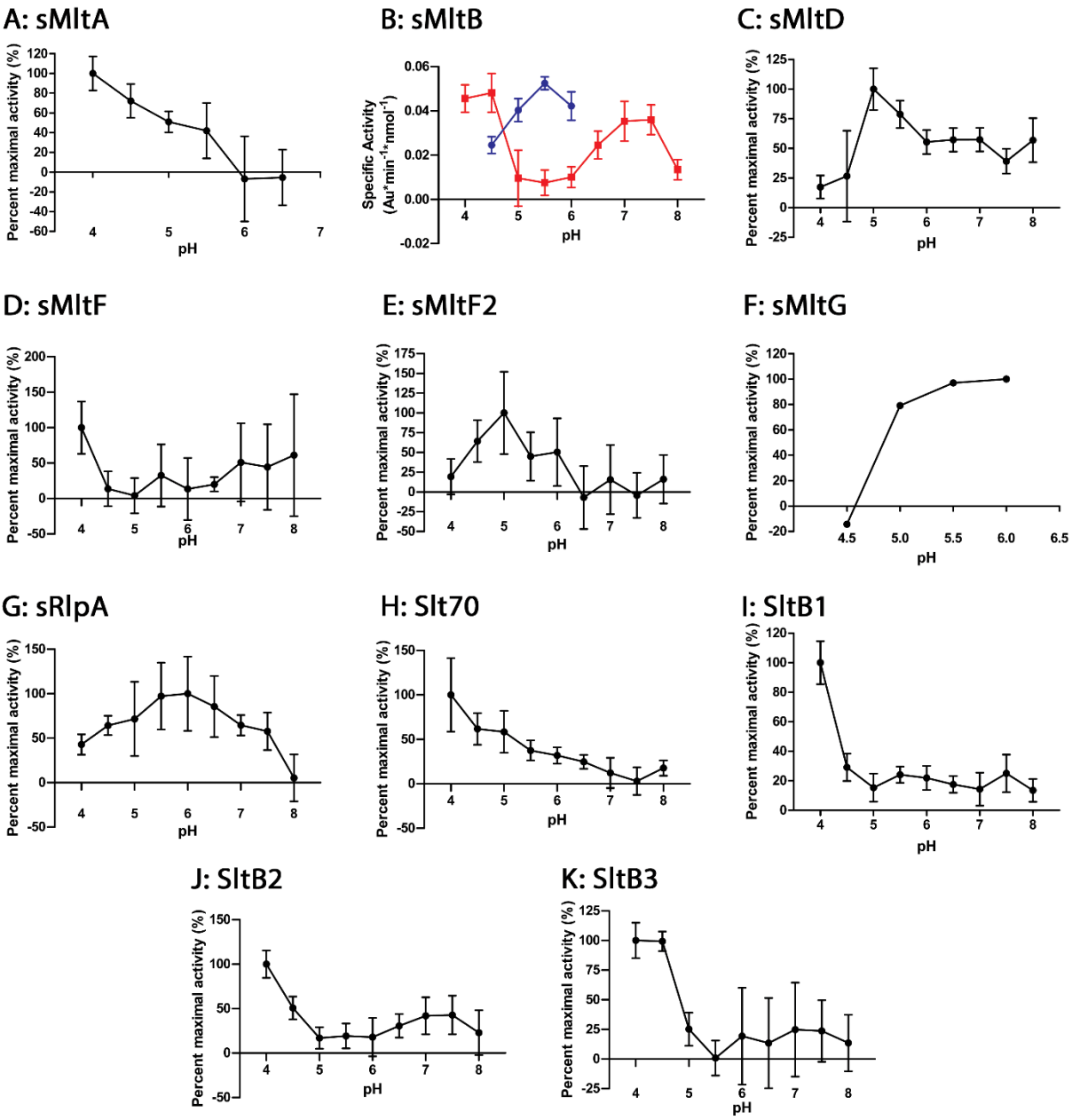

Figure 3.14 pH Activity Profiles of LTs - Turbidity assays were performed with each LT using 0.4 mg/mL M. luteus cells as substrate suspended in the acetate-MES-Tris buffer system at the pH values indicated, unless otherwise indicated. (A) sMltA (400 nM); (B) sMltB (400 nM) assayed with the tripartite buffer (red) and 10 mM NaOAc buffer (blue); (C) sMltD (100 nM); (D) sMltF (400nM); (E) sMltF2 (200 nM); (F) sMltG (500 nM) assayed in 10mM NaOAc buffer containing 10mM $MgCl_2$ at pH 4.5–6.0; (G) sRlpA (400 nM); (H) Slt70 (400 nM); (I) SltB1 (400 nM); (J) SltB2 (400 nM); (K) SltB3 (1 μM).

Table 3.1 pH optimum for each LT as determined in this study

Enzyme	MltA	MltB	MltD	MltF	MltF2	MltG	RlpA	Slt70	SltB1	SltB2	SltB3
pH Optimum	4.0	5.5	5.0	4.0	5.0	6.0	6.0	4.0	4.0	4.0	4.0

3.11.5 sMltF2

The pH activity profile of 200 nM sMltF2 was relatively sharp and revealed this LT had optimal lytic activity at slightly acidic pH of 5.0 (Fig. 3.15E). Lytic activity was virtually non-existent at pH conditions > 6.0.

3.11.6 sMltG

The tripartite buffer described above with pH ranging from 4.0 to 8.0 was not used to obtain a pH activity profile for sMltG because the yield obtained from sMltG purification was below the amount required to perform the test across all 9 pH values. Instead, the turbidity assay was performed with 500 nM sMltG using 0.4 mg/mL *M. luteus* cells as substrate in 10mM NaOAc buffer containing 10mM $MgCl_2$ at pH 4.5–6.0 (0.5 intervals). The pH activity profile revealed sMltG had optimal lytic activity closer to neutral pH conditions (pH 5.5–6.0), with decreasing rates of activity as pH was decreased (Fig. 3.15F).

3.11.7 sRlpA

The pH activity profile of this LT revealed a bell-shaped curve where 400 nM sRlpA had optimal lytic activity at pH 5.5–6.0 and held moderate levels of activity towards pH 4.0 and pH 7.5 (Fig. 3.15G). Lytic activity was virtually nonexistent at pH 8.0.

3.11.8 Slt70

With 250 nM Slt70, the pH activity profile revealed a downward trend where the LT had optimal lytic activity at pH 4.5 and decreased in activity with increasing pH (Fig. 3.15H). Lytic activity was virtually nonexistent at pH 7.5.

3.11.9 SltB1

SltB1 had optimal lytic activity at pH 4.0 when assayed at 400 nM concentrations, after which it experienced a significant decline in activity from pH 4.5 onwards (Fig. 3.15I).

3.11.10SltB2

SltB2 had optimal lytic activity at pH 4.5 (Fig. 3.15J). The activity of SltB1 diminished significantly as pH was increased up to 5.0, after which the activity remained relatively constant at this lower level.

3.11.11SltB3

In assays with 1 μM SltB3, this LT had optimal lytic activity at pH 4.0-4.5 (Fig. 3.15K). The activity of SltB1 diminished significantly with increasing pH up to 5.5, after which the activity remained relatively unchanged.

3.12 pH Effects on Interactions Between HEWL and Ivyp1

Having been characterized as an inhibitor of HEWL, previous inhibitor studies with Ivyp1 had been conducted in neutral to slightly alkaline conditions, the pH optimum of HEWL. As the current investigations with Ivyp1 were conducted in more acidic conditions, it was necessary to assess the effect of pH on the ability of Ivyp1 to inhibit HEWL. Thus, the turbidimetric assay was applied to determine the inhibitory effect of Ivyp1 toward HEWL in the same 10 mM sodium acetate buffer used for many of the LT studies. At pH 5.5, nearly complete inhibition of HEWL activity was observed with an equimolar and 2-fold excess of Ivyp1. While the specific activity of HEWL decreased slightly with decreasing pH levels, the continued ability for Ivyp1 to inhibit HEWL activity was evident; only small changes to the inhibitory capacity of Ivyp1 were observed (Fig. 3.16). These data indicate that Ivyp1 remains functional as a proteinaceous inhibitor over the pH range used to investigate the LTs.

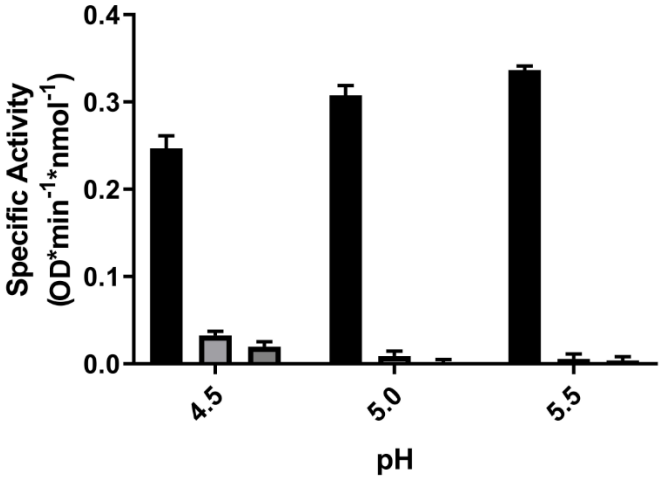

Figure 3.15 Effect of pH on HEWL Inhibition by Ivyp1 – Turbidimetric assays were performed in 10 mM NaOAc, 10mM $MgCl_2$ using 0.4mg/mL *M. luteus* cells as substrate to measure the pH dependency of Ivyp1 inhibition of HEWL. The specific activity of HEWL was determined at the three different pH values indicated in the absence (black), and presence of equimolar (light grey), and a 2-fold molar excess (dark grey) of Ivyp1. Error bars denote standard deviation (n=3).

3.13 Inhibition of Lytic Activity of LTs by Ivyp1 and Ivyp2

Purified Ivyp1 and Ivyp2 were tested as inhibitors against each of the LTs in buffer conditions optimal for their respective activities. Representative assays for each LT are presented in Figs. B1-B11 of Appendix B. Varied responses were obtained where in some cases obvious inhibition was observed while with others, there was apparent inhibition was minimal. An Ordinary One-Way ANOVA statistical analysis was carried out using GraphPad Prism v8.0 to determine whether the means within a group (*e.*g. Ivyp1:MltA at 0:1, 5:1, 10:1, 20:1) differed significantly from one another. A p-value of <0.05, indicating a significant difference between at least 2 means, was identified for six interactions: Ivyp1-MltD, Ivyp2- MltD, Ivyp1-MltG, Ivyp2-MltG, Ivyp2-Slt70, Ivyp1-SltB1 (Fig. 3.17). Whereas this analysis of the interactions of sMltD with Ivyp1 and Ivyp2 were indicated to be significant, visual inspection of the assay data revealed that the interaction was is in fact stimulatory in nature, rather than inhibitory (Fig. B3). The inhibition profiles for each of the other significant interactions (*i.e.* Ivyp1-MltG, Ivyp2-

MltG, Ivyp2-Slt70, Ivyp1-SltB1) revealed inhibition of lytic activity in the presence of a 20-fold molar excess of the proteinaceous inhibitor.

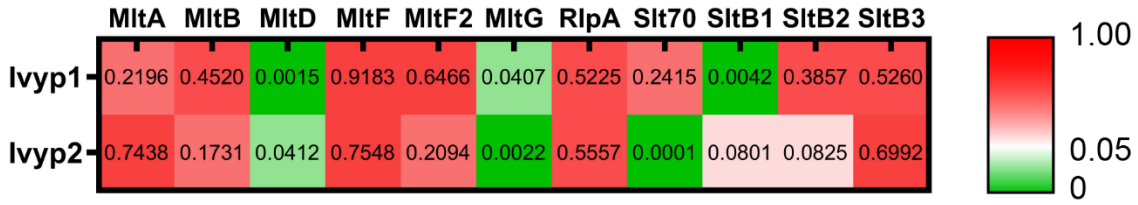

Figure 3.16 Statistical Analysis of Apparent Inhibition Data by Ordinary One-Way ANOVA – The p-values comparing the means for each LT-Ivyp combination are shown here as a heat map. P-values <0.05 are coloured in green, while P-values >0.05 are coloured in red.

The details for the interactions of each of the LTs with Ivyp1 and Ivyp2 are presented in the following.

3.13.1 sMltA

Reactions of 400nM sMltA at pH 4.5 with lower concentrations of Ivyp1 or Ivyp2 suggested some inhibition (Figs. 3.18A and B1). However, neither Ivyp1 nor Ivyp2 were capable of inhibiting the lytic activity of sMltA at increasing concentrations to20-fold molar excess and complete inhibition of sMltA was never achieved. Although lytic activity of sMltA varies with different ratios of Ivyp1 and Ivyp2, the differences were found to be statistically insignificant (Fig. 3.17). The data presented here reveal that both Ivyp1 and Ivyp2 are not inhibitors of sMltA.

3.13.2 sMltB

Purified Ivyp1 and Ivyp2 were tested against 2 µM sMltB in 25 mM NaH_2PO_4 buffer, pH 5.8, containing 100 mM $NaCl_2$ and 0.1 % Triton X-100. Under these conditions, a slight trend was observed where increasing concentrations of Ivyp1 and Ivyp2 led to decreasing lytic activity of sMltB (Figs. 3.18B and B2), but the differences were never statistically significant (Fig. 3.17). Neither Ivyp1 nor Ivyp2 were capable of inhibiting the lytic activity of sMltB at molar ratios up to 20:1 of Ivyp:sMltB (Fig. 3.18B).

3.13.3 sMltD

Purified Ivyp1 and Ivyp2 were tested against 100 nM sMltD at pH 5.0. Neither Ivyp1 nor Ivyp2 were capable of inhibiting the lytic activity of sMltD at molar ratios up to 20:1 of Ivyp:sMltD (Fig. 3.18C and B3). In fact, the opposite trend was observed in which the lytic activity of sMltD increased with increasing concentrations of Ivyp1 and Ivyp2. Interestingly, these results were statistically significant (Fig. 3.17) and suggest that Ivyp1 and Ivyp2 may potentially play a synergistic role with sMltD.

3.13.4 sMltF

Purified Ivyp1 and Ivyp2 were assayed against 400 nM sMltF at pH 4.5. Although the lytic activity of sMltF varied with different ratios of Ivyp1 (Figs. 3.18D and B4a), the differences were determined to be statistically insignificant (Fig. 3.17). Ivyp1 was incapable of inhibiting the lytic activity of this LT at molar ratios up to 20:1 of Ivyp2:sMltF (Fig. 3.18D and B4b). The data presented here reveal that both Ivyp1 and Ivyp2 are not inhibitors of sMltF.

3.13.5 sMltF2

Neither Ivyp1 nor Ivyp2 were capable of inhibiting the lytic activity of 200 nM sMltF2 at molar ratios up to 20:1 of Ivyp:sMltF2 when assayed at the optimal pH of 5.0 for this LT (Fig. 3.18E and B5). As with sMltF, the data presented here reveal that neither Ivyp1 nor Ivyp2 are potent inhibitors of sMltF2.

3.13.6 sMltG

Both Ivyp1 and Ivyp2 were found to inhibit the lytic activity of 500 nM sMltG with at pH 5.5 in a concentration dependent manner (Fig. 3.18F and B6), however complete inhibition of sMltG could not be achieved due to the solubility limits of the proteins under the assay conditions employed. Nonetheless, the inhibitions of sMltG activity were found to be statistically

significant (Fig. 3.17). These data reveal that both Ivyp1 and Ivyp2 are effective inhibitors of sMltG.

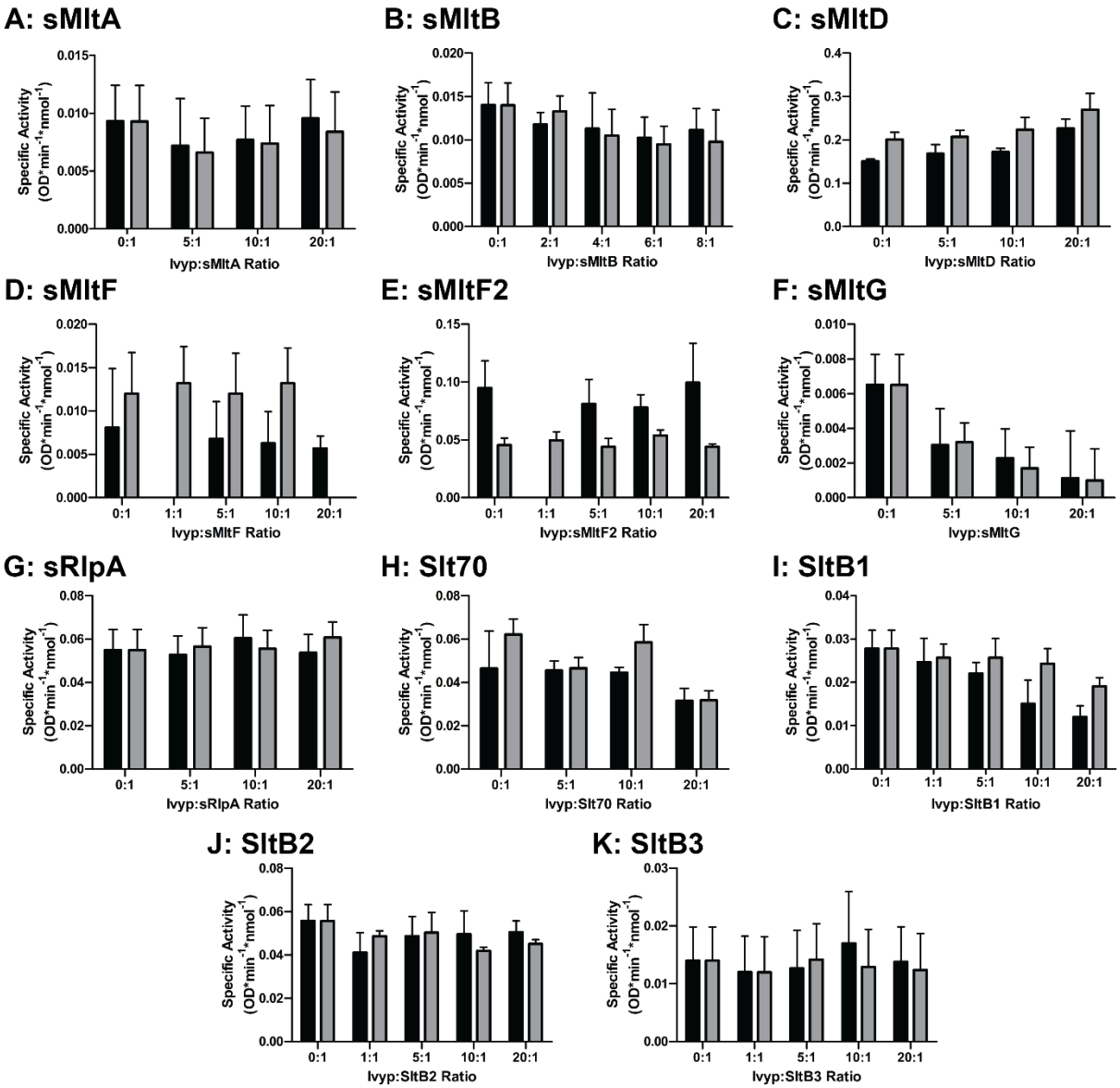

Figure 3.17 Inhibition of LTs by Ivyp1 and Ivyp2 – Each inhibition profile presents the specific activity of the respective LT in the presence of increasing molar excess of Ivyp1 (black) and Ivyp2 (grey). Unless otherwise indicated, the LTs were assayed in 10 mM sodium acetate buffer containing 10 mM $MgCl_2$ at their optimal pH, and in concentrations as indicated: (A) sMltA (400 nM), pH 4.5 buffer containing 10µg/mL BSA; (B) sMltB (2 µM) in 25mM NaH_2PO_4 pH 5.8, 100 mM $NaCl_2$, 0.1 % Triton X-100; (C) sMltD (100 nM), pH 5.0; (D) sMltF (400 nM), pH 4.5; (E) sMltF2 (200 nM), pH 5.0; (F) sMltG (500 nM), pH 5.5; (G) sRlpA (400 nM), pH 6.0; (H) Slt70 (250 nM), pH 5.5; (I) SltB1 (300 nM), pH 4.5; (J) SltB2 (250 nM), pH 4.5; (K) SltB3 (500 nM), pH 5.0. Error bars denote standard deviation (n=3).

3.13.7 sRlpA

When assayed against 400 nM sRlpA at pH 6.0, neither Ivyp1 nor Ivyp2 were capable of inhibiting the lytic activity of this LT at 20-fold molar excess concentrations (Fig. 3.18G and B7). Statistical analyses of the results showed no difference between the different ratios of Ivyp:sRlpA (Fig. 3.17), confirming that both Ivyp1 and Ivyp2 are not inhibitors of sRlpA.

3.13.8 Slt70

Ivyp2 was observed to inhibit this 250 nM Slt70 in a concentration dependent manner when assayed at pH 4.5 (Fig. 3.18H and B8). Statistical analysis confirmed this apparent inhibitory activity (Fig. 3.17), complete inhibition of Slt70 was never achieved. Whereas lytic activity of Slt70 varied with different ratios of Ivyp1, particularly at the 20:1 ratio where some inhibition was observed, the differences were never statistically significant (Fig. 3.17). Thus, of the two proteinaceous inhibitors, only Ivyp2 has some specificity for Slt70.

3.13.9 SltB1

In direct contrast to the activities of Ivyp1 and Ivyp2 towards Slt70, only Ivyp1 was found to inhibit the lytic activity of 300 nM SltB1 at pH 4.5 with increasing concentrations (Fig. 3.18I and B9), which was confirmed by statistical analysis (Fig. 3.17). However, under the experimental conditions employed, complete inhibition of SltB1 was never achieved. Again, in the converse situation with Slt70, the lytic activity of SltB1 varied with different ratios of Ivyp2, but these differences were statistically insignificant (Fig. 3.17). The data presented here thus indicate that Ivyp1 serves as an apparent inhibitor of SltB1.

3.13.10 SltB2 & SltB3

Some minor perturbations of SltB2 (250 nM) and SltB3 (500 nM) activity were observed when treated with Ivyp1 and Ivyp2 at their optimal pH of 4.5 and 5.0, respectively (Figs. 3.18J,

B10 and 3.18K, B11, respectively) but the differences were not statistically significant (Fig. 3.17). These data indicate that neither Ivyp1 nor Ivyp2 serve to inhibit SltB2 and SltB3.

4 Discussion

The research presented here continues the work originally started by Clarke *et al*. (70) and further expanded upon by other members of the Clarke lab (76–79). It offers insight into the spectrum of interaction of Ivyp1 and Ivyp2 with the eleven known LTs produced by *P. aeruginosa*. Ivyp1 and Ivyp2 were both found to inhibit sMltG, while Slt70 was inhibited by only Ivyp2, and SltB1 by Ivyp1. Statistical analyses strengthened the confidence of these findings. Interestingly, the data revealed an unanticipated observation in which Ivyp1 and Ivyp2 were both found to slightly enhance the lytic activity of sMltD, rather than inhibit it. Perhaps the most surprising finding, and one of concern, was the inability of either Ivyp1 or Ivyp2 to inhibit sMltB, as was initially reported.

This research project began by addressing two major problems faced in the past when working with LTs, low detectable lytic activity and test-to-test variability. The *M. luteus* undefined PG substrate was the greatest barrier to producing clean and highly reproducible results. Having a variable substrate from a Gram-positive cell that was foreign to the LTs from a Gram-negative bacterium is less than ideal. Ideally, the substrate would be synthesized to reflect the PG composition found in *P. aeruginosa*, which required knowledge and skills in chemical synthesis. Other efforts have been made to develop new assays that would change the mode of measuring lytic activity, such that fluorescence would be measured rather than absorbance (76). This was met with success for tests conducted with HEWL but did not translate once again to the LTs (76). Thus, instead of changing the substrate or mode of measurement, I sought to alter the assay environment in order to optimize the conditions that led to the greatest detection of lytic activity. This was accomplished by determining the pH-activity profiles for each LT to find their pH optimum. Also, the concentration of LTs used in the *in vitro* assays was decreased by ~10×

from the 2-10μM to 100-500nM range. Originally, the LT concentration was increased with the expectation to observe a greater rate of activity for an enzyme that exhibited low activity compared to its HEWL counterpart. However, under these conditions, the LTs were found to readily precipitate from solution, particularly when combined with the proteinaceous inhibitors. As a result, large standard deviations were realized for the assay of LTs at μM concentrations. Decreasing the concentration to nM levels alleviated these issues.

Although the determination of pH-activity profiles was conducted using a tripartite buffer (*viz.* 100mM Tris, 50mM MES, 50mM acetic acid), subsequent inhibition assays with Ivyp1 and Ivyp2 were performed using 10mM NaOAc buffer containing 10mM $MgCl_2$. Initially, the primary reason for this change was due to prior and continued success with the buffer system, particularly in studies involving sMltA. The pH-activity profiles generated in this study revealed that the pH optimum for most of the LTs (Fig. 3.15) centered around 4.0-4.5. The pH optimum of the other LTs fell around 5.0-5.5 (sMltD, sMltF2) or 5.5-6.0 (sMltG, sRlpA). Thus, sodium acetate, with a buffering range of 3.7-5.6, was the ideal buffer for a group of LTs with acidic pH optima.

For LTs with pH optima of 4.0 (sMltA, sMltF, Slt70, SltB1, SltB2), inhibition tests were conducted at pH 4.5 (Fig. 3.15, 3.18, 3.23, 3.24). This was due to a phenomenon observed in which lysed cell contents were precipitating out of solution at pH 4.0, as detected by an upwards trend in optical density of the *M. luteus* cell control (data not shown). Such precipitation of released cellular material would have had an effect in significantly masking the lytic (*i.e.* clearing) activity, particularly for LTs like sMltF, SltB1, and SltB2, which held a very specific pH optimum of 4.0.

The observation that the pH-activity optimum of all eleven LTs of *P. aeruginosa* is within an acidic range of pH (<4.0-6.0) led to the consideration of potential influences that pH may have on the interactions between Ivyp1 and Ivyp2 with the LTs. To test this, I investigated an interaction that had already been confirmed, Ivyp1 and HEWL. Previous experiments to confirm the inhibition of HEWL by Ivyp1 were conducted under a relatively neutral pH of 7.4. Here, the interaction of Ivyp1 and HEWL was tested at pH 4.5, 5.0, and 5.5. HEWL is still strongly inhibited by Ivyp1 at a 1:1 and 2:1 ratio at pH 5.5 and 5.0 (Fig. 3.16). A slight decline in the ability for Ivyp1 to inhibit HEWL was detected when assayed at pH 4.5. These data parallel an experiment done which showed no effect of pH on the ability for MliC to inhibit HEWL (S. Gilbert, unpublished). Thus, it can be concluded with some degree of confidence that at least Ivyp1 retains its structural integrity under acidic conditions, and thereby is still capable of serving as an inhibitor of muralytic enzymes that function in more acidic (micro)environments.

The finding that LTs favour acidic conditions is intriguing given our current understanding of the periplasmic environment. The periplasmic pH of *E. coli* was shown by Wilks and Slonczewski to match similarly to that of the cytoplasmic pH, about 7.5-7.6 (80). Whereas cytoplasmic pH remained relatively unchanged in the presence of an acidic (pH 5.5) or basic stressor (pH 7.5), periplasmic pH continued to consistently reflected the pH of the external medium (80). However, it is conceivable that a pH gradient of acidic to neutrality is established closer to the cell membrane through the generation of proton motive force. This potential for a pH gradient extending from the membrane out toward the centre of the periplasm may play a role in both the localization and, perhaps more so, the control of LT activity. It may also explain some of the apparent redundancy associated with the production of 11 LTs that otherwise catalyze the same chemical reaction. Having LTs with discrete acidic pH optima might reflect

their specific localization and function within the PG sacculus. For example, those with more acidic pH-activity optima may act below the PG closer to the cytoplasmic membrane to facilitate PG biosynthesis, while others that are more active at pH approaching neutrality are engaged with the outer layer(s) of the sacculus to catalyze PG remodeling and/or turnover. Clearly, experimental evidence for such discrete localizations across the relatively thin PG sacculus will require advances in current technologies. It should be noted, however, that the concept of pH as influenced by the proton motive force as a means of control of autolytic activity is not new, at least in Gram-positive bacteria. Such was proposed by Doyle and co-workers in studies with *Bacillus subtilis* where it was demonstrated that a potential pH gradient is established across the thicker PG sacculus of this Gram-positive bacterium such that its major autolysin would only be active at is outer layers (81).

Comparing the specific activities obtained in conditions of their respective pH optima indicates that sMltD is the most active of the 11 *P. aeruginosa* LTs (Fig. 4.1). This does not align with a recent study by Lee et al. which reports the activity of each LT assayed using a synthetic PG substrate, and where the products of the reaction were analyzed via mass spectrometry (82). In this earlier study, the relative activity of each LT was normalized to the most active enzyme in their experiment, which was SltB1, followed closely by SltB3 (82). Applying the same approach to the data obtained herein reveals some key differences (Fig. 4.1). The greatest disparities concern MltD, Slt70 and SltB3. With the earlier study, MltD and Slt70 were two of the least active enzymes, while I found these LTs to be two of the most active enzymes under the conditions employed. SltB3, on the other hand, was one of the most active in enzymes reported by Lee *et al.*, while it was the second to least active LT characterized herein.

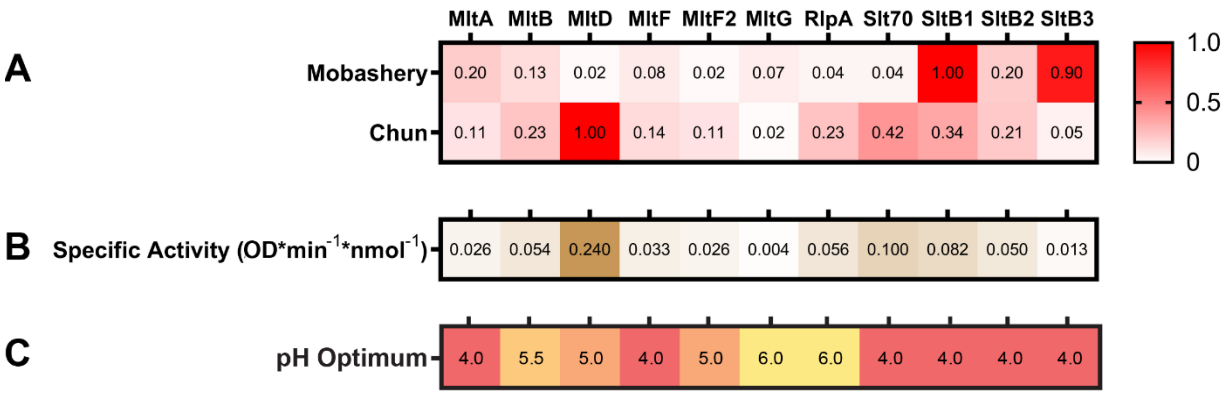

Figure 4.1 Comparison of LT Activities Assayed under Different Conditions – (A) Heat map representations of the relative activity of each LT. The activity for each LT was normalized to the value for the LT with the highest activity, within the respective series of data. (B) Heat map representation of the specific activities for each LT as determined in the current study. (C) Heat map representation of the pH optimum for each LT as determined in the current study. Colour representation follows the universal pH indicator with a gradient from neutral (pH 7, green) to acidic (pH 0, red).

The reasons for these apparent disparities are likely due to the methodology used to measure LT activities. Lee *et al*. assayed each of the LTs at neutral pH, and therefore none of the enzymes would have been operating under optimal pH conditions, according to my data under my conditions. However, what is surprising is that the LTs that performed best in the earlier study were the ones that had a strict adherence to a pH optimum of 4.0 (Fig. 4.1). This is counter-intuitive as one would have expected the LTs with a higher pH optimum to perform better than the LTs with a lower pH optimum. It is conceivable that this discrepancy is due to the nature of the substrate used. As noted above, Lee *et al.* used a defined synthetic substrate which may have accommodated particular substrate specificities of only a subset of the respective LTs. In the current study, the enzymes were assayed at their optimal pH, and against whole PG sacculi that would accommodate any specificity. Moreover, Lee *et al.* reported the amount of product produced from an end-point assay. These calculations would differ significantly from activity determined by monitoring the initial rate of change in optical density within a 5-minute interval.

This is because the activity of the LTs cannot be guaranteed to be linear throughout the entirety of a reaction. In general though, despite the differences in methodology, and aside from the differences with the three LTs Slt70, MltD, and SltB3, the trend for the relative activities of each series of eleven LTs is comparably similar in both cases. It can be concluded that both sets of data are reliable for comparing the relative activities of each LT to one another.

The inhibition tests revealed four potential targets by Ivyp1 and Ivyp2. Ivyp1 was found to interact with MltD, MltG, and SltB1, while Ivyp2 was found to interact with MltD, MltG, and Slt70 (Fig. 3.26). A potentially confounding phenomenon is the lack of a shared commonality between all four of these LTs. For example, Slt70 and MltD are both members of the Family 1 superfamily, while SltB1 and MltG are members of Family 3 and 5, respectively. MltD has endolytic activity and SltB1 is exolytic, while Slt70 and MltG catalyze both forms of activity (35, 82, 83). Of these four LTs, only MltG and SltB1 have been shown to cleave nascent PG without the peptide stem (82). Structurally, both MltG and Slt70 form a doughnut shape, although MltG forms this structure as a homodimer. SltB1 uniquely has an EF-hand motif, and is thereby stabilized by a Ca^{2+} ion, a common feature of the Family 3 LTs (84). A crystal structure of MltD has yet to be reported and so it is possible that this LT shared one or both of these structural features. Perhaps the only commonality shared between all four LTs is that each possesses a lysozyme-like fold catalytic domain (35, 84, 85). This is a distinguishing feature of all of the LTs except for Family 2 enzymes, which have an endoglucanase V fold (22, 31). Given that catalytic domains of each of the Family 3 enzymes form the lysozyme-like fold, it is surprising that SltB1 is the only member that is inhibited by Ivyp1.

One distinguishing feature shared by the four LTs inhibited by Ivyp1 and/or Ivyp2 is that they are also the only LTs that are inhibited by the natural product and antibiotic adjuvant

Bulgecin A (86). This sulfonated glycopeptide produced by *Pseudomonas acidophila* and *Pseudomonas mesoacidophila* (87), which coincidently inhibits both C- and G-type lysozymes (85, 88, 89), potentiates the activity of specific β-lactam antibiotics. With *P. aeruginosa*, Bulgecin A enhances the activity of the β-lactams ceftazidime, which preferentially inhibits PBP1a and PBP3, as well as meropenem, which preferentially inhibits PBP2 and PBP3 (86, 90, 91). Recently, Dik *et al.* (86) demonstrated that Bulgecin A binds strongly to Slt70, MltD, and MltG (K_d values of 8.5 μM, 1.4 μM, and 24μM, respectively) and to a lesser extent to SltB1 (K_d 160 μM), while only weakly to RlpA (K_d 1200 μM) and other LTs (86).On the basis of these data, combined with subsequent mutagenesis, growth, and imaging studies, Dik *et al.* conclude that Slt70, MltD and MltG (and perhaps SltB1), collaborate with the essential PBPs of the elongasome (PBP1a and PBP2) and divisome (PBP1a and PBP3) for the biosynthesis and general maintenance of the PG sacculus (86). Given the apparent importance of these LTs, together with the unique specificity of Bulgecin A inhibition, it is tempting to speculate that the specificities of the same LTs for Ivyp1 and Ivyp2 is not a mere coincidence. It is conceivable that the two Ivy proteins exist in the periplasm to inhibit any of the four LTs if and when they dissociate from their respective biosynthetic complexes to preclude their uncoordinated autolytic activity.

The structure of Slt70 has been solved with bound bulgecin A (85). Examination of this structure reveals that Bulgecin A interacts with the catalytic Glu478 in a manner similar to that which occurs between *e.g.* Ivyc and HEWL (1GPQ). In the same way that the central His residue of the Ivyc His60 binds to the catalytic diad of HEWL (Asp52 and Glu35), the central pyrrolidine ring of Bulgecin A, which resembles the imidazole in histidine, binds to the single catalytic acid of the LT (Figure 4.2). This suggests that the LTs may also interact with the key

His residue of the Ivy proteins in the same way. However, Dali Pairwise modeling of both Slt70 (1SLY) and Ivyp1 (1UUZ) onto the structure of Ivyc bound to HEWL (1GPQ) reveals significant steric hindrance between Ivyp1 and Slt70. Of course, such modelling does not accommodate any subtle conformational changes that may occur in the aqueous state, but the partial interference may in part explain why an Ivyp1:Slt70 ratio of up to 20:1 is required to see some inhibition of Slt70. Also, it should be noted that the structure of bulgecin A bound to Slt70 reveals that inhibition may also occur from the other face of the Slt70 doughnut. Whether this mode of inhibition is possible or not will require further crystallographic studies.

In addition to the synergistic potentiation of β-lactams by LT inhibition, another link between LTs and PBPs could be the possibility of direct binding interactions leading to activation. The idea that an LT-PBP interaction may be a prerequisite for activation of either enzyme is further strengthened by studies that have shown binding interaction between certain LTs and PBPs, such as Slt70 with PBP3 and PBP7/8 in *E. coli*, MltA with PBP1b and scaffolding protein MipA in *E. coli*, MltG with PBP1b in *E. coli* and SltB1 with PBP2 in *P. aeruginosa* (35, 74, 84, 92, 93). Most of these interactions were identified via pull-down assays. Other studies have also shown that overproduction of MltG led to a lethal phenotype in strains defective for PBP1b (35). Different theories have been proposed regarding why these interactions exist. One possibility is that these interactions are responsible for forming membrane adhesion sites, otherwise known as Bayer junctions, with the LTs anchored in the outer membrane and PBP's in the cytoplasmic membrane (93). Another theory is that the association of PBPs with LTs would lead to the activation, or even hyperactivation, of the LTs (35). This theory was validated by a previous student in the Clarke lab, who showed increased activity of MltB in the presence of a PBP (94). If this is true, then there is a possibility that Ivyp1 and Ivyp2

may act either directly through blocking the active site of the LTs and/or by complexing with the enzymes to prevent further activation through PBP bindings. The mode of inhibition could thus be through direct active site inhibition, or by allostery.

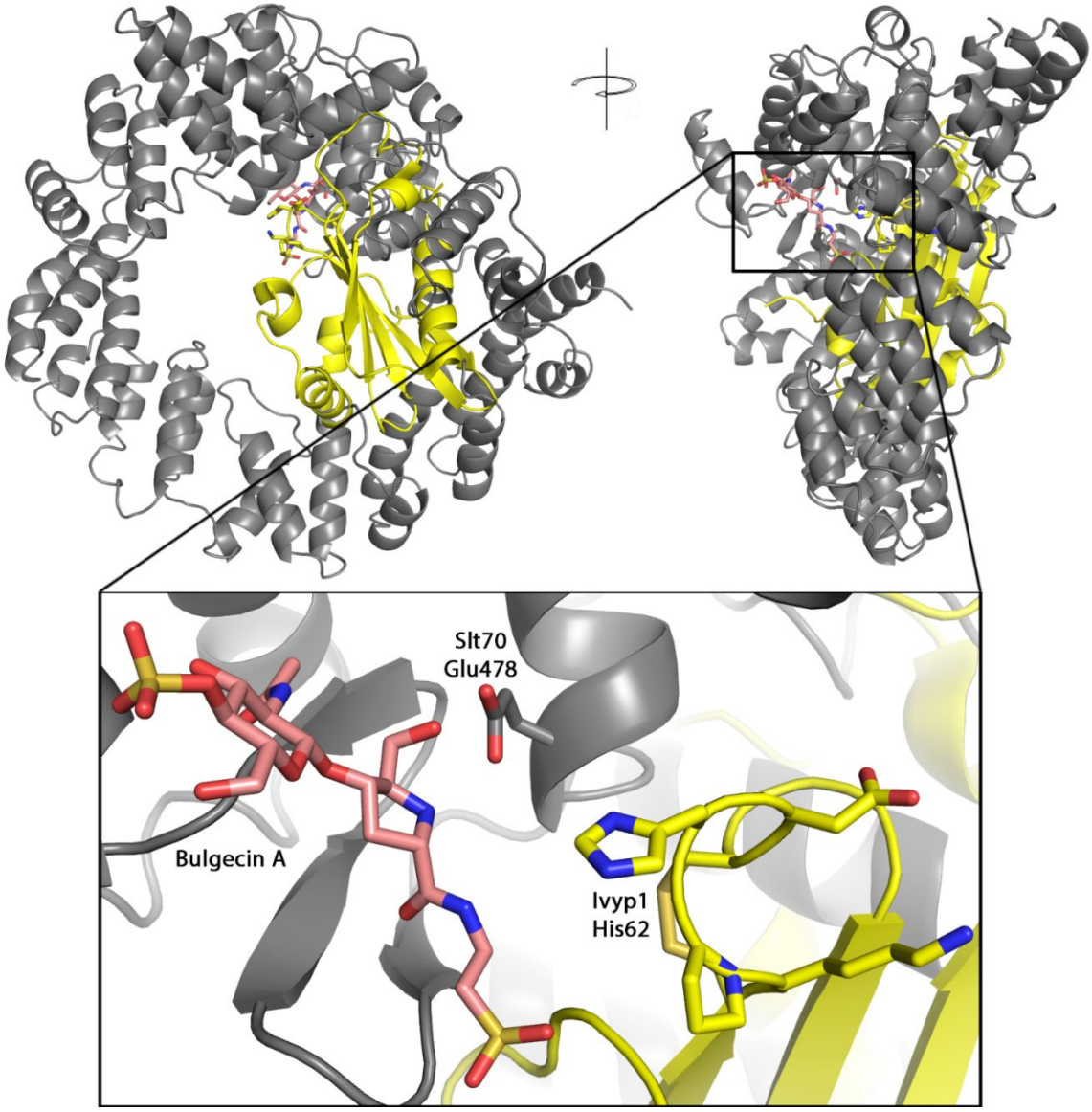

Figure 4.2 Pairwise Dali modeling of Ivyp1 to Slt70- Both Ivyp1 (yellow, PDB ID 1UUZ) and Slt70 (grey, PDB ID 1SLY) were modeled onto the structure of Ivyc bound to HEWL (not shown, PDB ID 1GPQ) to offer a rough insight into how Ivyp1 may interact with Slt70. Crystal structure of Slt70 was solved with bound Bulgecin A (pink) (85).

Conclusion & Future Directions

The redundancy of LTs in *P. aeruginosa* along with many other bacterial species, though initially confounding, means that there are multiple factors that play into regulating these enzymes. A single regulatory mechanism would not be enough to manage the fine-tuning required to control the activation/deactivation of eleven different LTs. The results presented in this thesis show that indeed Ivyp1 and Ivyp2 can directly inhibit a selection of LTs, namely MltG, Slt70, and SltB1. The results also reveal a range of pH optima across the LTs, suggesting that control of the pH environment may play one factor in regulating the LTs.

There are some potential experiments that could be done in the future to expand upon the work reported in this thesis. Currently, crystal structures of *P. aeruginosa* LTs exist only for MltF (PDB ID:4P11, 5A5X, 4OWD, 4OXV, 4OYV, 4OZ9, 4P0G, 5AA1, 5AA2, 5AA3), SltB1 (PDB ID 4ANR) and SltB3 (PDB ID 5ANZ). Crystal structures of *E. coli* LTs exist for Slt70 (PDB ID: 1QSA, 1QTE), MltA (PDB ID: 2AE0, 2PIC), MltB (PDB ID: 1D0L, 1D0M, 1QDR, 1QDT, 1QUS, 1QUT, 1D0K) and MltG (PDB ID 2R1F). No crystal structures exist for the following LTs: MltD, MltF2, SltB2, and RlpA. There is a clear lack of structural data, not just for *P. aeruginosa* LTs, but for LTs in general. In particular, a crystal structure of MltD would be useful as it has been shown thus far to interact with Ivyp1, Ivyp2, and Bulgecin A (86). Furthermore, kinetic analysis in the form of surface plasmon resonance (SPR) will be useful in providing data on the strength of the interaction between Ivyp1 and Ivyp2 with MltD, MltG, Slt70, and SltB1. Already some preliminary work has been started to determine the best mode of protein immobilization onto the chip and some tests have been done to minimize non-specific binding of analytes (C. Blinn, unpublished data). Additionally, growth curve experiments can be done with Ivyp1 and Ivyp2 overexpression strains in the presence of meropenem, which was

shown to cause cell lysis when used synergistically with Bulgecin A (86). It will be interesting to see if Ivyp1 and Ivyp2 can inhibit Slt70 and MltG *in vivo* like Bulgecin A, and whether this interaction will be detrimental to cell viability. The experiment can be expanded upon by testing different cell-wall acting antibiotics to determine any synergistic effects. Finally, activity of the LTs can be tested in the presence of certain PBPs to determine whether LT-PBP interaction influences the activity of either enzyme. These experiments can be further challenged by the addition of Ivyp1 or Ivyp2 to again assess whether these changes affect the activity of either enzyme. The culmination of all these experiments will provide a larger framework for understanding how Ivyp1 and Ivyp2 interact with LTs and further aid in determining the potential of this interaction for use in drug discovery.

REFERENCES

1. Scheffler RJ, Colmer S, Tynan H, Demain AL, Gullo VP. 2013. Antimicrobials, drug discovery, and genome mining. Appl Microbiol Biotechnol 97:969–978.
2. Rice LB. 2008. Federal Funding for the Study of Antimicrobial Resistance in Nosocomial Pathogens: No ESKAPE. J Infect Dis 197:1079–1081.
3. Boucher HW, Talbot GH, Bradley JS, Edwards JE, Gilbert D, Rice LB, Scheld M, Spellberg B, Bartlett J. 2009. Bad bugs, no drugs: no ESKAPE! An update from the Infectious Diseases Society of America. Clin Infect Dis 48:1–12.
4. Spellberg B, Guidos R, Gilbert D, Bradley J, Boucher HW, Scheld WM, Bartlett JG, Edwards Jr. J. 2008. The epidemic of antibiotic-resistant infections: a call to action for the medical community from the Infectious Diseases Society of America. Clin Infect Dis 46:155–164.
5. Lewis K. 2013. Platforms for antibiotic discovery. Nat Rev Drug Discov 12:371–87.
6. Coyette J, Van Der Ende A. 2008. Peptidoglycan: The bacterial Achilles heel. FEMS Microbiol Rev 32:147–148.
7. Alcorlo M, Martínez-Caballero S, Molina R, Hermoso JA. 2017. Carbohydrate recognition and lysis by bacterial peptidoglycan hydrolases. Curr Opin Struct Biol 44:87–100.
8. Van Delden C, Iglewski BH. 1998. Cell-to-cell signaling and Pseudomonas aeruginosa infections. Emerg Infect Dis 4:551–560.
9. Lister PD, Wolter DJ, Hanson ND. 2009. Antibacterial-resistant Pseudomonas aeruginosa: Clinical impact and complex regulation of chromosomally encoded resistance mechanisms. Clin Microbiol Rev 22:582–610.
10. Govan JRW, Deretic V, Colonization E, Environmental D. 1996. Microbial pathogenesis in cystic fibrosis: mucoid Pseudomonas aeruginosa and Burkholderia cepacia 60:539–574.
11. Moradali MF, Ghods S, Rehm BHA. 2017. Pseudomonas aeruginosa lifestyle: a paradigm for adaptation, survival, and persistence. Front Cell Infect Microbiol 7.
12. Koch AL. 1988. Biophysics of bacterial walls viewed as stress-bearing fabric. Microbiol Rev 52:337–353.
13. Dramsi S, Magnet S, Davison S, Arthur M. 2008. Covalent attachment of proteins to peptidoglycan. FEMS Microbiol Rev 32:307–320.
14. Neuhaus FC, Struve WG. 1965. Enzymatic synthesis of analogs of the cell-wall precursor. I. Kinetics and specificity of uridine diphospho-*N*-acetylmuramyl-L-alanyl-D-glutamyl-L-lysine: D-alanyl-D-alanine ligase (adenosine diphosphate) from Streptococcus faecalis R*. Biochemistry 4:120–131.
15. Vollmer W, Blanot D, De Pedro MA. 2008. Peptidoglycan structure and architecture. FEMS Microbiol Rev 32:149–167.

16. Schleifer KH, Kandler O. 1972. Peptidoglycan types of bacterial cell walls and their taxonomic implications. Bacteriol Rev 36:407–477.

17. Miller WR, Munita JM, Arias CA. 2014. Mechanisms of antibiotic resistance in enterococci. Expert Rev Anti Infect Ther 12:1221–36.

18. Sauvage E, Kerff F, Terrak M, Ayala JA, Charlier P. 2008. The penicillin-binding proteins: Structure and role in peptidoglycan biosynthesis. FEMS Microbiol Rev 32:234–258.

19. Tullio V, Roberta S, Manuela P. 2015. Lysozymes in the animal kingdom. J Biosci 35:45–57.

20. Ibrahim HR, Matsuzaki T, Aoki T. 2001. Genetic evidence that antibacterial activity of lysozyme is independent of its catalytic function. FEBS Lett 506:27–32.

21. Hoeltje J V., Mirelman D, Sharon N, Schwarz U. 1975. Novel type of murein transglycosylase in Escherichia coli. J Bacteriol 124:1067–1076.

22. Domínguez-Gil T, Molina R, Alcorlo M, Hermoso JA. 2016. Renew or die: The molecular mechanisms of peptidoglycan recycling and antibiotic resistance in Gram-negative pathogens. Drug Resist Updat 28:91–104.

23. Blackburn NT, Clarke AJ. 2001. Identification of four families of peptidoglycan lytic transglycosylases. J Mol Evol 52:78–84.

24. Herlihey FA, Clarke AJ. 2016. Controlling autolysis during flagella insertion in Gram-negative bacteria. Protein Rev Adv Exp Med Biol 925:41–56.

25. Thunnissen AMWH, Dijkstra AJ, Kalk KH, Rozeboom HJ, Engel H, Keck W, Dijkstra BW. 1994. Doughnut-shaped structure of bacterial muramidase revealed by X-ray crystallography. Nature 367:313–315.

26. Thunnissen A-MWH, Isaacs NW, Dijkstral BW. 1995. The catalytic domain of a bacterial lytic transglycosylase defines a novel class of lysozymes. Proteins Struct Funct Bioinforma 22:245–258.

27. Dominguez-Gil T, Lee M, Acebron-Avalos I, Mahasenan K V., Hesek D, Dik DA, Byun B, Lastochkin E, Fisher JF, Mobashery S, Hermoso JA. 2016. Activation by allostery in cell-wall remodeling by a modular membrane-bound lytic transglycosylase from Pseudomonas aeruginosa. Structure 24:1729–1741.

28. Artola-Recolons C, Lee M, Bernardo-Garcia N, Blazquez B, Hesek D, Bartual SG, Mahasenan K V., Lastochkin E, Pi H, Boggess B, Meindl K, Uson I, Fisher JF, Mobashery S, Hermoso JA. 2014. Structure and cell wall cleavage by modular lytic transglycosylase MltC of Escherichia coli. ACS Chem Biol 9:2058–2066.

29. Artola-Recolons C, Carrasco-López C, Llarrull LI, Kumarasiri M, Lastochkin E, Martínez De Ilarduya I, Meindl K, Usón I, Mobashery S, Hermoso JA. 2011. High-resolution crystal structure of MltE, an outer membrane-anchored endolytic peptidoglycan lytic transglycosylase from Escherichia coli. Biochemistry 50:2384–2386.

30. Scheurwater EM, Clarke AJ. 2008. The C-terminal domain of Escherichia coli YfhD functions as a lytic transglycosylase. J Biol Chem 283:8363–8373.

31. Van Straaten KE, Dijkstra BW, Vollmer W, Thunnissen AMWH. 2005. Crystal structure of MltA from Escherichia coli reveals a unique lytic transglycosylase fold. J Mol Biol 352:1068–1080.

32. Van Asselt EJ, Dijkstra AJ, Kalk KH, Takacs B, Keck W, Dijkstra BW. 1999. Crystal structure of Escherichia coli lytic transglycosylase Slt35 reveals a lysozyme-like catalytic domain with an EF-hand. Structure 7:1167–1180.

33. Fokine A, Miroshnikov KA, Shneider MM, Mesyanzhinov V V., Rossmann MG. 2008. Structure of the bacteriophage KZ lytic transglycosylase gp144. J Biol Chem 283:7242–7250.

34. Jorgenson MA, Chen Y, Yahashiri A, Popham DL, Weiss DS. 2014. The bacterial septal ring protein RlpA is a lytic transglycosylase that contributes to rod shape and daughter cell separation in Pseudomonas aeruginosa. Mol Microbiol 93:113–128.

35. Yunck R, Cho H, Bernhardt TG. 2016. Identification of MltG as a potential terminase for peptidoglycan polymerization in bacteria. Mol Microbiol 99:700–718.

36. Scheurwater E, Reid CW, Clarke AJ. 2008. Lytic transglycosylases: Bacterial space-making autolysins. Int J Biochem Cell Biol 40:586–591.

37. Lamers RP, Nguyen UT, Nguyen Y, Buensuceso RNC, Burrows LL. 2015. Loss of membrane-bound lytic transglycosylases increases outer membrane permeability and B-lactam sensitivity in Pseudomonas aeruginosa. Microbiologyopen 4:879–895.

38. Reid CW, Blackburn NT, Legaree BA, Auzanneau FI, Clarke AJ. 2004. Inhibition of membrane-bound lytic transglycosylase B by NAG-thiazoline. FEBS Lett 574:73–79.

39. Dik DA, Batuecas MT, Lee M, Mahasenan K V., Marous DR, Lastochkin E, Fisher JF, Hermoso JA, Mobashery S. 2018. A structural dissection of the active site of the lytic transglycosylase MltE from Escherichia coli. Biochemistry 6090–6098.

40. Byun B, Mahasenan K V., Dik DA, Marous DR, Speri E, Kumarasiri M, Fisher JF, Hermoso JA, Mobashery S. 2018. Mechanism of the Escherichia coli MltE lytic transglycosylase, the cell-wall-penetrating enzyme for Type VI secretion system assembly. Sci Rep 8:4110.

41. Fisher JF, Mobashery S. 2014. The sentinel role of peptidoglycan recycling in the β-lactam resistance of the Gram-negative Enterobacteriaceae and Pseudomonas aeruginosa. Bioorg Chem 56:41–48.

42. Koraimann G. 2003. Lytic transglycosylases in macromolecular transport systems of Gram-negative bacteria. Cell Mol Life Sci 60:2371–2388.

43. Heidrich C, Ursinus A, Berger J, Schwarz H, Höltje JV. 2002. Effects of multiple deletions of murein hydrolases on viability, septum cleavage, and sensitivity to large toxic molecules in Escherichia coli. J Bacteriol 184:6093–6099.

44. Jacobs C, Frère JM, Normark S. 1997. Cytosolic intermediates for cell wall biosynthesis and degradation control inducible β-lactam resistance in gram-negative bacteria. Cell 88:823–832.

45. Lee M, Dhar S, De Benedetti S, Hesek D, Boggess B, Blázquez B, Mathee K, Mobashery S. 2016. Muropeptides in Pseudomonas aeruginosa and their role as elicitors of β-lactam-antibiotic resistance. Angew Chemie Int Ed 55:6882–6886.

46. Jacobs C, Huang LJ, Bartowsky E, Normark S, Park JT. 1994. Bacterial cell wall recycling provides cytosolic muropeptides as effectors for beta-lactamase induction. EMBO J 13:4684–4694.

47. Holtje J-V, Kopp U, Ursinus A, Wiedemann B. 1994. The negative regulator of β-lactamase induction AmpD is a *N*-acetyl-anyhydromuramyl-L-alanine amidase. FEMS Microbiol Lett 122:159–164.

48. Korsak D, Liebscher S, Vollmer W. 2005. Susceptibility to antibiotics and β-lactamase induction in murein hydrolase mutants of Escherichia coli. Antimicrob Agents Chemother 49:1404–1409.

49. Kraft AR, Prabhu J, Ursinus A, Höltje JV. 1999. Interference with murein turnover has no effect on growth but reduces β-lactamase induction in Escherichia coli. J Bacteriol 181:7192–7198.

50. Moynihan PJ, Clarke AJ. 2011. *O*-Acetylated peptidoglycan: Controlling the activity of bacterial autolysins and lytic enzymes of innate immune systems. Int J Biochem Cell Biol 43:1655–1659.

51. Moynihan PJ, Sychantha D, Clarke AJ. 2014. Chemical biology of peptidoglycan acetylation and deacetylation. Bioorg Chem 54:44–50.

52. Hayashi H, Araki Y, Ito E. 1973. Occurrence of glucosamine residues with free amino groups in cell wall peptidoglycan from Bacilli as a factor responsible for resistance to lysozyme. J Bacteriol 113:592–598.

53. Amano K, Araki Y, Ito E. 1980. Effect of N-acyl substitution at glucosamine residues on lysozyme-catalyzed hydrolysis of cell-wall peptidoglycan and its oligosaccharides. Eur J Biochem 107:547–553.

54. Amano K, Hayashi H, Araki Y, Ito E. 1977. The action of lysozyme on peptidoglycan with N-unsubstituted glucosamine residues: Isolation of glycan fragments and their susceptibility to lysozyme. Eur J Biochem 76:299–307.

55. Vollmer W. 2008. Structural variation in the glycan strands of bacterial peptidoglycan. FEMS Microbiol Rev 32:287–306.

56. Vollmer W, Tomasz A. 2000. The pgdA gene encodes for a peptidoglycan *N*-acetylglucosamine deacetylase in Streptococcus pneumoniae. J Biol Chem 275:20496–20501.

57. Blair DE, Van Aalten DMF. 2004. Structures of Bacillus subtilis PdaA, a family 4 carbohydrate esterase, and a complex with *N*-acetyl-glucosamine. FEBS Lett 570:13–19.

58. Fukushima T, Kitajima T, Sekiguchi J. 2005. A polysaccharide deacetylase homologue, PdaA, in Bacillus subtilis acts as an *N*-acetylmuramic acid deacetylase in vitro. J Bacteriol 187:1287–1292.

59. Azuma I, Thomas D, Adam A, Ghuysen J, Bonaly R, Petit J, Lederer E. 1970. Occurence of N-glucosylmuramic acid in bacterial cell walls. Biochim Biophys Acta 20:444–451.

60. Bernard E, Rolain T, Courtin P, Guillot A, Langella P, Hols P, Chapot-Chartier MP. 2011. Characterization of *O*-acetylation of *N*-acetylglucosamine: A novel structural variation of bacterial peptidoglycan. J Biol Chem 286:23950–23958.

61. Laaberki MH, Pfeffer J, Clarke AJ, Dworkin J. 2011. *O*-acetylation of peptidoglycan is required for proper cell separation and S-layer anchoring in Bacillus anthracis. J Biol Chem 286:5278–5288.

62. Bera A, Herbert S, Jakob A, Vollmer W, Götz F. 2005. Why are pathogenic staphylococci so lysozyme resistant? The peptidoglycan *O*-acetyltransferase OatA is the major determinant for lysozyme resistance of Staphylococcus aureus. Mol Microbiol 55:778–787.

63. Weadge JT, Pfeffer JM, Clarke AJ. 2005. Identification of a new family of enzymes with potential *O*-acetylpeptidoglycan esterase activity in both Gram-positive and Gram-negative bacteria. BMC Microbiol 5:49.

64. Weadge JT, Clarke AJ. 2006. Identification and characterization of *O*-acetylpeptidoglycan esterase: A novel enzyme discovered in Neisseria gonorrhoeae. Biochemistry 45:839–851.

65. Weadge JT, Clarke AJ. 2007. Neisseria gonorrheae *O*-acetylpeptidoglycan esterase, a serine esterase with a Ser-His-Asp catalytic triad. Biochemistry 46:4932–4941.

66. Monchois V, Abergel C, Sturgis J, Jeudy S, Claverie JM. 2001. Escherichia coli ykfE ORFan gene encodes a potent inhibitor of C-type lysozyme. J Biol Chem 276:18437–18441.

67. Deckers D, Masschalck B, Aertsen A, Callewaert L, Van Tiggelen CGM, Atanassova M, Michiels CW. 2004. Periplasmic lysozyme inhibitor contributes to lysozyme resistance in Escherichia coli. Cell Mol Life Sci 61:1229–1237.

68. Abergel C, Monchois V, Byrne D, Chenivesse S, Lembo F, Lazzaroni J-C, Claverie J-M. 2007. Structure and evolution of the Ivy protein family, unexpected lysozyme inhibitors in Gram-negative bacteria. Proc Natl Acad Sci U S A 104:6394–9.

69. Geetha C, Venkatesh SG, Dunn BHF, Gorr S-U. 2003. Expression and anti-bacterial activity of human parotid secretory protein (PSP). Biochem Soc Trans 31:815–8.

70. Clarke CA, Scheurwater EM, Clarke AJ. 2010. The vertebrate lysozyme inhibitor Ivy functions to inhibit the activity of lytic transglycosylase. J Biol Chem 285:14843–14847.

71. Clarke AJ. 1993. Extent of peptidoglycan *O*-acetylation in the tribe Proteeae. J Bacteriol 175:4550–4553.

72. Callewaert L, Aertsen A, Deckers D, Vanoirbeek KGA, Vanderkelen L, Van Herreweghe

JM, Masschalck B, Nakimbugwe D, Robben J, Michiels CW. 2008. A new family of lysozyme inhibitors contributing to lysozyme tolerance in gram-negative bacteria. PLoS Pathog 4.

73. Blackburn NT, Clarke AJ. 2002. Characterization of soluble and membrane-bound family 3 lytic transglycosylases from Pseudomonas aeruginosa. Biochemistry 41:1001–1013.

74. Legaree BA, Clarke AJ. 2008. Interaction of penicillin-binding protein 2 with soluble lytic transglycosylase B1 in Pseudomonas aeruginosa. J Bacteriol 190:6922–6926.

75. Ellis KJ, Morrison JF. 1982. Buffers of constant ionic strength for studying pH-dependent processes, p. 405–426. *In* Methods in Enzymology.

76. Ciufo J. 2017. Inhibition of membrane-bound lytic transglycosylases A, B and F by membrane-bound lysozyme inhibitor of C-type lysozyme. University of Guelph.

77. Selander SI. 2014. Inhibition of membrane-bound lytic transglycosylase A by inhibitors of vertebrate lysozyme P1 and P2. University of Guelph.

78. Holland KA. 2014. Inhibition of membrane-bound lytic transglycosylase F (MltF) by inhibitors of lysozyme. University of Guelph.

79. Herlihey FA. 2016. Biochemical characterization of the activity and control of the autolysins involved in flagella assembly in Gram-negative bacteria. University of Guelph.

80. Wilks JC, Slonczewski JL. 2007. pH of the cytoplasm and periplasm of Escherichia coli: Rapid measurement by green fluorescent protein fluorimetry. J Bacteriol 189:5601–5607.

81. Kemper MA, Urrutia MM, Beveridge TJ, Koch AL, Doyle RJ. 1993. Proton motive force may regulate cell wall-associated enzymes of Bacillus subtilis. J Bacteriol 175:5690–6.

82. Lee M, Hesek D, Dik DA, Fishovitz J, Lastochkin E, Boggess B, Jed F. 2017. From genome to proteome to elucidation of reactions for all eleven known lytic transglycosylases from Pseudomonas aeruginosa. Angew Chemie Int Ed 1–6.

83. Chaput C, Labigne A, Boneca IG. 2007. Characterization of Helicobacter pylori lytic transglycosylases Slt and MltD. J Bacteriol 189:422–429.

84. Nikolaidis I, Izoré T, Job V, Thielens N, Breukink E, Dessen A. 2012. Calcium-dependent complex formation between PBP2 and lytic transglycosylase SltB1 of Pseudomonas aeruginosa. Microb Drug Resist 18:298–305.

85. Thunnissen AMWH, Rozeboom HJ, Kalk KH, Dijkstra BW. 1995. Structure of the 70-kDa soluble lytic transglycosylase complexed with Bulgecin A. Implications for the enzymatic mechanism. Biochemistry 34:12729–12737.

86. Dik DA, Madukoma CS, Tomoshige S, Kim C, Lastochkin E, Boggess WC, Fisher JF, Shrout JD, Mobashery S. 2019. Slt, MltD and MltG of Pseudomonas aeruginosa as targets of Bulgecin A in potentiation of β-lactam antibiotics. ACS Chem Biol.

87. Shinagawa S, Maki M, Kintaka Ka, Imada A, Asai M. 2012. Isolation and characterization of bulgecins, new bacterial metabolites with bulge-inducing activity. J Antibiot (Tokyo) 38:17–23.

88. Karlsen S, Hough E. 1996. Structure of a complex between bulgecin, a bacterial metabolite, and lysozyme from the rainbow trout. Acta Crystallogr Sect D Biol Crystallogr 52:115–123.

89. Karlsen S, Hough E, Rao ZH, Isaacs NW. 1996. Structure of a Bulgecin-inhibited G-type lysozyme from the egg white of the Australian black swan. A comparison of the binding of Bulgecin to three muramidases. Acta Crystallogr Sect D Biol Crystallogr 52:105–114.

90. Yang Y, Bhachech N, Bush K. 1995. Biochemical comparison of imipenem, meropenem and biapenem: Permeability, binding to penicillin-binding proteins, and stability to hydrolysis by β-lactamases. J Antimicrob Chemother 35:75–84.

91. Davies TA, Page MGP, Shang W, Andrew T, Kania M, Bush K. 2007. Binding of ceftobiprole and comparators to the penicillin-binding proteins of Escherichia coli, Pseudomonas aeruginosa, Staphylococcus aureus, and Streptococcus pneumoniae. Antimicrob Agents Chemother 51:2621–2624.

92. Romeis T, Höltje JV. 1994. Specific interaction of penicillin-binding proteins 3 and 7/8 with soluble lytic transglycosylase in Escherichia coli. J Biol Chem 269:21603–21607.

93. Vollmer W, Von Rechenberg M, Höltje JV. 1999. Demonstration of molecular interactions between the murein polymerase PBP1B, the lytic transglycosylase MltA, and the scaffolding protein MipA of Escherichia coli. J Biol Chem 274:6726–6734.

94. Adams CB. 2005. Studies on the non-penicillin binding domain of penicillin binding protein 2 from Pseudomonas aeruginosa. University of Guelph.

APPENDICES

Appendix A – Recipes and Formulations

Competent cells solution A:	30mM KAc, 100mM KCl, 10mM $CaCl_2$, 50mM $MnCl_2$, 15% glycerol
Competent cells solution B:	10mM MOPS, 75mM $CaCl_2$, 10mM KCl, 15% glycerol
TAE buffer	40mM Tris, 20mM Acetic Acid, 1mM EDTA
4% stacking gel	4% bis/acrylamide, 0.168M Tris-HCl pH 6.8, 0.1% SDS, 0.4% APS, 0.4% TEMED
12% separating gel	12% bis/acrylamide, 0.376M Tris-HCl pH 8.8, 0.1% SDS, 0.125% APS, 0.25% TEMED
5× protein sample buffer	60mM Tris-HCl pH 6.8, 25% glycerol, 2% SDS, 5% 2-mercaptoethanol, 0.1% bromophenol blue
Coomassie stain	1g/L Coomassie brilliant blue R-250, 45% v/v methanol, 10% v/v acetic acid
Destain	40% v/v methanol, 10% v/v acetic acid

Appendix B – Turbidity Graphs

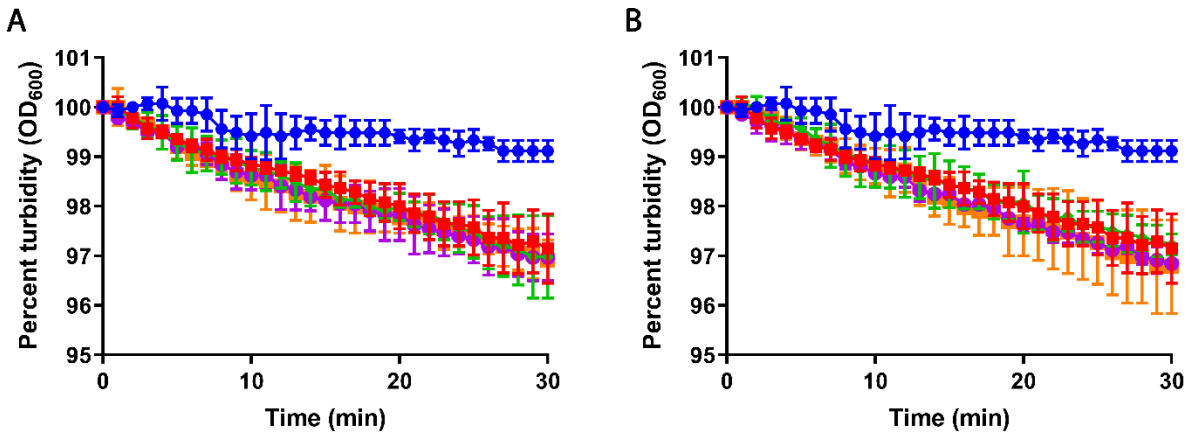

Figure B 1 Inhibition of sMltA with Ivyp1 and Ivyp2 – Turbidity graphs representing 400nM sMltA activity in 100mM NaOAc pH 4.5, 10mM $MgCl_2$, 10µg/mL BSA using 0.4mg/mL *M. luteus* cells as a substrate (red). Inhibition by Ivyp1 (A) and Ivyp2 (B) was performed at a 0:1 (blue), 5:1 (green), 10:1 (purple), and 20:1 (orange) ratio of Ivyp:sMltA.

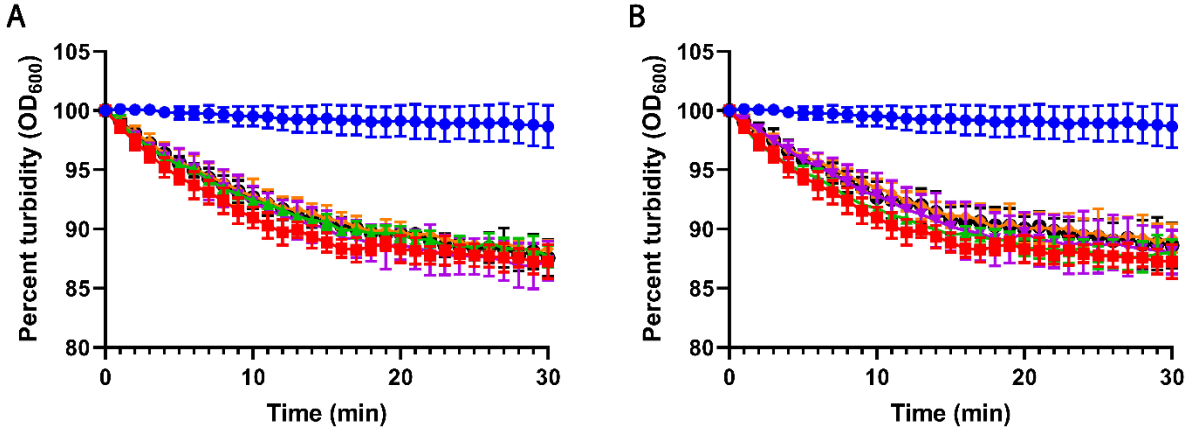

Figure B 2 Inhibition of sMltB with Ivyp1 and Ivyp2 – Turbidity graphs representing 2µM sMltB activity in 25mM NaH_2PO_4 pH 5.8, 100mM $NaCl_2$, 0.1% Triton X-100 using 0.4mg/mL *M. luteus* cells as a substrate (red). Inhibition by Ivyp1 (A) and Ivyp2 (B) was performed at a 0:1 (blue), 2:1 (green), 4:1 (purple), 6:1 (orange), and 8:1 (black) ratio of Ivyp:sMltB.

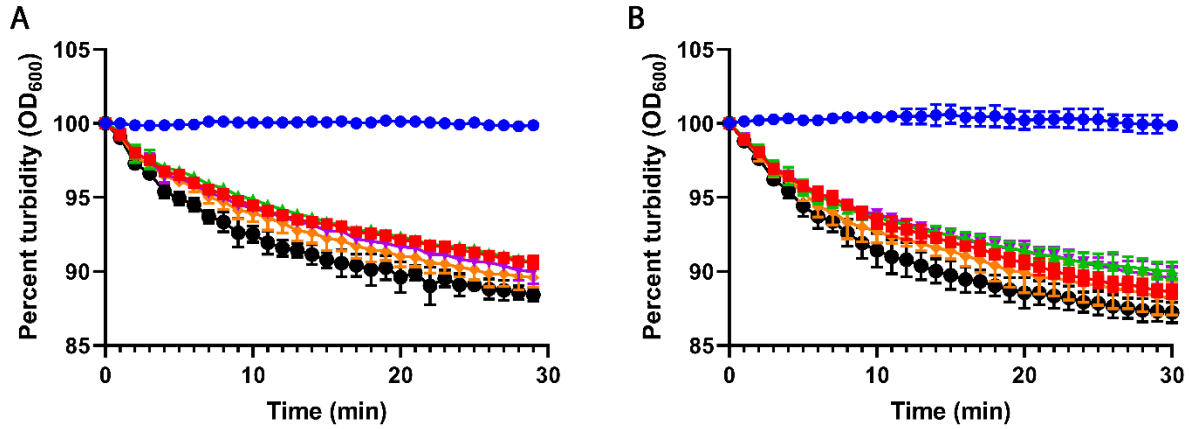

Figure B 3 Inhibition of sMltD with Ivyp1 and Ivyp2 – Turbidity graphs representing 100nM sMltD activity in 100mM NaOAc pH 5.0, 10mM $MgCl_2$ using 0.4mg/mL *M. luteus* cells as a substrate (red). Inhibition by Ivyp1 (A) and Ivyp2 (B) was performed at a 0:1 (blue), 1:1 (green), 5:1 (purple), 10:1 (orange), and 20:1 (black) ratio of Ivyp:sMltD.

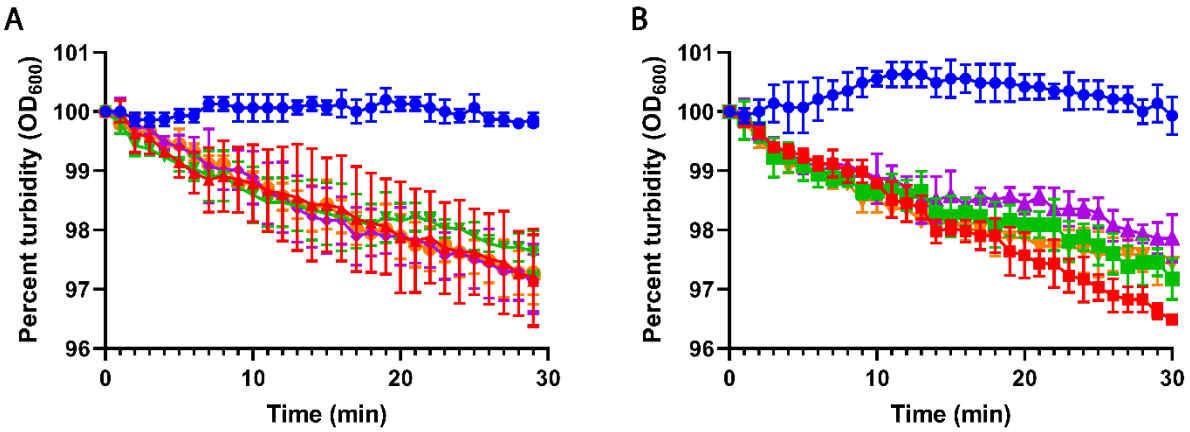

Figure B 4 Inhibition of sMltF with Ivyp1 and Ivyp2 – Turbidity graphs representing 400nM sMltF activity in 100mM NaOAc pH 4.5, 10mM $MgCl_2$ using 0.4mg/mL *M. luteus* cells as a substrate (red). Inhibition by Ivyp1 (A) was performed at a 0:1 (blue), 1:1 (green), 5:1 (purple), and 10:1 (orange) ratio of Ivyp1:sMltA, while inhibition by Ivyp2 (B) was performed at a 0:1 (blue), 5:1 (green), 10:1 (purple), and 20:1 (orange) ratio of Ivyp2:sMltF.

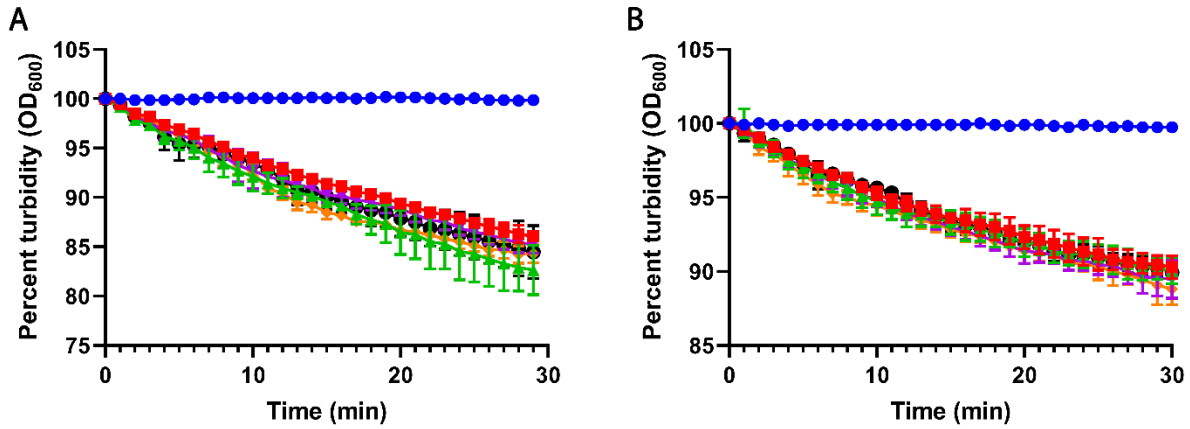

Figure B 5 Inhibition of sMltF2 with Ivyp1 and Ivyp2 – Turbidity graphs representing 200nM sMltF2 activity in 100mM NaOAc pH 5.0, 10mM $MgCl_2$ using 0.4mg/mL *M. luteus* cells as a substrate (red). Inhibition by Ivyp1 (A) and Ivyp2 (B) was performed at a 0:1 (blue), 1:1 (green), 5:1 (purple), 10:1 (orange), and 20:1 (black) ratio of Ivyp:sMltF2.

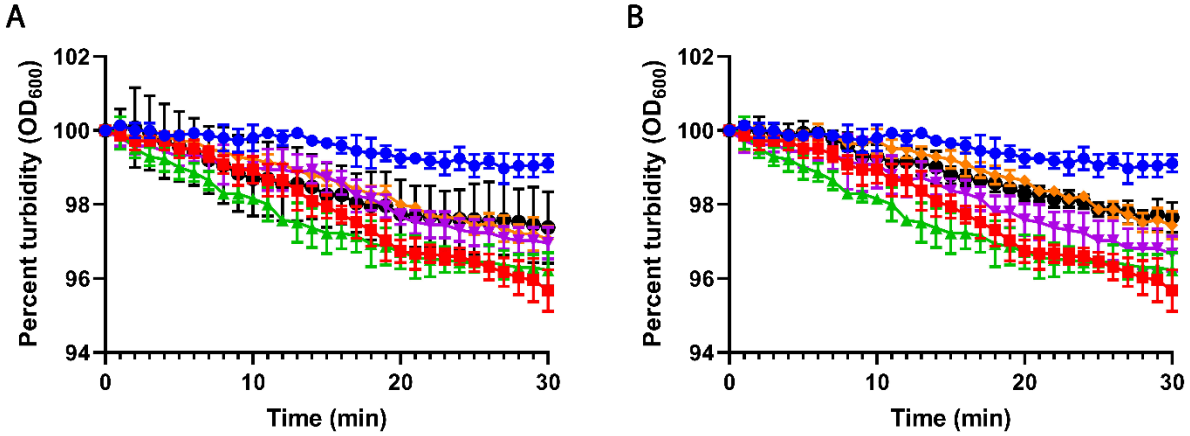

Figure B 6 Inhibition of sMltG with Ivyp1 and Ivyp2 – Turbidity graphs representing 500nM sMltD activity in 100mM NaOAc pH 5.5, 10mM $MgCl_2$ using 0.4mg/mL *M. luteus* cells as a substrate (red). Inhibition by Ivyp1 (A) and Ivyp2 (B) was performed at a 0:1 (blue), 5:1 (purple), 10:1 (orange), and 20:1 (black) ratio of Ivyp:sMltA. Buffer control is shown in green.

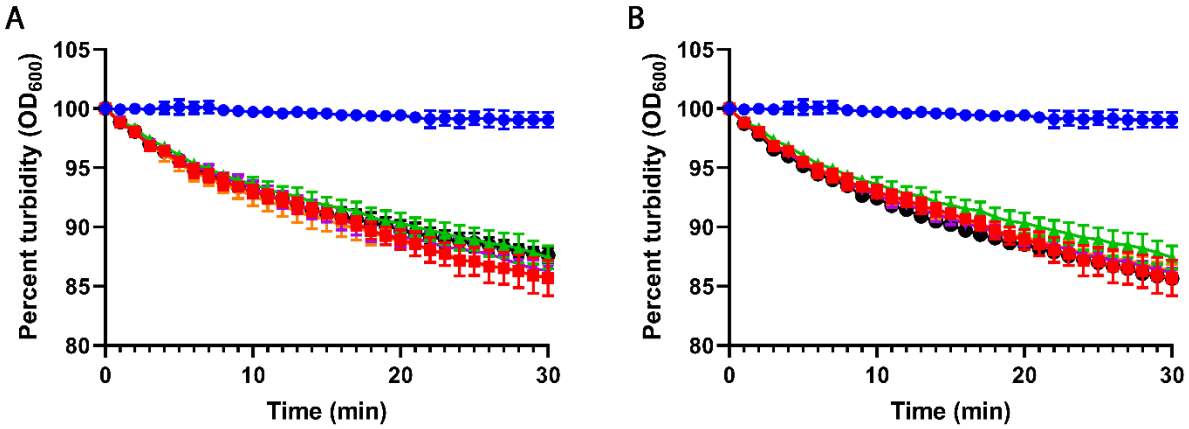

Figure B 7 Inhibition of sRlpA with Ivyp1 and Ivyp2 – Turbidity graphs representing 400nM sRlpA activity in 100mM NaOAc pH 6.0, 10mM $MgCl_2$ using 0.4mg/mL *M. luteus* cells as a substrate (red). Inhibition by Ivyp1 (A) and Ivyp2 (B) was performed at a 0:1 (blue), 5:1 (purple), 10:1 (orange), and 20:1 (black) ratio of Ivyp:sMltA. Buffer control is shown in green.

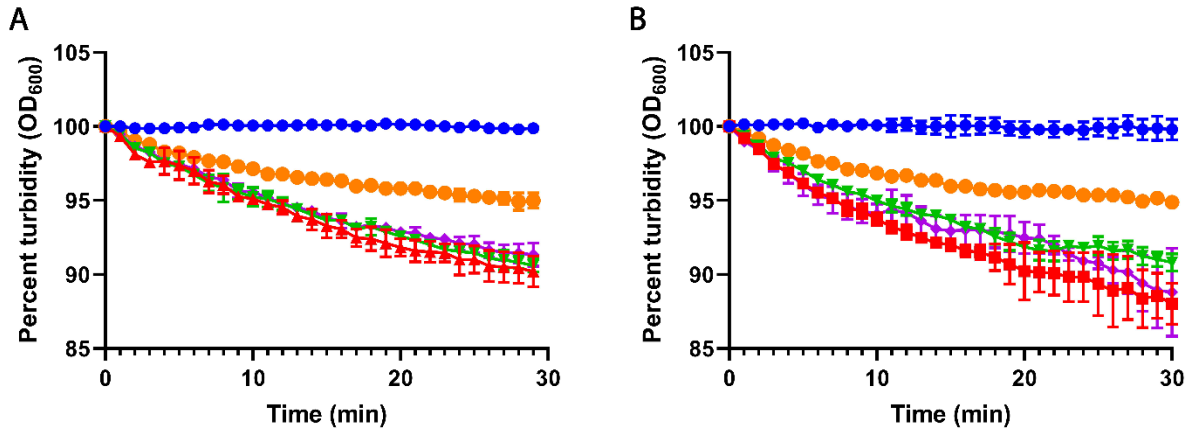

Figure B 8 Inhibition of Slt70 with Ivyp1 and Ivyp2 – Turbidity graphs representing 250nM Slt70 activity in 100mM NaOAc pH 5.5, 10mM $MgCl_2$ using 0.4mg/mL *M. luteus* cells as a substrate (red). Inhibition by Ivyp1 (A) and Ivyp2 (B) was performed at a 0:1 (blue), 5:1 (green), 10:1 (purple), and 20:1 (orange) ratio of Ivyp:Slt70.

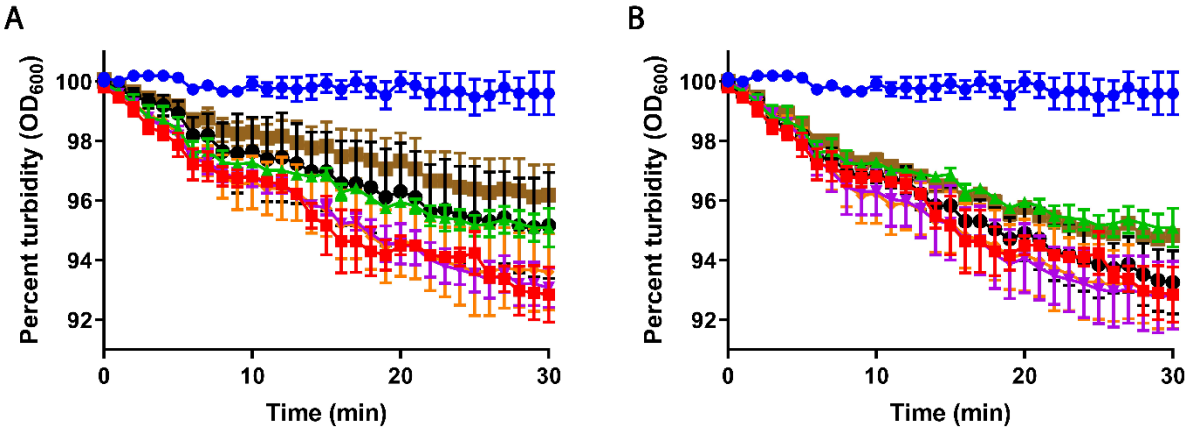

Figure B 9 Inhibition of SltB1 with Ivyp1 and Ivyp2 – Turbidity graphs representing 300nM SltB1 activity in 100mM NaOAc pH 4.5, 10mM $MgCl_2$ using 0.4mg/mL *M. luteus* cells as a substrate (red). Inhibition by Ivyp1 (A) and Ivyp2 (B) was performed at a 0:1 (blue), 1:1 (purple), 5:1 (orange), 10:1 (black) and 20:1 (brown) ratio of Ivyp:SltB1. Buffer control is shown in green.

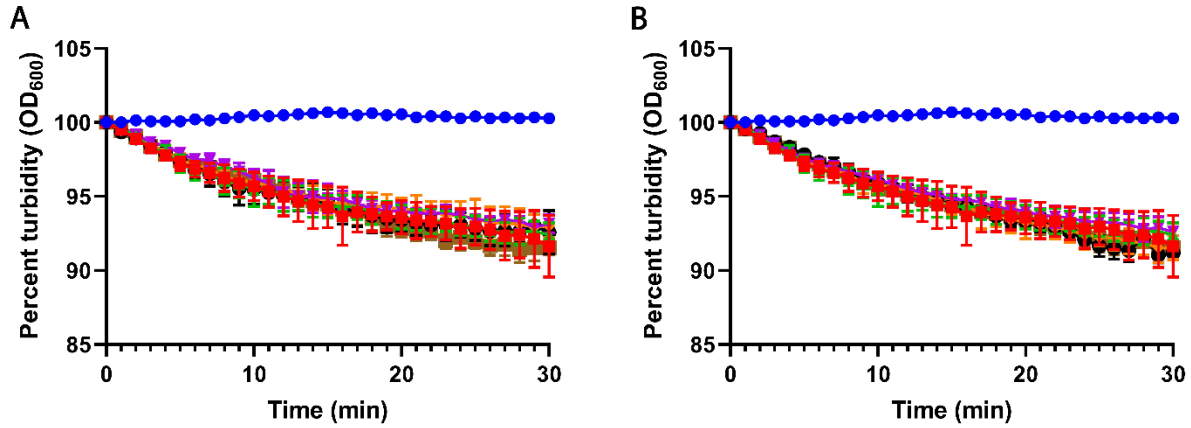

Figure B 10 Inhibition of SltB2 with Ivyp1 and Ivyp2 – Turbidity graphs representing 250nM SltB2 activity in 100mM NaOAc pH 4.5, 10mM $MgCl_2$ using 0.4mg/mL *M. luteus* cells as a substrate (red). Inhibition by Ivyp1 (A) and Ivyp2 (B) was performed at a 0:1 (blue), 1:1 (purple), 5:1 (orange), 10:1 (black) and 20:1 (brown) ratio of Ivyp:SltB2. Buffer control is shown in green.

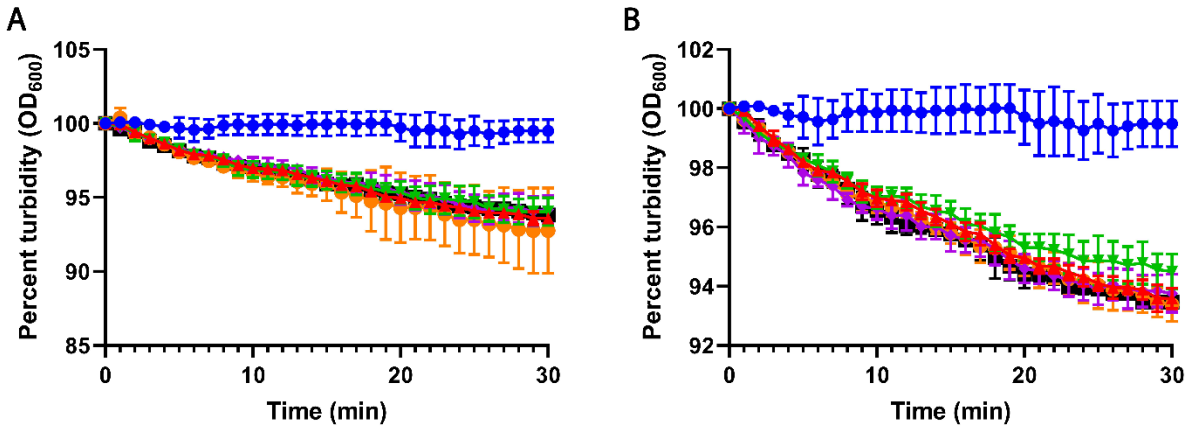

Figure B 11 Inhibition of SltB3 with Ivyp1 and Ivyp2 – Turbidity graphs representing 500nM SltB3 activity in 100mM NaOAc pH 5.0, 10mM $MgCl_2$ using 0.4mg/mL *M. luteus* cells as a substrate (red). Inhibition by Ivyp1 (A) and Ivyp2 (B) was performed at a 0:1 (blue), 1:1 (green), 5:1 (purple), 10:1 (orange) and 20:1 (black) ratio of Ivyp:SltB3.